Universitat Autònoma de Barcelona

Interrogating resistance mechanisms to PD-1 blockade therapy

Davis Yuri Torrejon Castro

Universitat Autònoma de Barcelona

Interrogating resistance mechanisms to PD-1 blockade therapy

A doctoral thesis presented

for the degree of Doctor

by

Davis Yuri Torrejon Castro

Directors:

Dr. Antoni Ribas Bruguera

Dr. Joan Seoane Suárez

Dr. Joan Carles Galceran

Tutor:

Dr. Jordi Giralt López de Sagredo

Doctoral Program in Medicine

Department of Medicine

Universitat Autònoma de Barcelona

Barcelona, 2021

This work is dedicated to my wife Marta, my son Nicolas and my daughter Olivia.

ACKNOWLEDGMENTS

I would like to express my gratitude to my mentor, Dr. Antoni Ribas. I still remember the day I received Toni's acceptance email to work in his lab. I took up the challenging arm in arm with my wife and son to start a life in other country. My deep commitment to bridging science and medicine drove me to leave the clinical practice to join his lab in 2015. Toni, your leadership, integrity, trust, collaborative spirit, work ethic and respect for your patients and colleagues inspire an entire generation of physician-scientists. I am really grateful for this opportunity!

Through these years, all members of Ribas lab, past and present, have been nothing but supportive, caring and great co-workers to contribute to the progress of my project. I would like to especially thank Dr. Siwen Hu-Lieskovan for her guidance and was the first one to train me on *in vivo* experiments. A special thanks to my friend, Gabriel Abril-Rodriguez for your help on crucial experiments and constructive criticism on the project.

To my mother Monica, thanks for your love, sacrifice and faith in the journey to turn my dream into a reality. My mother always taught me that life was about giving back. After she passed away from cancer, I have often reflected on my mission: To give the knowledge to help solve the puzzle which represents this devastating disease, and to drive to pursue strategies based on my scientific findings that will improve the lives of patients. I promise not to disappoint you.

To my father Andres, my genuine advisor and unflagging warrior, I cannot find the appropriate words that could properly describe my appreciation for your devotion and support. I always carry his teachings in my conscience. He always says, "The harder the life hit the harder you must fight". I only hope to be as good warrior and father as you are.

To my All – my wife Marta, my son Nicolas and my daughter Olivia- who give meaning to my days. Nothing would have been possible without Marta's support and advice. She lost everything along the way, nothing will ever be the same in Barcelona. But together we are building a new family and unlearning of fear and limits. Thanks for your love, patience and understanding. It may be a winding path, it may be longer and harder, but walking altogether makes it much more pleasant.

I would also like to express my thanks to all the members of the Vall d'Hebron Institute of Oncology thesis committee, Dr. Joan Seoane, Dr. Joan Carles and Dr. Jordi Giralt, for their support and encouragement through this process. Finally, I need to thank the funding sources that have supported my work, including a Young Investigator Award from American Society of Clinical Oncology, a grant from the Spanish Society of Medical Oncology for Translational Research in Reference Centers, and the V Foundation-Gil Nickel Family Endowed Fellowship in Melanoma Research.

ABBREVIATION LIST

ACK: Ammonium-Chloride-Potassium

APC: Allophycocyanin

APLNR: Apelin Receptor

APM: antigen presenting machinery

ATCC: American Type Culture Collection

B2M: Beta-2-Microglobulin

cnLOH: copy number neutral loss of heterozygosity

CSCC: cutaneous squamous-cell carcinoma

CTLA-4: cytotoxic T-lymphocyte-associated protein 4

CXCL10: Chemokine (C-X-C motif) ligand 10

CXCL11: Chemokine (C-X-C motif) ligand 11

CXCL9: Chemokine (C-X-C motif) ligand 9

CyTOF: Cytometry by Time-Of-Flight

DMEM: Dulbecco's Modified Eagle Medium

ELISA: enzyme-linked immunosorbent assay

EOMES: Eomesodermin

GAPDH: Glyceraldehyde 3-phosphate dehydrogenase

GAS: γ-activated sequence

GFP: green fluorescent protein

ICAM: Intercellular adhesion molecule

IFN: Interferon

IFNAR1: Interferon Alpha and Beta Receptor Subunit 1

IFNGR1: Interferon γ Receptor 1

IFNGR2: Interferon γ Receptor 2

IFNα: Interferon α

IFNβ: Interferon β

IFNγ: Interferon γ

IL15: Interleukin 15

IL2: Interleukin 2

IRF1: interferon regulatory factor 1

JAK1: Janus Kinase 1

JAK2: Janus Kinase 2

KO: knockout

LB: Lysogeny Broth

LoF: Loss of Function

MART1: Melanoma-associated antigen recognized by T cells

MFI: mean fluorescence intensity

MHC: Major histocompatibility complex

MITF: microphthalmia-associated transcription factor

MSI: Microsatellite Instability High

MTA: material transfer agreement

NK: natural killer

NSCLC: Non-small-cell lung carcinoma

NY-ESO-1: New York esophageal squamous cell carcinoma 1

PBAF: Polybromo-associated BAF complex

PBMCs: peripheral blood mononuclear cells

PCR: Polymerase chain reaction

PD-1: Programmed cell death protein 1

pDCs: plasmacytoid dendritic cells

PD-L1: Programmed death-ligand 1

PD-L2: Programmed death-ligand 2

PPRs: Pattern recognition receptors

PTPN2: Protein Tyrosine Phosphatase Non-Receptor Type 2

RFP: red fluorescent protein

RIG-1: retinoic acid-inducible gene I

RPMI: Roswell Park Memorial Institute medium

SCLC: Small cell lung cancer

sgRNA: single guide RNA

shRNA: short hairpin RNA

STAT1: Signal transducer and activator of transcription 1

STAT3: Signal transducer and activator of transcription 3

TAM: tumor-associated macrophages

TAP1: Antigen peptide transporter 1

TBET: T-box transcription factor TBX21

TCR: T-cell receptor

TIDE: Tracking of Indels by Decomposition

TIM3: T cell immunoglobulin and mucin-domain containing-3

TLR9: Toll-like receptor 9

TYK2: Tyrosine Kinase 2

VSV: Vesicular stomatitis virus

WT: wild-type

INDEX

SUMMARY

Immunotherapy with PD-1 or PD-L1 blockade has been proved to accomplish long term anti-tumor responses in patients with metastatic cancer, but it is extremely important to understand why some patients never respond to this mode of therapy, and how some patients respond and then progress. We have been studying resistance mechanisms to PD-1 blockade in patient biopsies and human melanoma cell lines mediated by *JAK1/2* loss-of-function mutations in the IFN-receptor pathway and the inactivation of *B2M* in the antigen presentation.

To characterize the biological significance and validate the role of these mutations leading to resistance to PD-1 blockade, we developed genetic acquired resistant models of *JAK1*, *JAK2* and *B2M* loss-of-function mutations by gene knockout in human melanoma cell lines and murine cell lines. Human melanoma cell lines with *JAK1/2* knockout became insensitive to interferon IFN-induced antitumor effects, while *B2M* knockout were no longer recognized by antigen-specific T cells and hence was resistant to cytotoxicity. All of these mutations led to resistance to anti-PD-1 therapy *in vivo*.

Based on the mechanistic understanding of these genetic acquired resistance mutations, we allowed the design of strategies aimed to overcome resistance. *JAK1/2* knockout resistance could be overcome with the activation of innate and adaptive immunity by intratumoral Toll-like receptor 9 agonist administration together with anti-PD-1, mediated by natural killer (NK) and CD8 T cells. *B2M* knockout resistance could be overcome by NK-cell and CD4 T-cell activation using the CD122 preferential IL2 agonist bempegaldesleukin. Therefore, mechanistically designed combination therapies can overcome genetic resistance to PD-1 blockade therapy.

RESUMEN

La immunoterapia basada en el bloqueo del PD-1/ PD-L1 ha logrado respuestas antitumorales a largo plazo en pacientes con cáncer metastásico, pero es importante conocer por qué algunos pacientes no responden o cómo otros inicialmente responden y después progresan. Nosotros estudiamos los mecanismos de resistencia al bloqueo del PD-1 en biopsias y líneas celulares de melanoma humano mediadas por las mutaciones de pérdida de función del *JAK1/2* en la vía del receptor del IFN y la inactivación del *B2M* en la presentación antigénica.

Con el fin de caracterizar el significado biológico y validar el rol de estas mutaciones, desarrollamos modelos genéticos de resistencia adquirida con las mutaciones de pérdida de función del *JAK1*, *JAK2* y *B2M* por desactivación específica de estos genes (knockout) en líneas celulares de melanoma humano y líneas murinas. Las líneas de melanoma con *JAK1/2* knockout se volvieron insensibles a los efectos antitumorales inducidos por el interferón, mientras que las células T específicas de antígeno ya no eran reconocidas en las líneas con *B2M* knockout y, por tanto, eran resistentes a la citotoxicidad. Todas estas mutaciones conducen a la resistencia a la terapia anti-PD-1 en los experimentos *in vivo*.

Basada en la comprensión mecanicista de estas mutaciones de resistencia adquirida, diseñamos estrategias destinadas a superarla. La resistencia al *JAK1/2* knockout pueden superarse con la activación de la inmunidad innata y adaptativa de la administración intratumoral del agonista de receptor tipo Toll 9 con anti-PD-1, dicha respuesta es mediada por los linfocitos T CD8 y células asesinas naturales (NK). La resistencia a la inactivación del *B2M* puede superarse mediante la activación de células NK y células T CD4 utilizando el CD122, agonista preferencial de IL2, bempegaldesleukin. Por lo tanto, las terapias de combinación diseñadas racionalmente mediante la comprensión mecanicista pueden superar la resistencia genética a la terapia de bloqueo del PD-1.

1. INTRODUCTION

1.1 Development of cancer immunotherapy based on PD-1 blockade therapy

Cancer is the second most common cause of death worldwide, exceeded only by heart disease. In 2018, there were around 18.1 million new cases of cancer worldwide including around 2.1 million cases in the U.S., and 9.6 million cancer-related deaths worldwide including 616,714 deaths in the U.S. The number of new worldwide cancer cases per year is expected to rise to 23.6 million by 2030. In the U.S., more than 1.8 million new cancer cases are expected to be diagnosed in 2021, and about 608,570 Americans are expected to die of cancer in 2021, which translates to about 1,670 deaths per day (1,2). This makes cancer a major public health issue. With the many challenges of traditional treatments such as chemotherapy and radiotherapy, there has been a significant interest in treating cancer using immunotherapy, which focuses on harnessing the power of the immune system to fight cancer.

The pioneering studies by James P. Allison releasing CTLA-4 (cytotoxic T-lymphocyte-associated protein 4), a negative checkpoint regulator of the immune system, provided a paradigm shift in cancer immunotherapy (3,4). Allison cited three reasons for studying the immune system in cancer. One is the great specificity of the immune system. Because cancer cells produce antigens that can trigger an immune response specific to the cancer, with few of the side effects normally associated with chemotherapy or radiotherapy. The second one is that immune memory. This is the hallmark of the immune system that make it different from the rest of cancer therapy. One memory T cell can produce multiple cytotoxic T cells which can directly kill tumor cells for the rest of life, while others have only a limited efficiency. The third one is that the immune system can adapt as the tumor changes. This new paradigm led to the

clinical development of other immune checkpoint inhibitors such antibodies blocking PD-1 (programmed cell death protein 1) or its main ligand PD-L1 (programmed death-ligand 1).

PD-1 is an inhibitory receptor induced in activated T cells, B lymphocytes, and NK cells. The interaction between PD-1 and ligands, PD-L1 and PD-L2 suppresses T cell function primarily by inactivating CD28 signaling and play a crucial role in the maintenance of peripheral tolerance (5,6). Anti-PD-1/PD-L1 antibodies restore antitumor immune responses, stimulating T cells to attack cancer cells, providing patients with remarkable and durable clinical responses of various cancer types.

There are currently six anti-PD-1/PD-L1 antibodies approved by the FDA, Pembrolizumab (Keytruda®), nivolumab (Opdivo®) and cemiplimab-rwlc (Libtayo®) are PD-1 receptor inhibitors, while atezolizumab (Tecentriq®), avelumab (Bavencio®), and durvalumab (Imfinzi®) block the engagement of PD-L1. These agents have been shown to have significant antitumor activity in a wide range of malignancies, in particular in carcinogen-induced cancers or cancers driven by viral infections (**Table 1**).

Despite the promising anticancer activity offered by anti-PD-1/PD-L1 antibodies, there are many critical parameters remain unknown, such as the predictive primary sensitivity or resistance biomarkers as well as the resistance mechanisms and disease progression on or after therapy. A significant number of patients do not respond to this type of therapy (innate resistance) or they experience the reappearance and progression after responding (acquired resistance) (7,8). Therefore, there has been an urgent need to understand the biology of resistance mechanisms to anti-PD-1 therapy and develop more effective immunotherapeutic approaches to overcome the resistance to immunotherapy.

Table 1. Major indications approved for the use of anti–PD-1/PD-L1 therapies and the suspected mechanism of action of the antitumor response

Group	Indication	Objective response rate (%)	Agents approved	Main driver of response
High response rate	Hodgkin's disease	87	nivolumab pembrolizumab	PDJ amplicon
	Desmoplastic melanoma	70	nivolumab pembrolizumab	Mutations from chronic sun exposure
	Merkel cell	56	avelumab pembrolizumab	Merkel cell virus
	Microsatellite Instability High (MSI-h) cancers	53	nivolumab pembrolizumab	Mutations from mismatch repair deficiency
Intermediate response rate	Skin melanoma	35 to 40	nivolumab pembrolizumab	Mutations from intermittent sun exposure
	Cutaneous squamous-cell carcinoma (CSCC)	34 to 46	cemiplimab-rwlc pembrolizumab	Mutations from sun exposure
	Non-small-cell lung carcinoma (NSCLC)	20	atezolizumab cemiplimab-rwlc nivolumab pembrolizumab	Mutations from cigarette smoking
	Small cell lung cancer (SCLC)	19	pembrolizumab	Mutations from cigarette smoking
	Head and neck	15	nivolumab pembrolizumab	Mutations from cigarette smoking
	Gastroesophageal	15	pembrolizumab	Mutations from cigarette smoking
	Bladder and urinary tract	15	atezolizumab avelumab durvalumab nivolumab pembrolizumab	Mutations from cigarette smoking
	Renal cell carcinoma	25	nivolumab pembrolizumab	Insertions and deletions (indels)
	Hepatocellular carcinoma	20	nivolumab	Hepatitis virus

Table was adapted with permission from Ribas et al. Science 2018.

1.2 Tumor cell resistance to interferon γ signaling

Interferon γ (IFNγ) is produced by activated T-cells and is often used as the primary marker of T-cell activation. IFNγ engagement to its receptor (*IFNGR1* and *IFNGR2*) on tumor cells leads to *JAK1* and *JAK2* activation resulting in *STAT1* and *STAT3* recruitment and phosphorylation. Upon *STATs* phosphorylation and activation, the complex is translocated to the nucleus where it binds to the γ-activated sequence (*GAS*), resulting in interferon regulatory factor 1 (*IRF1*) activation which is known to be essential to induce PD-L1 expression (9). IFNγ has direct pro-apoptotic/anti-proliferative effects on target cells, while its pro-inflammatory effects include enhancing antigen presentation through Major histocompatibility complex (MHC) class I and Antigen peptide transporter 1 (*TAP1*) upregulation, and also production of chemokines (CXCL9, 10, 11) and ICAM expression for T-cell recruitment (10,11) (**Figure 1A**).

Because inducible PD-L1 expression in tumors upon tumor antigen-specific T cell infiltration appears to be associated with response to PD-1 blockade therapies, the elucidation of the mediators required to upregulate PD-L1 during adaptive resistance provide essential information for the understanding of the pathways involved in immune resistance. Although PD-L1 could also be constitutively expressed by activation of different oncogenic pathways, interferon-induced PD-L1 expression seems to be a mechanism of cancer cells resistance against T cell attack (12,13).

In order to elucidate the molecular mechanisms underlying PD-L1 expression, we performed an IFN receptor pathway shRNA (short hairpin RNA) screen in which melanoma cells were transduced with the PD-L1 promoter attached to a firefly luciferase (14). We demonstrated that the IFNγ-*JAK1/2-STAT1/3-IRF1* axis regulates PD-L1 expression and revealed the potential

role of key molecules (such as *JAK1*, *JAK2* or *IRF1*) in the regulation of PD-L1 expression when mutating or epigenetically silencing (14). This mechanism of cancer immunoediting, with loss of signaling through *JAK1* or *JAK2*, would result in lack of PD-L1 expression, thereby resulting in cancer cells that would be genetically negative for inducible PD-L1 expression. In such a scenario, blocking PD-1 or PD-L1 with therapeutic antibodies would not be useful (**Figure 1B).**

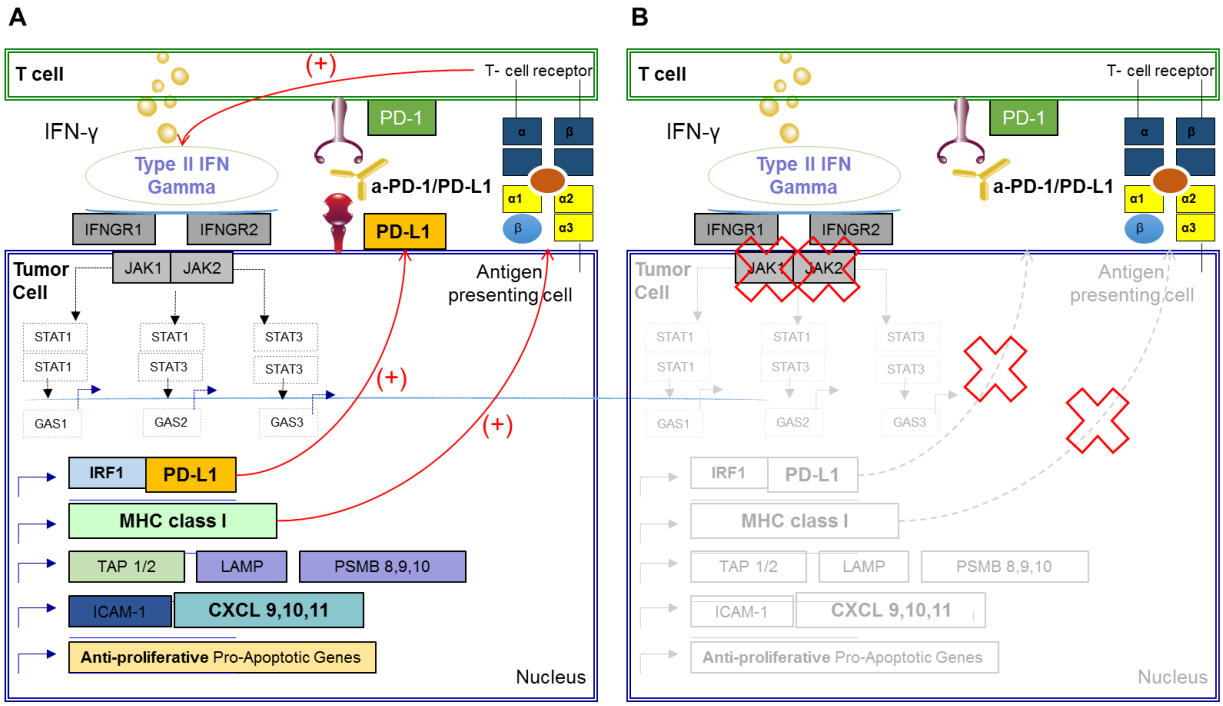

Figure 1. (A) IFN-induce adaptive PD-L1 expression in response to tumor-specific T cell response. Tumor-reactive T cells, which recognize tumor neoantigens in the context of MHC class I, release IFNγ, resulting in activation of *JAK1/2*, with both being necessary for downstream signaling (bottleneck in the pathway), leading to activation of *STAT1/3* and *IRF1*. This results in the adaptive expression of PD-L1 on the surface of tumor cells, which negatively regulates the antitumor T cell response. In this setting, an anti-PD-1/PD-L1 antibody releases this immune checkpoint and leads to tumor response. **(B) Resistance to anti-PD-1/PD-L1 blocking antibody by Loss of Sensitivity to IFNγ signaling.** A tumor with genetic deficiencies in the IFNγ signaling (*JAK1* or *JAK2*) will not respond to IFNγ by expressing PD-L1. In the absence of adaptive PD-L1 expression, anti-PD-1/PD-L1 immune checkpoint blockade is ineffective. The circuit is broken leading to innate resistance to these class of agents.

1.3 Disruption of the *B2M* gene in antigen presentation

T cells are activated by tumor antigens to proliferate and differentiate into effector cells only when the antigens are presented in a peptide-MHC complex. This multistep process involves multiple genes that constitute the antigen presenting machinery (APM) and are essential in the efficiency of T cell-based immunotherapies. Downregulation of MHC genes or the APM, including the proteasome components, transporters associated with antigen processing (TAP), β-2-microglobulin, peptide transporters, endoplasmic reticulum chaperones and the Golgi apparatus leading to antigen escape variants not recognized by the immune system (15).

Beta-2-Microglobulin (*B2M*) is a critical membrane protein component of the MHC class I found on the surfaces of all nucleated cells. *B2M* function is to interact with and stabilize the tertiary structure of MHC-I α-chain, thereby presenting antigenic peptides to cytotoxic T lymphocytes. During the process of recognizing the foreign peptide antigen on the cell surface, T cells can actively bind and dissolve the cancer cells presented by the antigen. Without *B2M* on the tumor cell surface, MHC class I molecules are not stable and unable to present antigen to CD8 T cells, resulting the *B2M* loss as a genetic mechanism of resistance to cancer immunotherapy.

Early pioneering work demonstrated that mutations resulting in loss of *B2M*, rendering melanoma tumors resistance to T cell infiltration (16,17). This mechanism of resistance has also highlighted in our study of acquired resistance to anti-PD-1 therapy in melanoma patients where the whole-exome sequencing of the resistant tumor had a new and homozygous truncating mutation in *B2M* leading to lack of surface expression of MHC class I and acquired resistance mechanism to anti-PD-1 in the patient (18) (**Figure 2**).

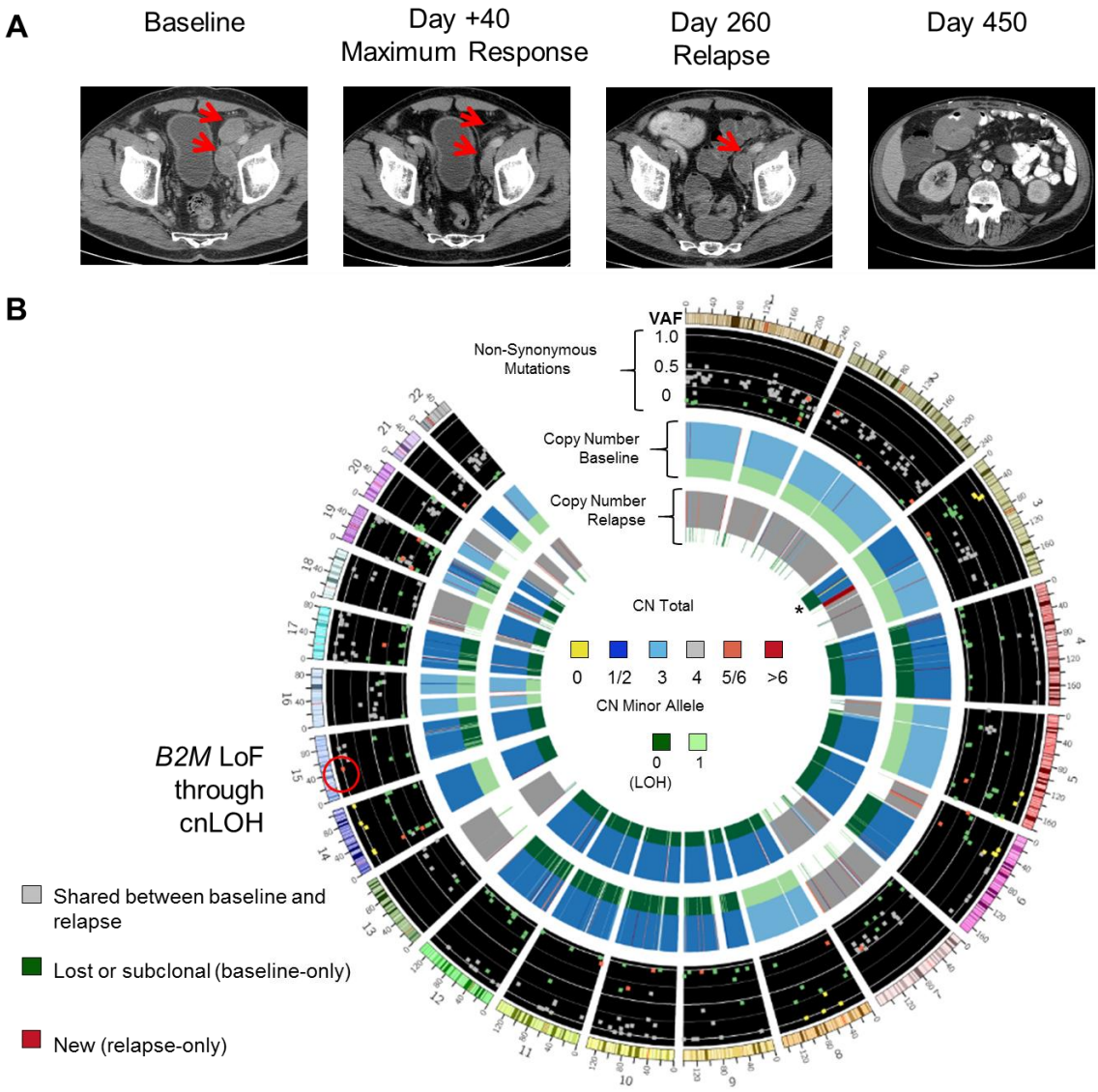

Figure 2. . Acquired *B2M* LoF Mutation at Relapse Tumor. (A) CT images correspond time-points indicated by colored dots. The relapse biopsy comes from a small bowel lesion first visualized at 264 days, with clear progression 453 days from therapy start. **(B)** Circos plot. Cell line (M437) derived from the baseline biopsy is compared to the progressing tumor. Both lesions shared a core of 304 non-synonymous mutations and a similar copy number profile with mostly shallow gains/losses. Most baseline-specific mutations were subclonal (62% of 149 mutations with allele frequency <0.35), while others were eliminated in loss-of-heterozygosity events on chromosomes 3p, 5q, 6p, 8, 14, and 20. Relapse was notable for a strong amplification of the MITF locus on chromosome 3 (asterisk), and a four basepair S14fs frameshift deletion in the MHC class I component *B2M* (red circle). Figure was adapted with permission from Zaretsky et al. NEJM 2016.

1.4 Resistance to PD-1 blockade therapy

Our studies in patient biopsies and human melanoma cell lines, provided the first evidence that melanoma could escape anti-PD-1 therapy through alterations in the IFNγ receptor pathway through loss of the *JAK1/2*, and in the APM through loss of *B2M* (18,19). In Zaretsky *et al*, 2016, we did whole-exome sequencing on tumor samples taken from four patients with metastatic melanoma who had relapsed after more than 6 months of tumor response to treatment with pembrolizumab. The tumors in two of the patients showed over 90% of the same mutations both before and after disease progression. But their relapsed tumors had developed mutations in the *JAK1* or *JAK2* genes, respectively (**Figure 3**). In the third patient, the relapsed tumor showed a mutation in *B2M* gene and the fourth patient had no apparent mutations related to acquire resistance to T cells (18).

Of note, in acquired resistance cases mediated by *JAK1/2* and *B2M* mutations, among the 20,000 plus genes in the genome the only ones that had a new, homozygous mutation were these particular genes. In all cases, it was through the process of copy number neutral loss of heterozygosity (cnLOH), which requires that multiple genetic steps happen to lead to the homozygous gene and protein loss (18). These cannot be chance events, and can only be explained by active immunoediting of the cancer genome.

The translational relevance of these findings have been corroborated in patient biopsies for *JAK1/2* mutations (20,21), as well as in melanoma (22–24) and lung cancer (25) for *B2M* mutations. Additional data from five preclinical models based on CRISPR screens provide orthogonal support to the key role of the IFNγ receptor pathway and APM as the two dominant

pathways involved in resistance (26–30). Loss of genes such as the IFNγ receptor chains (*IFNGR1/2*), *JAK1*, *JAK2* or *STAT1*, or the APM molecules MHC class I, *B2M*, TAP transporters or proteasome subunits, result in decreased antitumor activity of cancer immunotherapy.

The frequency of such mutations is low in the limited studies to date (31,32), but instead are biologically important events that unquestionably lead to acquired resistance in the few cases where they develop de novo in the relapsed tumors. The genetic changes leading to resistance are defined mechanisms that we can study with the anticipation that other cancer cells may try to achieve the same goals through harder to study non-genetic mechanisms. Indeed, recent CRISPR/Cas9 screens studies have identified additional molecules that modulate the IFNγ receptor pathway without a genetic alteration, such as changes in PTPN2 (26), APLNR (27), and PBAF (33) expression, demonstrating that down- or up-regulation of molecules besides JAK kinases can achieve the same advantage to cancer cells as *JAK1/2* Loss-of-Function (LoF) mutations.

We acknowledge that the biology of these Loss-of-Function mutations is not straightforward, as several well-documented cases of patients with metastatic melanoma with *B2M* mutations at baseline were reported to respond to anti–PD-1 or anti-CTLA4 therapy (22,34–37). In addition, it is envisioned that a subset of cases with primary and acquired resistance to PD-1 blockade therapy can obtain the similar resistant phenotypes through epigenetic changes in the same pathways, which are harder to study in patient-derived biopsies (7,37–39). Based on these data, we propose a focused functional characterization of the genetic resistance mechanisms that we have described in patient biopsies, and how the knowledge will lead to rational combination therapies to treat the cancers with these resistance mechanisms.

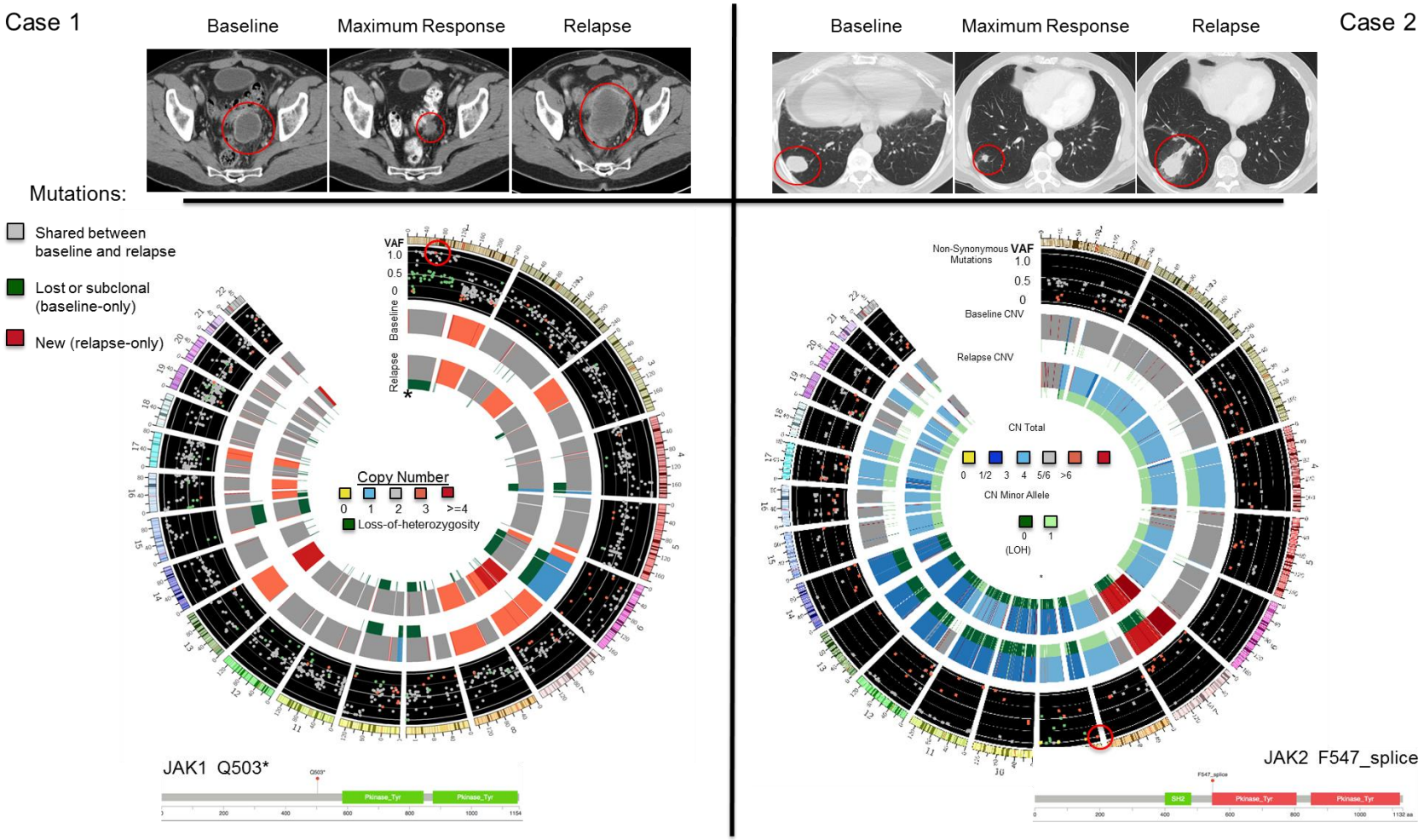

Figure 3. Acquired *JAK1/2* LoF Mutation at Relapse, with Accompanying Loss of Heterozygosity. (Top) CT images correspond time-points indicated by colored dots. Circos plot of Patient 1 and 2 shows differences in whole-exome sequencing between the pre-pembrolizumab and post-relapse biopsies. The red circle highlights a new, high-allele-frequency, relapse-specific *JAK1* **(left)** and *JAK2* **(right)** mutation in the context of chromosomal loss of heterozygosity. cBioPortal Diagram **(bottom)** revel as the JAKs mutation is upstream of the kinase domains. Figure was adapted with permission from Zaretsky et al. NEJM 2016.

We originally reported that the dinucleotide 2'-3'-cGAMPa (cyclic guanosine monophosphate–adenosine monophosphate), an endogenous STING (stimulator of interferon genes) which is produced in response to cytosolic double-strand DNA provided a downstream signal leading to cell death in human melanoma cell lines with a JAK2 mutation but not with JAK1 mutation (18). This, because the STING agonist still requires type I IFN signaling to exhort its antitumor properties, which is maintained with a JAK2 mutation. In this sense, the convergence of data on the IFNγ receptor signaling pathway suggests that the use of combinatorial approaches to reactivate the IFN pathway could overcome resistance driven by JAK mutations (40).

For instance, Toll-like receptor 9 (TLR9) agonists that mimic bacterial DNA sequences stimulate both innate and adaptive immune responses by inducing the production of type I IFNs, in particular by plasmacytoid dendritic cells (pDCs), a cell type with exquisite sensitivity to TLR9 agonists (41). SD-101 is an agonist of TLR9 that stimulates pDCs to release IFNα and mature into antigen-presenting cells to activate T cell anti-tumor responses. We hypothesize that the downstream activation of a type I IFN response, in cancer cells or in pDCs in the tumor microenvironment, should be able to overcome acquired resistance to *JAK1/2* LoF tumors.

On the other hand, it is well known that MHC class I deficient tumors are susceptible to NK cell–dependent cytotoxicity (42–44). NK inhibitory receptors on the surface of the NK cell recognize cognate MHC class I molecules and produce a signal to inhibit lysis. As a result, NK cells may be activated to recognize "missing self" caused by the lack of expression of MHC class I on tumor cells originated from the genetic mutation in the *B2M* (43).

Interleukin 2 (IL2) promotes immune responses by inducing CD4+T cell proliferation and differentiation into helper T cells, including Th1 and Th2 cells, and activating CD8+ T effectors

and NK cells (45). Bempegaldesleukin is an engineered PEGylated IL2 agonist (46) that demonstrated superior activity over aldesleukin in a murine model of ACT therapy (47). Given the mechanistic model of how *B2M* loss tumors can escape from T-cell-mediated immunity point us to the hypothesis that inducing this potent IL2 agonist can restore the full functionality of NK cells and CD4+ T cells that could recognize and destroy the tumor cells in an MHC class I-independent manner.

To define the IFN signaling and antigen presentation mechanisms of resistance by *JAK1*, *JAK2* and *B2M* loss of function mutations we developed *in vitro* and *in vivo* models and studied the biological significance of these mutations leading to resistance to PD-1 blockade therapy. Using CRISPR/Cas9 genome editing, we created sublines lacking *JAK1*, *JAK2* and *B2M* expression in four human melanoma cell lines to characterize their biology in terms of response to IFNγ exposure and evaluation of cell proliferation, growth inhibition and signaling changes by RNAseq. We also created established knockout sublines in the murine MC38 colon carcinoma, which is a well-characterized model with high mutational burden that responds well to anti-PD-1 therapy (48,49), and validated key results in the widely used primary anti–PD-1 blockade–resistant B16 murine melanoma model. Based on the molecular understanding of these pathways, we hypothesized that a TLR9 agonist could initiate a potent type I IFN systemic response overcoming anti-PD-1 resistance in *JAK1/2* deficient models and that a CD122 preferential IL2 pathway agonist could overcome resistance in *B2M* deficient tumors by enhancing NK –cell and CD4 T-cell antitumor activity.

2. HYPOTHESIS

My hypothesis is that the genetic absence of *JAK1/2* or *B2M* results in cancer cells that are not infiltrated by tumor antigen-specific immune cells due to lack of signaling through the IFNγ receptor resulting in absence of T cell attraction due to lack of chemokine production (for *JAK1/2*), or due to absence of T cell recognition of the cancer (for *B2M*).

Understanding the immune escape mechanisms will allow developing new rational design combinatorial therapies to overcome these resistance mechanisms, and better treat patients with advanced melanoma and other cancers.

3. OBJECTIVES

MAIN OBJECTIVE

Characterization and biological significance of the *JAK1/2*, and *B2M* Loss-of-Function mutations we described in patients by generating *in vitro* and *in vivo* model systems, and how the knowledge will lead to rational combination therapies to treat the cancers with these resistance mechanisms.

SECONDARY OBJECTIVES

Aim 1: Understand how IFN-receptor pathway alterations and *B2M* mutations leading to resistance to PD-1 blockade.

1.1. Generate a panel of *JAK1*, *JAK2* and *B2M* knockout sublines in human melanoma cell lines.

1.2 Functional studies in human melanoma cell lines and established knockout sublines exposed to IFNs (cell proliferation, antigen processing, T cell recognition and growth inhibition).

1.3 Analyze signaling changes in human melanoma cell lines exposed to IFNγ.

Aim 2: Modeling resistance to PD-1 blockade in mouse melanoma models.

2.1 Generate anti-PD-1 acquired resistance in MC38 murine model by *in vivo* treatment with anti-PD-1 therapy.

2.2 Analysis of models of *in vitro* IFNγ and *in vivo* anti-PD-1 acquired resistance mechanisms.

2.4 Study the role of *B2M* in acquired resistance to anti-PD-1 therapy.

Aim 3: Overcome resistance with combination immunotherapy.

3.1 Test downstream activation of the IFN-receptor pathways with TLR 9 agonist in *JAK1/2* knockout tumors.

3.2 Test IL2 pathway agonist against *B2M* knockout tumors.

3.3 Validation of combinatorial strategies in an aggressive B16 murine melanoma model.

4. MATERIAL AND METHODS

4.1 Human melanoma cell lines, cell culture and conditions

Patient-derived melanoma cell lines were thawed and cultured at 37° C with 5% CO_2 in RPMI-1640 medium supplemented with 10 % fetal bovine serum, 100 units/ml penicillin, 100 µg/ml streptomycin and 0.25 µg/ml amphotericin B. Cells were maintained and tested for mycoplasma with the MycoAlert Mycoplasma Detection Kit (Lonza). Cell lines were periodically sampled and used the GenePrint 10 System for cellular authentication, and matched with the earliest passage cell lines. Cell lines were subject to experimental conditions after reaching two passages from thawing.

4.2 CRISPR/Cas9-mediated knockout

4.2.1 CRISPR/Cas9 sgRNAs, cloning

The human melanoma cell lines M202, M233, M407 and M420 were subjected to CRISPR/Cas9-mediated knockout of *JAK1, JAK2*, and *B2M*. MC38 murine cell line was subjected to CRISPR/Cas9-mediated knockout of *JAK1, JAK2, B2M* and *IFNAR1*. B16 murine cell line was subjected to CRISPR/Cas9-mediated knockout of *JAK1, JAK2* and *B2M*. Single guide RNA (sgRNA) targeting were designed using the CRISPR design tool at http://www.deskgen.com, and are shown in the **Tables 2-4**.

Table 2. List of CRISPR sgRNA sequences in human melanoma cell lines.

Gene	sgRNA
JAK1	sgRNA1 FW 5-CATCCGGTAGTGGAGCCGGA-3
	sgRNA1 RV 5-TCCGGCTCCACTACCGGATG-3
	sgRNA2 FW 5-TCTCGTCATACAGGGCAAAG-3
	sgRNA2 RV 5-CTTTGCCCTGTATGACGAGA-3
JAK2	sgRNA1 FW 5-ATCTGCCTCAGATTTCCCAA-3
	sgRNA1 RV 5-TTGGGAAATCTGAGGCAGAT-3
	sgRNA2 FW 5-CTTACGATGACAGAAATGGA-3
	sgRNA2 RV 5-TCCATTTCTGTCATCGTAAG-3
B2M	sgRNA2 FW 5-ATACTCATCTTTTTCAGTGG-3
	sgRNA2 RV 5-CCACTGAAAAAGATGAGTAT-3
	sgRNA3 FW 5-GAGTAGCGCGAGCACAGCTA-3
	sgRNA3 RV 5-TAGCTGTGCTCGCGCTACTC-3

Table 3. List of CRISPR sgRNA sequences in MC38 mouse cell line

Gene	sgRNA
JAK1	sgRNA1 FW 5-CAGCGGAGAGTATACAGCCG-3
	sgRNA1 RV 5-CGGCTGTATACTCTCCGCTG-3
	sgRNA2 FW 5-CATTTTAGCACAGAACGCCA-3
	sgRNA2 RV 5-TGGCGTTCTGTGCTAAAATG-3
	sgRNA3 FW 5-CTGGACAACCGAATAAATGC-3
	sgRNA3 RV 5- GCATTTATTCGGTTGTCCAG-3
JAK2	sgRNA1 FW 5-ATATCACCATTCTGATGTAC-3
	sgRNA1 RV 5-GTACATCAGAATGGTGATATC-3
	sgRNA2 FW 5- CATCAGAATGGTGATATTCC-3
	sgRNA2 RV 5- GGAATATCACCATTCTGATG-3

B2M	sgRNA1 FW 5-CTGGTGCTTGTCTCACTGAC-3
	sgRNA1 RV 5-GTCAGTGAGACAAGCACCAGC-3
	sgRNA2 FW 5-TCACGCCACCCACCGGAGAA-3
IFNAR1	sgRNA2 RV 5-TTCTCCGGTGGGTGGCGTGAC-3
	sgRNA1 FW 5-CTCGCTGTCGTGGGCGCGG-3
	sgRNA1 RV 5-CCGCGCCCACGACAGCGAGC-3
	sgRNA2 FW 5-CACTGCCCATTGACTCTCCG-3
	sgRNA2 RV 5-CGGAGAGTCAATGGGCAGTGC-3

Table 4. List of CRISPR sgRNA sequences in B16 mouse cell line

Reagent	Sequence(s)
***JAK1* CRISPR guide**	CAGCGGAGAGTATACAGCCG
***JAK2* CRISPR guide**	CATCAGAATGGTGATATTCC
***B2M* CRISPR guide**	TCACGCCACCCACCGGAGAA

Human melanoma M407 with CRISPR/Cas9 mediated *JAK1* and *JAK2* knockouts were generated by lentiviral transduction using particles encoding guide RNAs, a fully functional CAS9 cassette, GFP, and puromycin as selectable markers (Sigma-Aldrich), as previously described (18). All other sgRNAs were cloned into the pSpCas9(BB)-2A-GFP vector (Addgene, Cambridge, MA) using Zhang's protocol (50) and then transformed into One Shot® Stbl3™ Chemically Competent E. coli (Invitrogen) and cultured overnight in Lysogeny Broth (LB) medium with ampicillin plates. Selected colonies were grown in LB overnight and DNA was isolated using the QIAprep midiprep kit (QIAGEN). Plasmids were then sequence-verified using a U6 promoter primer forward 5'-GCCTATTTCCCATGATTCCTTC–3'.

4.2.2 Cell lines transfection

Cells were transfected using lipofectamine 3000 manufacturer's protocol (Thermo Fisher Scientific, Waltham, MA). Cells were seeded one day before transfection and cultured in medium without antibiotics. GFP positive cells were collected and single-cell sorted 48-72 hours after transfection at the University of California (UCLA) Flow Cytometry core.

4.2.3 Genomic DNA isolation and PCR amplification of target regions

Genomic DNA was isolated for each clone (NucleoSpin Tissue XS, Macherey-Nagel, Düren, Germany) and after a 700 base pair (bp) region containing the sgRNA was amplified by PCR using the HotStarTaq Master Mix (QIAGEN). Forward and reverse primers were located 200 and 500 base pairs from the sgRNA respectively. PCR products were then purified using the QIAquick PCR purification kit protocol (QIAGEN) and then sent for Sanger sequencing at UCLA core facility.

4.2.4 CRISPR/Cas9 validation by TIDE analysis and western blot

Disruption was confirmed by Sanger sequencing with Tracking of Indels by Decomposition (51) (TIDE) web tool. TIDE works by aligning the wild-type (WT) gene sequence to CRISPRed sample sequences. The program predicts the expected WT sequence for insertions and deletions ranging from -10 to +10 and then computes the percentage of sample sequences that match with your expected WT sequence for each of the possible insertions and deletions. Finally protein knockout was confirmed with Western blot.

4.3 Cell-proliferation and growth-inhibition assays

Cell-proliferation and growth-inhibition assays were performed by real-time live cell imaging in an Incucyte ZOOM (Essen Biosciences, Ann Arbor, MI). Two thousand to five thousand cells were seeded in 96-wells plates and cultured at 37^{o} C. Twenty-four hours after plating, culture media were replaced with fresh media with or without 5000 IU/ml IFNα (Merck Millipore, Cat# IF007), 500 IU/ml IFNβ (Merck Millipore, Cat# IF014) and 100 ng/ml IFNγ (BD Pharmingen, Cat# 554616) in human melanoma cell lines and IFNα (Merck Millipore, Cat# IF009), IFNβ (Merck Millipore, Cat# IF011) and IFNγ (Peprotech, Cat# 315-05) in mouse cell lines at the same concentrations. IFN concentrations were defined after dose-dependent growth inhibition optimization processes for all three IFNs (18).

4.4 Surface flow cytometry analysis of PD-L1 and MHC Class I

Melanoma and murine cell lines were seeded into 6-well plates during day 1, targeting 70-80% of confluence on the day of surface staining. The following day, culture media were replaced with fresh media with or without IFNα 5000 IU/ml, β 500 IU/ml, or γ 100 ng/ml (same conditions as above) for 18 hours. During day 3, after incubation time, cells were trypsinized and incubated at 37°C for 2 hours with media containing the same concentrations of IFNα, β, or γ. Then media were removed by centrifugation and cells were resuspended with 100% FBS and stained with Allophycocyanin (APC) anti-PD-L1 and PE-Cy7 anti-HLA-ABC in human melanoma cell lines or PE anti-PD-L1 and APC anti-MHC I in mice cell lines, on ice for 20 minutes. To continue, cells were washed once with 3 ml PBS and resuspended in 300 µL of PBS. Dead cell

discriminator, 7-AAD, was added to samples prior to data acquisition by LSRII (Becton, Dickinson and Company). Data were analyzed using Flowjo software (version 10.0.8r1, Tree Star Inc., Ashland, OR). Experiments were performed at least twice for each cell line.

4.5 Functional coculture assays and IFNγ production by ELISA

Parental human M202 melanoma cell line and established *JAK1*, *JAK2* and *B2M* knockout sublines were HLA-A*0201^{+}MART1^{+} cell lines used to analyze recognition by T-cell receptor transgenic T cells with the use of *in vitro* coculture assays. Cells were cocultured with effector peripheral blood mononuclear cells PBMCs (untransduced and MART1 F5 specific TCR) at an effector/target ratio of 1:1, 2.5:1 and 10:1. Supernatants from six replicate wells for each condition were collected 24 hours post-coculturing and measured IFNγ release by ELISA (eBioscience, San Diego, CA).

Cytotoxicity assay were conducted by real-time live cell imaging in an IncuCyte ZOOM (Essen Biosciences, Ann Arbor, MI) and expressed as percentage of cells that were killed by effector cells over period of coculture. Cell lines were stably transfected with a nuclear localizing RFP (NucLight Red Lentivirus EF1a Reagent, Essen Biosciences) to facilitate cell counts. All experiments were performed in a minimum of three independent runs. Graph production and statistical data were analyzed via Prism software (Graphpad, La Jolla, CA).

4.6 RNA isolation and RNA-seq analysis of human melanoma cell lines

Melanoma cell lines were plated at 1.5-2.0 x 10^6 cells per 10 cm dish or 2x10^5 per 6-well plate well for IFNγ treatment. 24 hours after plating, culture media was replaced with fresh media with or without 100 ng/ml IFNγ (BD Pharmingen, Cat# 554616). Cells were harvested 6 hours after the start of IFNγ treatment, pellets were lysed in TRIzol reagent (Invitrogen, Cat# 15596018) and stored at -80°C before RNA extraction.

Total RNA was extracted using a protocol that combined the TRIzol method and the RNeasy mini kit (Qiagen Cat# 74104). Briefly, the aqueous phase containing RNA from the TRIzol extraction method was mixed with an equal amount of 70% Ethanol and loaded on an RNeasy mini column. The column was washed according to the kit manual and total RNA was eluted in 60 ul RNase free water. RNasin RNase inhibitor (Promega, Cat# N2511) was added to a final concentration of 2 U/ul. Total RNA was submitted for RNA-seq to the UCLA Technology Center for Genomics & Bioinformatics.

Single-end reads 50bp in length were mapped using HISAT2 (52) version 2.0.4 and aligned to the hg19 genome using default parameters. Reads were quantified using HTSeq (53) version 0.6.1 with the intersection-nonempty mode and counting ambiguous reads if fully overlapping. Raw counts were then normalized to fragments per kilobase of exon per million fragments mapped (FPKM) expression values. FPKM values were log2 transformed with an offset of 1, and normalized by gene for heatmap visualization. Change in gene expression was quantified by calculating the log2 fold change, comparing IFNγ treated to untreated cell lines. Genes were

annotated as processes and pathways using the MSigDB (54), Kyoto Encyclopedia of Genes and Genomes (KEGG (55)), and Reactome (56) gene sets. Heatmaps were created using the R statistical language (https://www.R-project.org) and the ggplot2 (57) package.

4.7 Western blots

Selected cell lines were maintained in 10 cm culture dishes and analyzed when 70-80% confluent. Western blot was performed as previously described (58). Primary antibodies included *JAK1, JAK2, B2M* and *GAPDH* (all were obtained from Cell Signaling Technology, Danvers, MA). Immuno-reactivity was analyzed with the ECL-Plus kit (Amersham Biosciences Co, Piscataway, NJ), using the ChemiDoc MP system (Bio-Rad Laboratories, Hercules, CA). Experiments were performed at least twice for each cell line.

4.8 Mice, cell lines and reagents

C57BL/6 mice were bred and kept under defined-flora pathogen-free conditions at the Association for the Assessment and Accreditation of Laboratory Animal Care approved animal facility of the Division of Experimental Radiation Oncology, University of California, Los Angeles (UCLA), and used under the UCLA Animal Research Committee protocol #2004-159-43I.

The MC38 cell line was originally generated at the NCI Surgery Branch (originally labeled as Colo38), and was obtained from Dr. Robert Prins (Department of Neurosurgery, UCLA). The

B16-F10 mouse melanoma cell lines were purchased from American Type Culture Collection (ATCC). The MC38 cell line, B16-F10 mouse melanoma cell line, and established knockout cell lines were cultured at 37° C with 5% CO_2 in DMEM medium (Invitrogen, Carlsbad, CA) supplemented with 10 % fetal bovine serum, 100 units/ml penicillin, 100 µg/ml streptomycin and 0.25 µg/ml amphotericin B. Cells were tested negative for mycoplasma with the MycoAlert Mycoplasma Detection Kit (Lonza) and periodically tested for authentication. For *in vivo* experiments, early-passage cell lines were used (less than ten passages).

Antibodies for *in vivo* experiments: anti-mouse-PD-1 (clone RMP1-14), anti-mouse CD8 (clone YTS 169.4, BE0117), anti-mouse CD4 (clone GK1.5, BE0003), anti-mouse NK1.1 (clone PK136, BE0036) and isotype control antibody (clone 2A3, BE0089), all from BioXCell (West Lebanon, NH). The CpG-C oligodeoxynucleotide SD-101 were obtained under a material transfer agreement (MTA) with Dynavax. SD-101 was synthesized and purified by standard techniques as previously described (59). Bempegaldesleukin (NKTR-214 (60)) was provided by Nektar Therapeutics. Both are diluted in the recommended product formulation buffer for *in vivo* studies.

4.9 Antitumor studies in mouse models

To establish subcutaneous tumors, $0.3x10^6$ of MC38 wild-type or established *JAK1, JAK2, B2M and IFNAR1* knockout cells per mouse were injected into the flanks of C57BL/6 mice. When tumors became palpable (day 5 or 6), four doses of 300 µg of anti–PD-1 or isotype control antibody were injected intraperitoneally (i.p.) every 3 days. Intratumoral treatment of SD-101

was used at 50 µg per injection. Bempegaldesleukin (NKTR-214) was used at 0.8 mg/kg every 9 days x 2 doses, intravenous (tail vein). For depletion studies, 300 µg of anti-CD8, 300 µg of anti-CD4, 300 µg of anti-NK1.1, or the combination were administered every 3 days starting the day before SD-101 or bempegaldesleukin until the end of the experiment. Splenocytes from control and depleted corresponding mice were taken to validate depletion efficacy. Tumors were followed from caliper measurements two or three times per week and tumor volume was calculated using the following formula: tumor volume= ((width)2 x length)/2. Mean and error standard of the tumor volumes per group was calculated.

4.10 Mass cytometry (CyTOF) analysis

MC38 wild-type or established *JAK1, JAK2* and *B2M* knockout tumor cells ($0.3x10^6$) were implanted into the flanks of C57BL/6 mice. On day 13 following inoculation, tumors were harvested from mice at pre-defined treatment. Tumors were digested using the tumor dissociation kit mouse (Miltenyi, Bergisch Gladbach, Germany). Spleens were dissociated and filtered with a 70-micrometer filter following digestion with the ACK lysis buffer (Lonza, Basel, Switzerland). Samples staining and data acquisition were performed as previously described (61) except that used 3% paraformaldehyde and samples were not barcoded. A full list of immune markers used was described in the **Table 5**.

Table 5. List of antibodies used for CyTOF

Tag	Target	Clone	Source
191/3 Ir	DNA-single cells	-	Fluidigm
Cisplatin	Dead cells	-	Fluidigm
89Y	CD45	30-F11	DVS
142Nd	CD11c	N418	DVS
143Nd	CD69	H1.2F3	DVS
146Nd	F4/80	BM8	DVS
148Nd	CD11b	M1/70	DVS
149Nd	CD62L (L-selectin)	MEL-14	Biolegend
150Nd	Ly6C	Hk1.4	DVS
151Eu	Ly6G	1A8	DVS
152Sm	CD3e	145-2C11	DVS
153Eu	CD274 PD-L1	10F.9G2	FDM
155Gd	CD25 (IL2R)	3C7	Biolegend
159Tb	CD279 PD1	29F.1A12	DVS
162Dy	CD366 (TIM3)	RMT3-23	DVS
166Er	CD19	6D5	DVS
167Er	CD335 (Nkp46)	29A1.4	DVS
168Er	CD8a	53-6.7	DVS
170Er	CD161 (NK1.1)	PK136	DVS
171Yb	CD44	IM7	DVS
172Yb	CD4	RM4-5	DVS
174Yb	I-A/I-E (MHC class II)	M5/114.15.2	DVS
175Lu	CD103	2E7	Biolegend
176Yb	CD45R_B220	RA3-6B2	DVS
	Intracellular		
115IN	Ki67	SolA15	ThermoScientific
141Pr	TNFα	MP6-XT22	DVS
147Sm	Eomes	Dan11mag	ThermoScientific
158Gd	FoxP3	FJK-16s	DVS
161Dy	T-bet	B56	DVS

Samples were analyzed using Fluidigm® Helios™ (San Francisco, CA) mass cytometry system at the UCLA Flow Cytometry core. Samples were manually gated for cells, singlets and double expression of the viable CD45 single-cell–positive population (**Figure 4**) using FlowJo software (version 10.4.2, Ashland, OR) and data files were analyzed using Cytofkit package (62) (R version 3.5.1). To identify and annotate each of the clusters obtained, cluster median data were normalized, and a threshold of >0.5 was used to define positive immune markers. T-distributed stochastic neighbor embedding plots were generated by Pheno-Graph clustering through cytofkiyShinyAPP from Cytofkit. We used FlowSom, an unsupervised automated algorithm which orders cells according to their phenotypic similarities. FlowSom clustered the T-CD8 cells into three branches and thus distinguished exhausted T-CD8 populations.

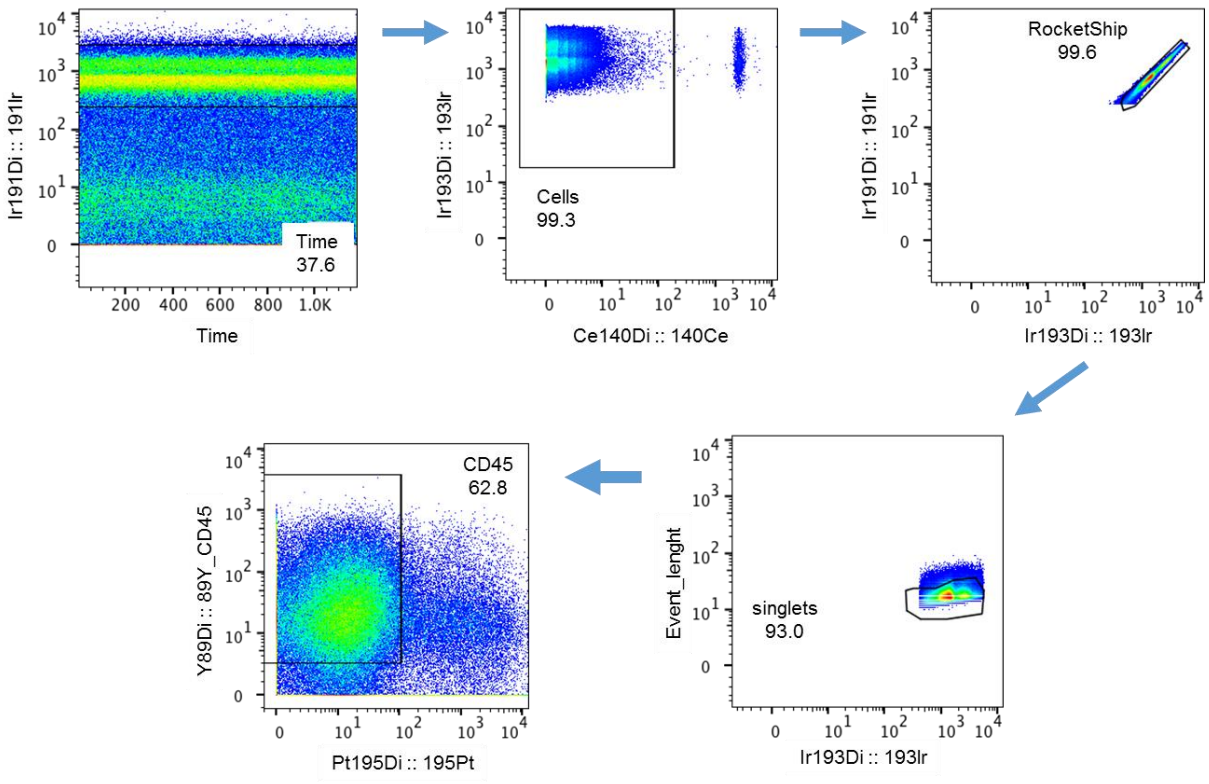

Figure 4. Analysis of tumor-infiltrating immune cells by CyTOF: Representative manual gating strategy for MC38 tumor-infiltrating CD45 cell subpopulation from mass cytometry data.

4.11 Metacyto analyses

MetaCyto was performed using the default workflow for both flow and mass cytometry (CyTOF) data as previously described (63). By combining and clustering the markers for all datasets, MetaCyto is able to identify and track specific immune cell populations present across heterogeneous studies. We merged cytometry data from seven studies according to the cell line phenotype in **Table 6**. We included the MetaCyto automated unsupervised clusters determined from the aggregated experiments and additionally supplied a list of pre-determined functional clusters as listed **Table 7** for the analysis. For each phenotype, we performed a regression analysis to estimate effect sizes and *P* values of the treatment relative to isotype in each immune cluster. Results were plotted via Prismv8 software (Graphpad, La Jolla, CA). MetaCyto is available as an R package on Bioconductor: (http://bioconductor.org/packages/release/bioc/html/MetaCyto.html).

4.12 Gene-expression assays

Total RNAs were extracted using the PureLink RNA Mini Kit (Invitrogen). CXCL9 and CXCL10 expression were measured by reverse transcription PCR following the manufacturer's protocol for the Power SYBR Green RNA-to-CT 1-Step Kit (Applied Biosystems) and using the following primers: CXCL9: 5′-CCCAATTGCAACAAAACTGA-3′ and 5′-AGTCCGGATCTAGGCAGGTT-3′ and CXCL10: 5′-AATCATCCCTGCGAGCCTAT-3′ and 5′-TTTTTGGCTAAACGCTTTCAT-3′.

Table 6. A summary of seven studies included in the meta-analysis.

Phenotype	Experiment name	Variables	n
Wild-type	CyTOF_ex_04122018 CyTOF_ex_05232018	Control vs a-PD-1 Control vs a-PD-1, Control vs SD-101, Control vs a-PD-1+SD-101, Control vs Bempegaldesleukin	6 21
***JAK1* KO**	CyTOF_ex_02282018 CyTOF_ex_Jul18 CyTOF_ex_10032018	Control vs a-PD-1 Control vs a-PD-1 Control vs a-PD-1, Control vs SD-101, Control vs a-PD-1+SD-101	4 6 18
***JAK2* KO**	CyTOF_ex_02282018 CyTOF_ex_Jul18 CyTOF_ex_03192019	Control vs a-PD-1 Control vs a-PD-1 Control vs a-PD-1, Control vs SD-101, Control vs a-PD-1+SD-101	6 6 22
***B2M* KO**	CyTOF_ex_04122018 CyTOF_ex_Jul18 CyTOF_ex_02122019	Control vs. a-PD-1 Control vs. a-PD-1 Control vs. a-PD-1 Control vs bempegaldesleukin, Control vs a-PD-1 +Bempegaldesleukin	6 6 14

Table 7. Cell definitions used to identify the 26 cell populations in the meta-analysis

Name	Cell Definitions
T_cells	CD3+CD11b-CD19-CD45R_B220-CD16-CD335-
B_cells	CD3-CD11b-CD19+CD45R_B220+
NK_cells (NKp46+)	CD3-CD11b-CD19-CD161-CD335+
NK_cells (NKRP1+)	CD3-CD11b-CD19-CD161+CD335-
naïve_CD4_T_cells	CD3+CD11b-CD19-CD45R_B220-CD16-CD335-CD4+CD62L+CD44-
naïve_CD8_T_cells	CD3+CD11b-CD19-CD45R_B220-CD16-CD335-CD8+CD62L+CD44-
Eff_CD4_Tcells	CD3+CD11b-CD19-CD45R_B220-CD16-CD335-CD4+CD62L-CD44-
Eff_CD8_Tcells	CD3+CD11b-CD19-CD45R_B220-CD16-CD335-CD8+CD62L-CD44-
Tregs	CD3+CD11b-CD19-CD45R_B220-CD16-CD335-CD4+CD25+FoxP3+

5. RESULTS

5.1 Understand how IFN-receptor pathway alterations and *B2M* mutations leading to resistance to PD-1 blockade

We started studying how IFNγ regulates PD-L1 expression by analyzing a panel of 48 human melanoma cell lines (**Figure 5**). Our findings documented that three cell lines (M364, M395 and M412b) that did not upregulate PD-L1 at all upon IFNγ exposure. Two of these cell lines (M364 and M395) harbored *JAK1/2* homozygous LoF mutations, similar to what we were seeing in patients who did not respond or became resistant to anti-PD-1 therapy (18,19).

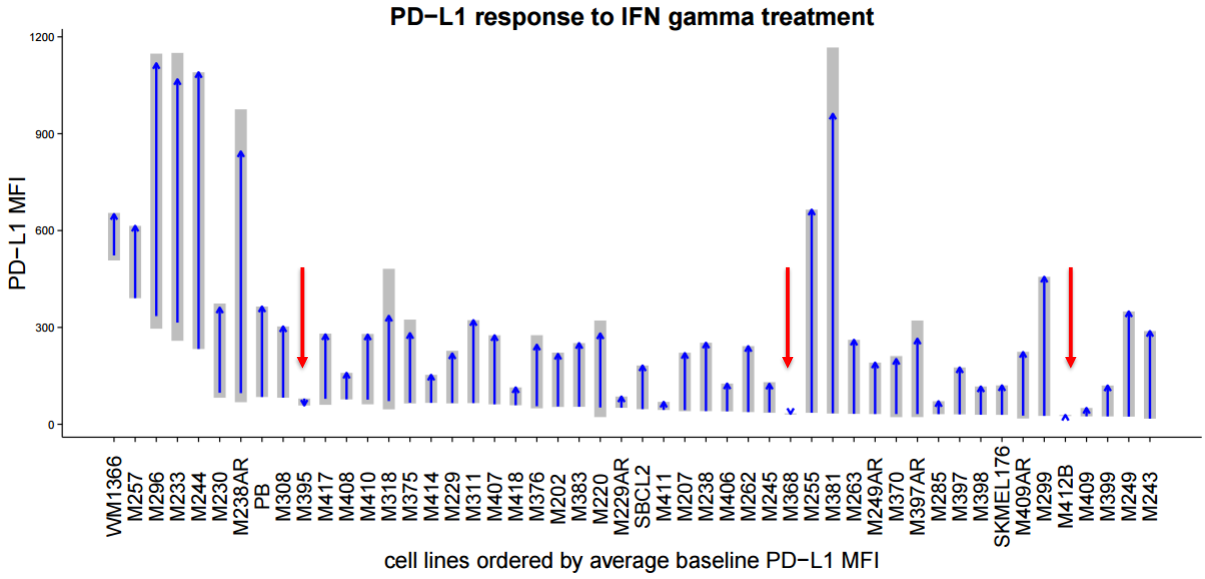

Figure 5. PD-L1 response to IFNγ by surface flow cytometry staining in 48 human melanoma cell lines. Blue arrows represent average change from baseline level of surface PD-L1 by mean fluorescence intensity (MFI) upon IFNγ exposure. Three cell lines did not respond at all to IFNγ (marked with red arrows). M395 has a *JAK1* mutation, M368 a *JAK2* mutation, but M412b has no IFNγ pathway mutations. Grey shades show the full range of measured values (n = 2 or 3). Figure was adapted with permission from Shin et al. Cancer Discovery 2017.

On the basis of this panel, we selected four representative melanoma cell lines to generate *JAK1* and *JAK2* CRISPR/Cas9 knockout sublines: M202 (MART1-positive), intermediate response to IFNγ; M233, good response; M407 (NY-ESO-1 positive), intermediate response, and the addition of M420 generated from a patient at baseline and upon acquired resistance (M464, with a *JAK2* LoF mutation) to anti-PD-1 therapy that we described in Zaretsky et al. (18).

5.1.1 Generating a panel of *JAK1, JAK2* and *B2M* knockout sublines in melanoma cell lines using CRISPR/Cas9 genome editing

We first generated and validated *JAK1* and *JAK2* knockout sublines in four human melanoma cell lines (M202, M233, M407 and M420), and *B2M* knockout sublines in two human melanoma cell lines (M202 and M233) using CRISPR/Cas9 gene editing. We designed a set of sgRNAs for each gene, targeting the first exons as out of frame insertions or deletions at the beginning of the sequence are more likely to generate non-functional proteins (**Tables 2-4**). Chromatograms were analyzed using the TIDE web tool, which aligns the WT gene sequence to CRISPRed sample sequences and predicts the expected WT sequence for indels ranging from -10 to +10 (see “Methods” section).

For each gene, one knockout clone was selected. Clones were suspected to DNA and protein analyses. First, genomic DNA was isolated, sequenced, and then interrogated by TIDE. Only those clones which did not present any WT form by TIDE were kept for protein analyses. Selected clones were completely WT deficient by TIDE and the protein expression was completely lost by Western blot (**Figure 6**).

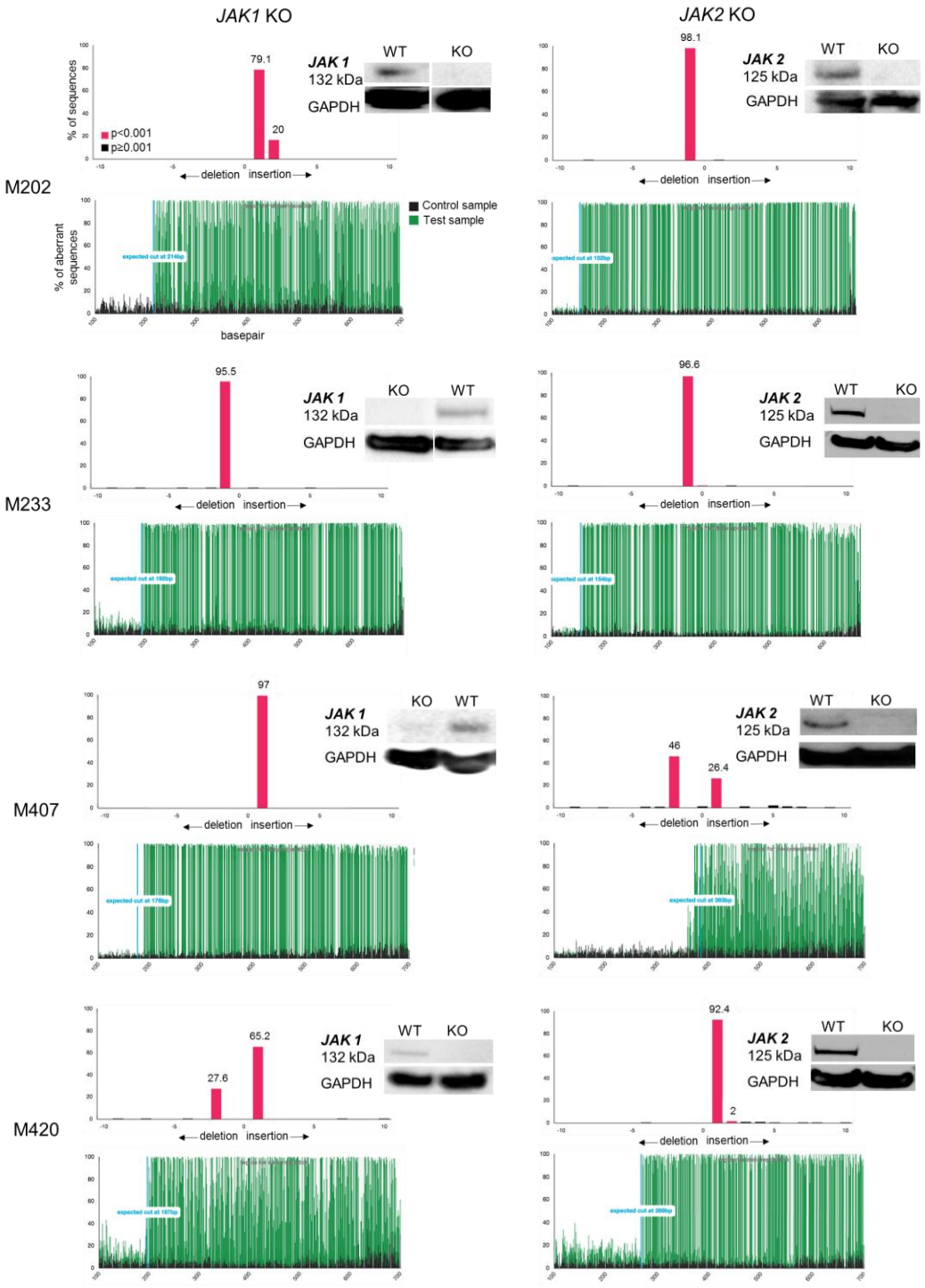

Figure 6. Validation of the generation of *JAK1* and *JAK2* KO from M202, M233, M407 and M420 melanoma cell lines. Clone's TIDE analysis histogram and quality control showing the percentage of each insertion and deletion ranging from -10 to +10, being 0 the WT form. Western blot analysis in the right, protein expression is completely lost in the KO selected clones.

5.1.2 *JAK1/2* knockouts in human melanoma cells results in insensitivity to IFNγ

We characterized the biology of *JAK1/2* knockout cells in terms of response to IFNα, β and γ stimulation. M233, M407, and M420 melanoma cell lines showed growth inhibition in response to direct *in vitro* treatment with IFNα, β or γ , ($P < 0.0001$, IFNγ compared with baseline) whereas M202 was mostly resistant with only a small amount of growth inhibition with IFNβ. All *JAK1* knockout sublines were insensitive to all three IFNs (P = ns, IFNs compared with baseline), which is in line with the role that *JAK1* plays in signaling downstream of both type I and II IFN receptors (64). As expected, since *JAK2* is only involved in type II IFN signaling, *JAK2* knockout sublines were insensitive to IFNγ but remained sensitive to IFNα and β (P = ns, IFNγ vs. baseline; $P < 0.0001$, IFNα and IFNβ compared with baseline in M233, M407, and M420; and $P < 0.05$, IFNα compared with baseline in M202) (**Figure 7**).

We also evaluated the surface expression of PD-L1 and MHC class I after exposure to IFNs. In all *JAK1* knockout sublines, PD-L1 and MHC class I surface expression did not increase after exposure to the three IFNs, while the *JAK2* knockout sublines did not respond to IFNγ but still responded to IFNα and -β (**Figure 8**). In contrast, B2M knockout in the M233 cell line did not affect the sensitivity to any of the three IFNs on cell growth inhibition ($P < 0.0001$, IFNγ compared with baseline) and B2M knockout in the M202 was mostly resistant with only a small amount of growth inhibition with IFNβ but upregulate the PD-L1 surface expression comparable to the wild-type, but instead led to the loss of surface expression of MHC class I (**Figure 9**).

Therefore, *JAK1* knockout cell lines lose the ability to respond to type I and II IFNs, *JAK2* knockout cell lines lose the ability to respond to type II IFN, and *B2M* knockout cell lines continue to respond to all three IFNs and lose expression of MHC class I.

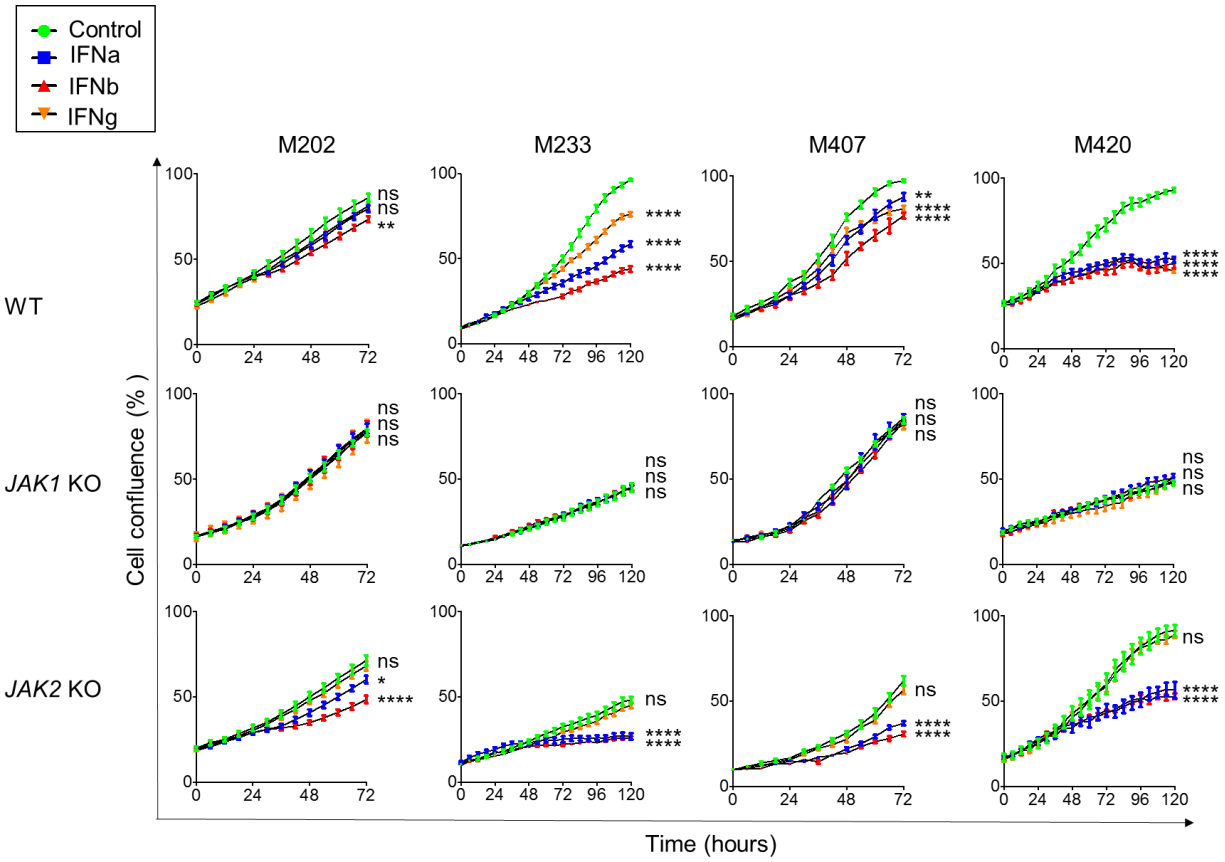

Figure 7. Growth inhibition in response to direct *in vitro* treatment with IFNα, IFNβ, or IFNγ. Growth curves represent the percent in the confluence of cells (y-axis) over time (x-axis), treated with IFNα, IFNβ or IFNγ (fill color) as measured by IncuCyte continuous live-cell imaging. Error bars reflecting the SEM across six replicates of each cell line and treatment combination. ns, not significant; *, $P < 0.05$; **, $P < 0.01$; ****, $P < 0.0001$ for the percent in growth with the treatment shown at the 72-hour (in M202 and M407) or 120-hour (in M233 and M420) endpoint as compared with the untreated control, with Dunnett multiple comparisons test. One representative experiment of three independently conducted experiments is shown.

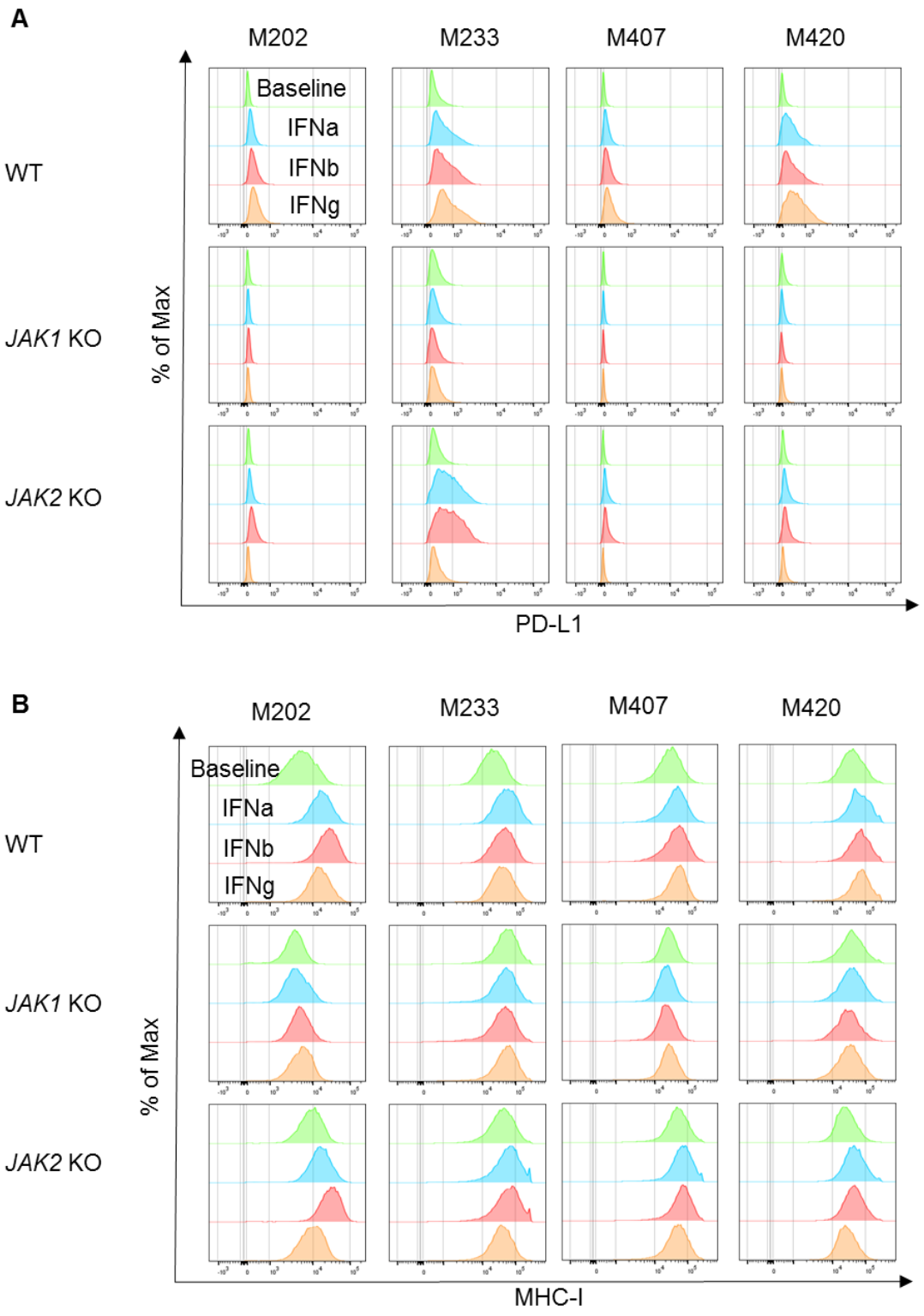

Figure 8. Flow cytometry analysis of **(A)** PD-L1 and **(B)** MHC class I surface expression upon IFNα, IFNβ, or IFNγ stimulation in the panel of M202, M233, M407 and M420 parental and generated *JAK1/2* KO human melanoma cell lines. Histograms represent changes in MFI by flow cytometry.

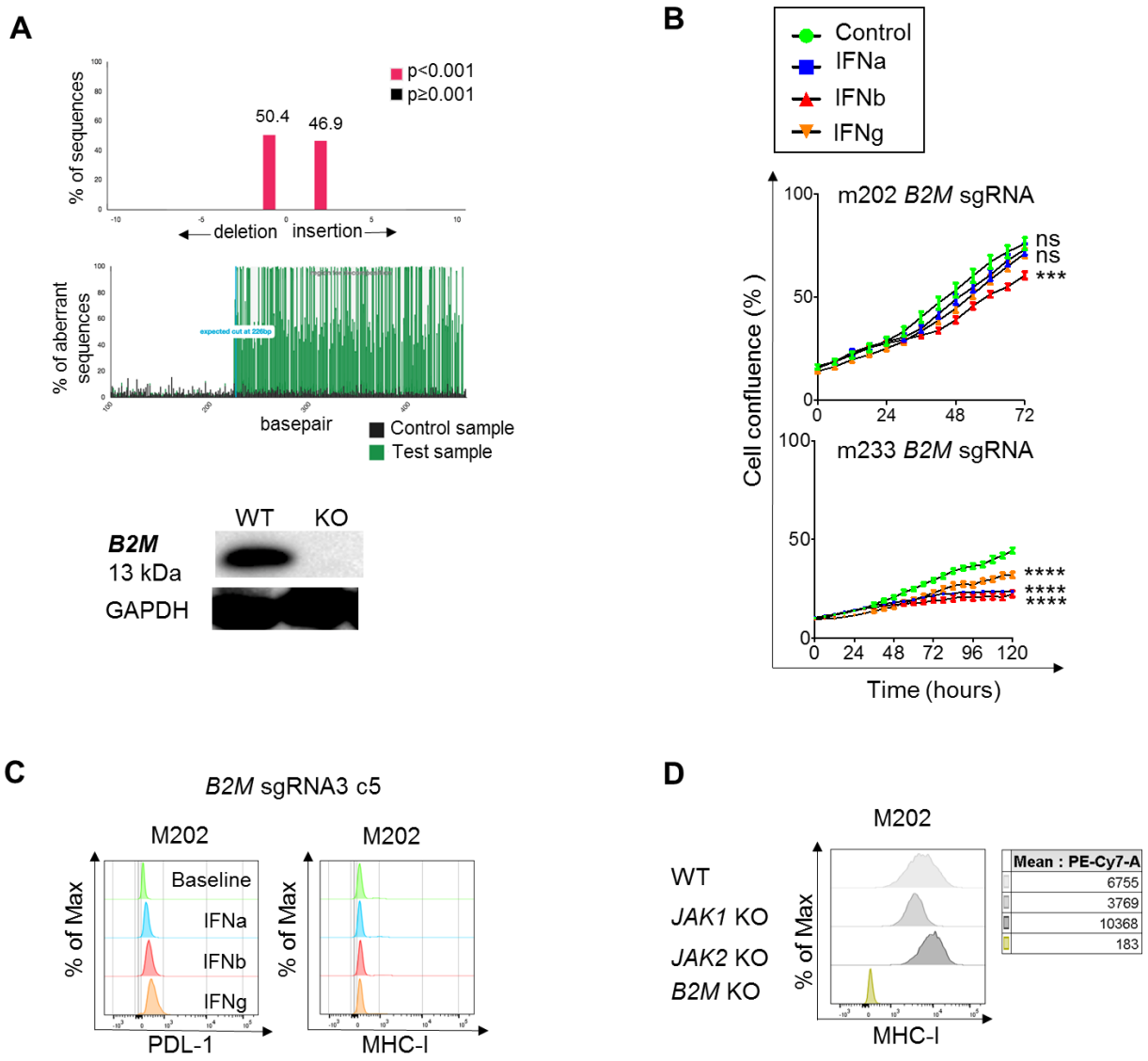

Figure 9. Functional effects of *B2M* KO mutations in human melanoma cell lines. (A) Validation of the generation of *B2M* KO from M202 sgRNA3 clone 5. TIDE analysis histogram and quality control showing the percentage of each insertion and deletion and WB analysis at the bottom. **(B)** Growth inhibition in response to direct *in vitro* treatment with IFNα, -β, or -γ in M202 and M233 *B2M* KO tumor. Error bars reflecting the standard error of the mean across six replicates of each cell line and treatment combination. ns, not significant; ***$P < 0.001$, ****$P < 0.0001$ for the percent in growth with the treatment shown at the 72 or 120-hour end point as compared with the untreated control, with Dunnett's multiple-comparison correction. **(C)** The measure of PD-L1 and MHC class I expression by flow cytometry after IFNs stimulation in M202 *B2M* KO tumor. **(D)** Basal expression of MHC class I by flow cytometry in *B2M* KO in comparison with other *JAK1/2* KO tumors. In (C) and (D): Histograms represent changes in MFI by flow cytometry.

5.1.3 *B2M* knockout results in lack of antigen presentation to T cells

In order to assess the impact of *JAK1/2* and *B2M* knockout mutations in the ability of T cells to recognize and attack tumor cells, we used HLA-A*02:01 MART1-positive M202 melanoma cells and set up a coculture using human T cells that were retrovirally transduced to express the F5 transgenic T-cell receptor (TCR) specific for MART1 (65,66). Cells were cocultured at an effector/target ratio of 1:1, 2.5:1 and 10:1.

MART1 TCR transgenic T cells had strong *in vitro* antitumor cytotoxicity against both M202 *JAK1* single-guide RNA (sgRNA) 2 clone 6 and *JAK2* sgRNA1 clone 41 knockout MART1-positive melanoma cells comparable to the parental cells (effector/target 10:1; 77% compared with 75% and 77% cytotoxicity, respectively; $P = 0.9$, Dunnett multiple comparisons test), with intact IFNγ production by these T cells in coculture experiments **(Figure 10).** This observation was consistent across different clones of the *JAK1* (sgRNA1 clone 4, sgRNA2 clone 1 and sgRNA2 clone 4) and *JAK2* (sgRNA1 clone 7, sgRNA1 clone 15 and sgRNA1 clone 24) knockout cell lines with similar ability to be recognized and killed by antigen-specific T cells **(Figure 11 and 12).** On the other hand, M202 *B2M* sgRNA 3 clone 5 knockout MART1-positive melanoma cells were not recognized by MART1 TCR transgenic T cells (effector/target 10:1; *B2M* knockout 0% vs. parental 77% cytotoxicity; $P < 0.0001$), exemplified by the lack of IFNγ production and cell killing when cocultured **(Figure 10).**

Taken together, *JAK1/2* knockout cell lines have intact T-cell cytotoxicity likely due to sufficient baseline levels of MHC class I expression allowing T-cell recognition. However, both T-cell recognition and cytotoxicity are lost when *B2M* was knocked out.

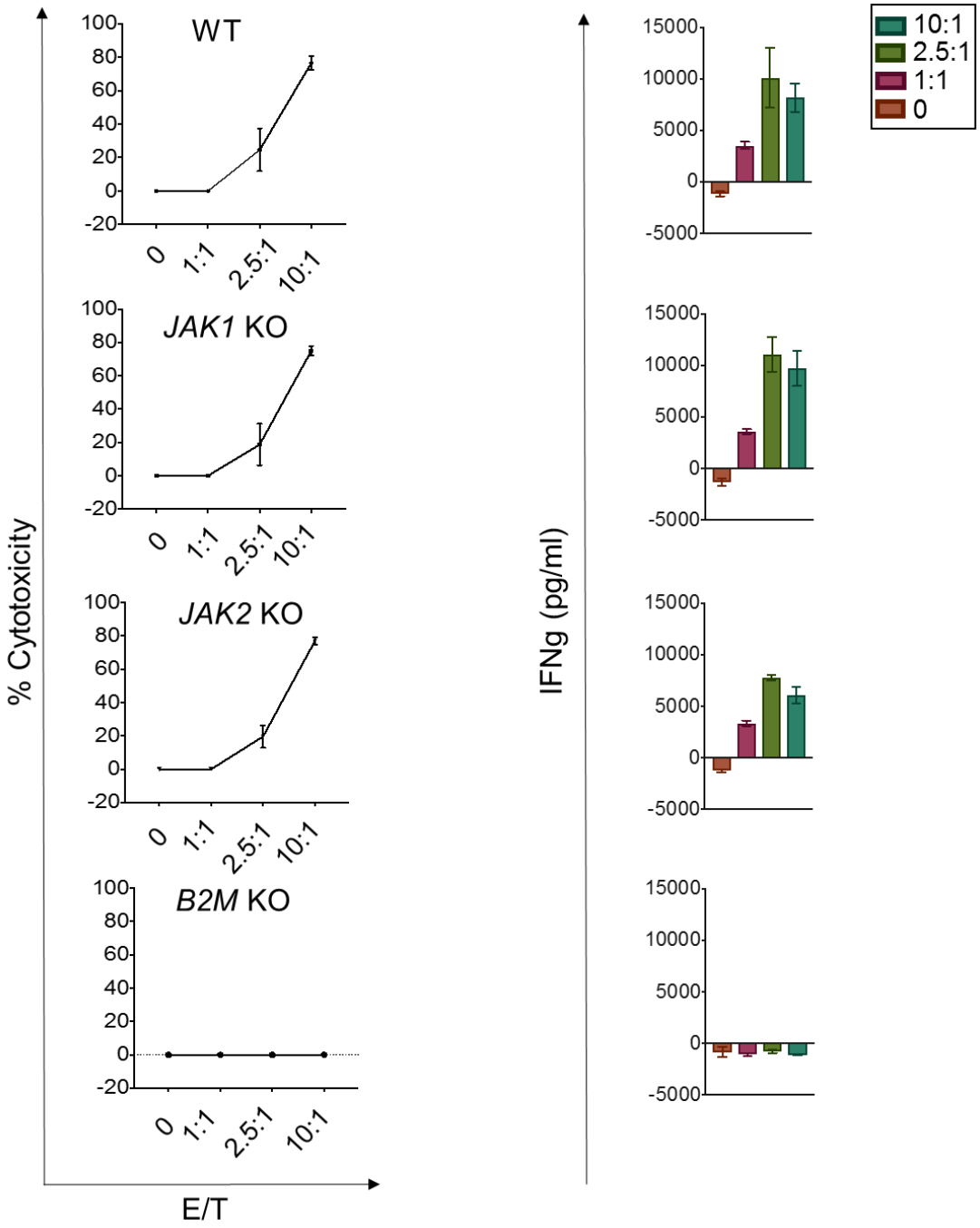

Figure 10. Coculture of HLA-A*02:01 MART1-positive M202 melanoma cells by MART1 TCR transgenic T cells. Target cancer cells were stably transfected with a nuclear localizing red fluorescent protein (NucLight Red Lentivirus EF1a Reagent, Essen Biosciences) and cocultured with MART1-specific TCR-engineered T cells. The percent of cytotoxicity (y-axis) was measured after 24 hours of coculture at an effector:target (E:T) ratio between 1:1 and 10:1 (x-axis) and the IFNγ production (y-axis) after 24 hours of *in vitro* coculture at different E:T ratios. WT, wild-type.

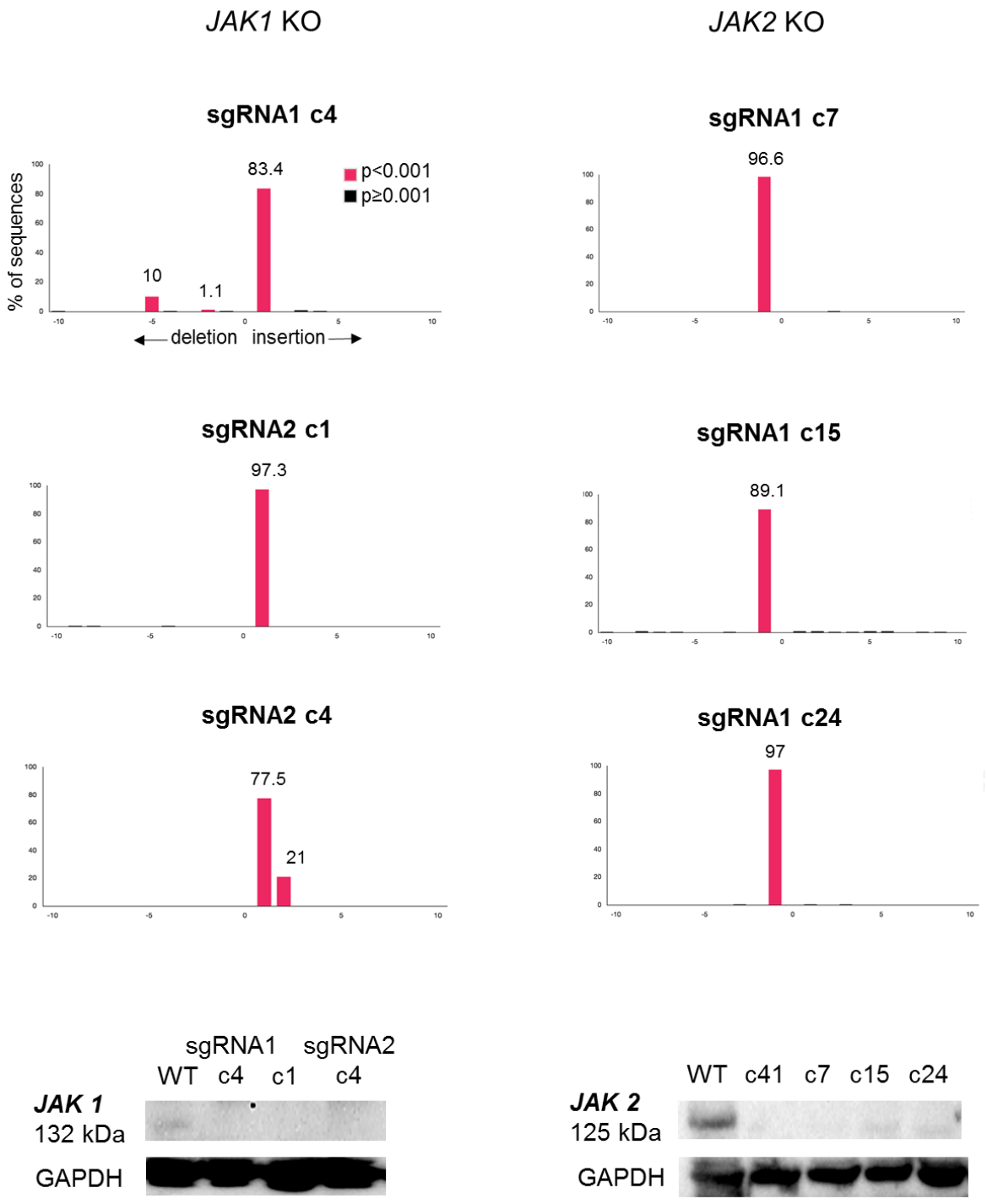

Figure 11. Validation of the generation of *JAK1* and *JAK2* knockouts from M202 melanoma cell lines. Clone's TIDE analysis histogram showing the percentage of each insertion and deletion ranging from -10 to +10, being 0 the WT form. Western blot analysis at the bottom, protein expression is completely lost in the knockout selected clones.

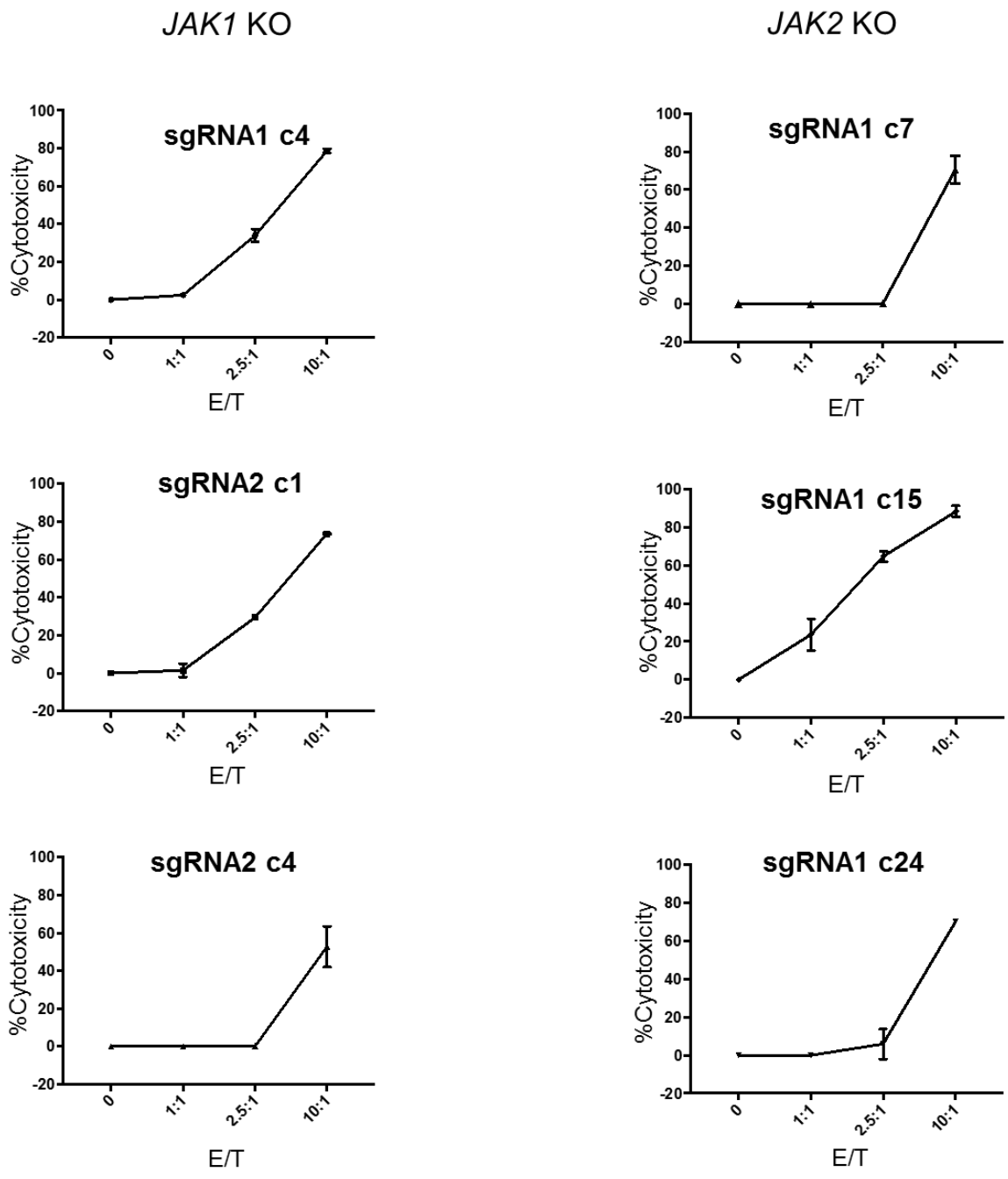

Figure 12. Coculture of HLA-A*02:01 MART1-positive M202 *JAK1/2* knockouts melanoma cells by MART1 TCR transgenic T cells. *In vitro* cytotoxicity assay: Target tumors were stably transfected with a nuclear localizing RFP (NucLight Red Lentivirus EF1a Reagent, Essen Biosciences) and cocultured with MART1 specific TCR engineered T cells. The percent of cytotoxicity (y-axis) was measured after 24 hours of coculture at E:T ratio between 1:1 and 10:1 (x-axis).

5.1.4 Downstream signaling alterations in human cell lines exposed to IFNγ

In order to investigate the change of response to IFNγ exposure, we cultured the four cell lines with and without *JAK1/2* or *B2M* knockout mutations with IFNγ. We harvested RNA at 6 hours after IFNγ stimulation for genome-wide transcriptome comparison to baseline by RNA sequencing (RNA-seq). We then filtered for gene sets involved in immune response and IFNγ signaling and obtained a total of 61 genes that had greater than a 2-fold change difference in expression in all parental cell lines upon IFNγ treatment. These genes were also upregulated in *B2M* knockout sublines upon IFNγ exposure, but not in sublines with *JAK1/2* knockout **(Figure 13).**

Overall, wild-type cell lines generally increased gene expression involved in APM (such as *B2M, HLA-A, HLA-B, HLA-C, HLA-F HLA-G, HLA-DRB1, HLA-DRB5, CIITA, TAP1, TAP2, PSMB8, PSMB9* and *PSMB10*), IFNγ signaling (such as *JAK1, JAK2, SOCS1, SOCS3, STAT1, STAT2, IRF1, IRF2, IRF7* and *IRF9*) and chemokines (*CXCL9* and *CXCL10*). These changes were also observed in *B2M* knockout sublines. However, the ability to upregulate these genes by IFNγ was lost in both *JAK1/2* knockout sublines **(Figure 14).**

In summary, human melanoma cell lines with *JAK1/2* knockout mutations do not respond to IFNs, as determined by upregulation of corresponding IFN-response target genes as well as surface expression of PD-L1 and MHC class I, but they can still be recognized by antigen-specific T cells leading to specific cytotoxicity provided they have constitutive baseline MHC class I expression. On the contrary, human melanoma cell lines with *B2M* knockout mutations respond to IFNs with expression of corresponding IFN-response genes, but they are not recognized by antigen-specific T cells due to lack of surface MHC class I expression, and therefore are resistant to specific cytotoxicity.

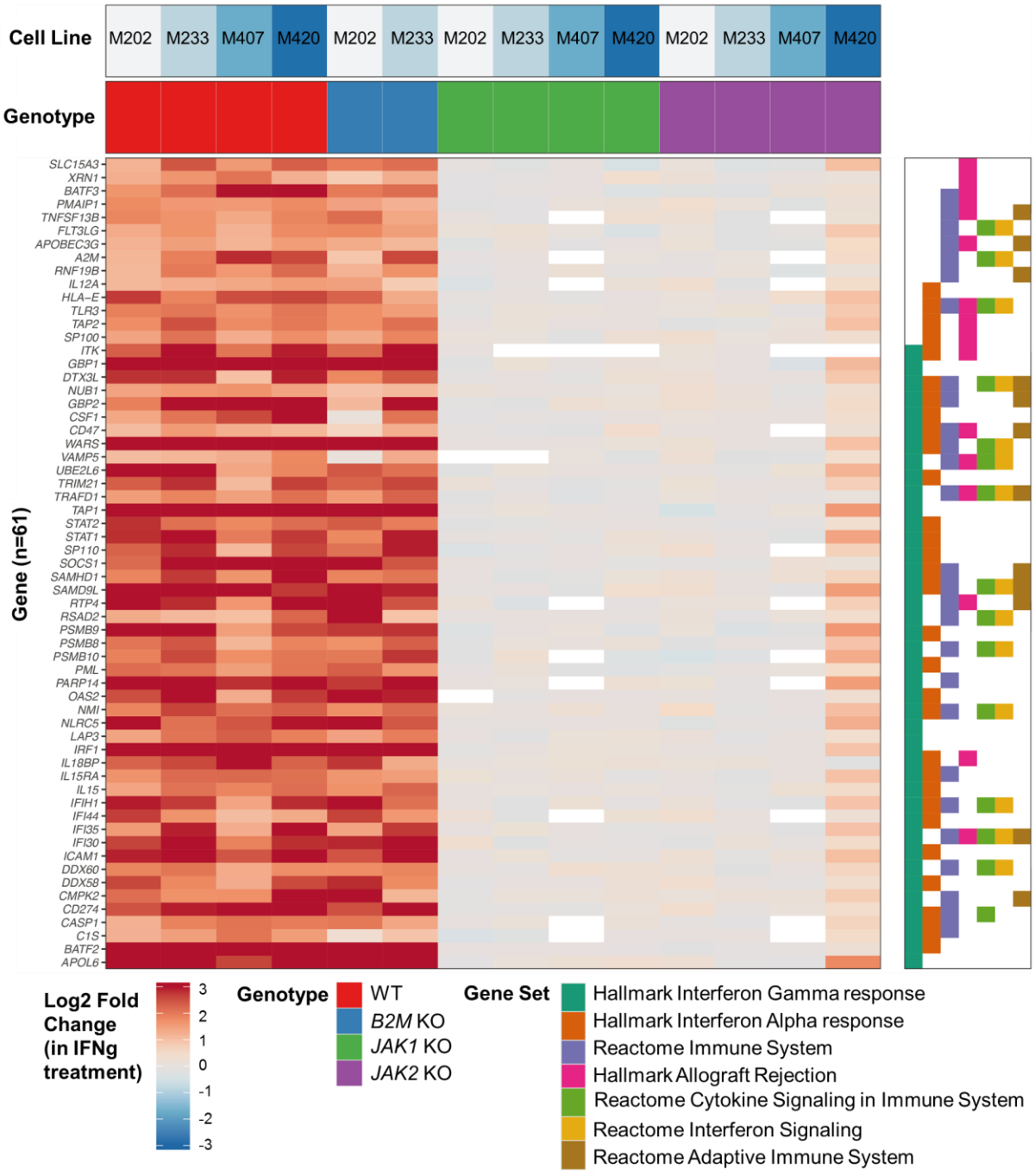

Figure 13. Altered IFNγ-induced gene transcription in *JAK1/2*-KO melanoma cell lines. Heat map displaying the change in gene expression due to IFNγ treatment. Genes were filtered to those that had at least 2-fold change in expression in all four groups of melanoma cell lines: M202, M233, M407, and M420. Associated cell line (top row) and genotype (second row) are indicated. Hallmark, Kyoto Encyclopedia of Genes and Genomes, and Reactome gene sets were filtered to those with at least 10 genes differentially expressed (right plot). Genes were sorted by the most highly enriched pathways.

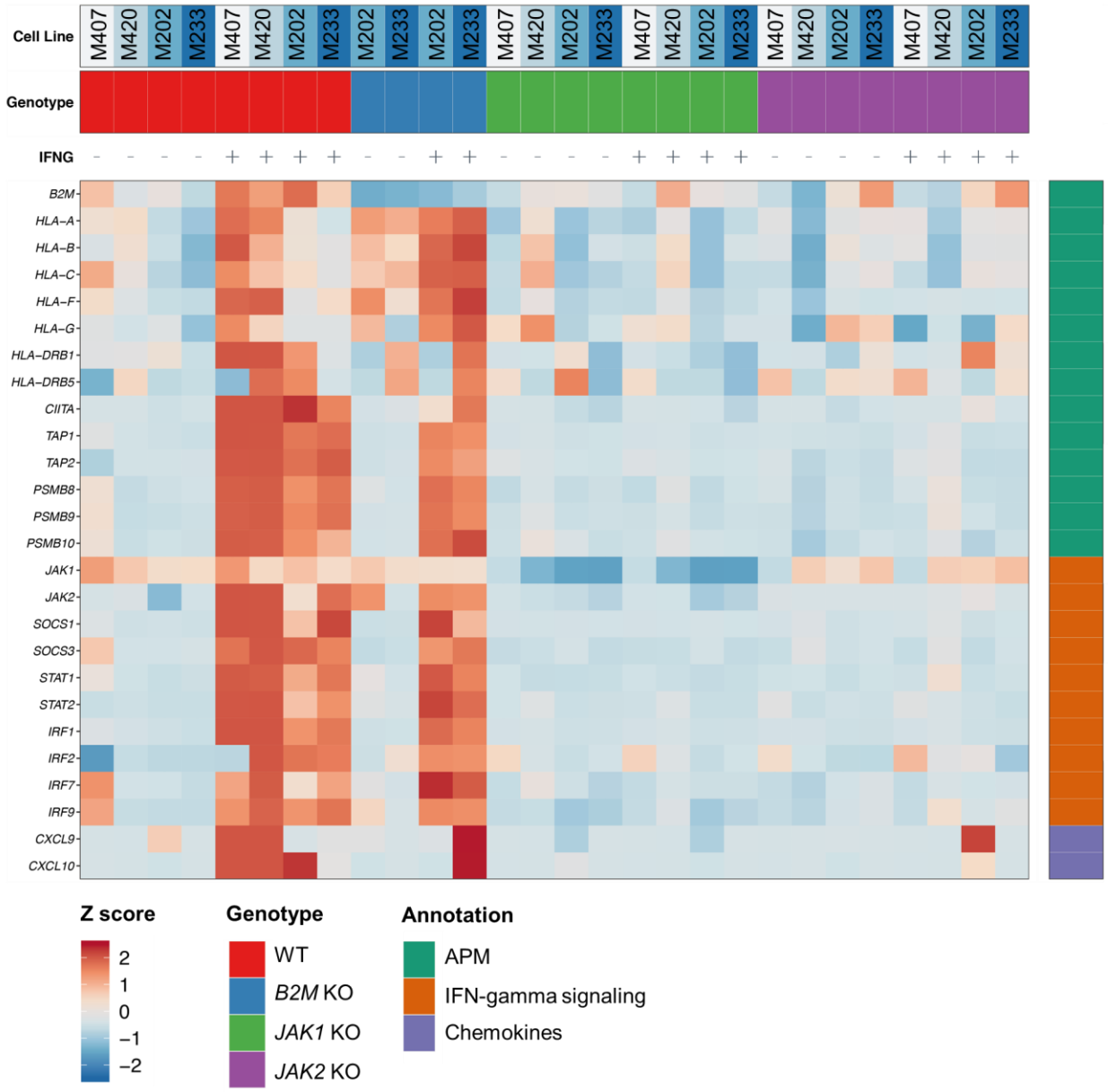

Figure 14. The IFNγ-induced increased expression of APM, IFNγ signaling and chemokines is lost with *JAK1/2* KO mutations. Gene expression heatmap from 28 cell lines (x-axis), including the four groups of melanoma cell lines: M407, M420, M202 and M233 illustrating changes from before/after IFNγ exposure. Associated cell line (top row panel), genotype (second row panel), and IFNγ treatment (before [-], after [+]) are indicated. Gene expression is depicted as the Z score of gene expression (in FPKM) across all samples. Genes (y axis) are ordered by those associated with APM, IFNγ signaling response, and chemokines, indicated by 'Annotation'.

5.2 Modeling resistance to PD-1 blockade in MC38 murine carcinoma model

5.2.1 CRISPR/Cas9-knockout (KO) tumors of *JAK1/2* and *B2M* result in resistance to anti–PD-1 in the MC38 model

There are very few syngeneic animal models that respond to PD-1 blockade. The murine colon adenocarcinoma MC38 has been previously shown to partially respond to PD-1 blockade therapy (48,49,61). It is a carcinogen-induced cell line with high mutational burden which shows an increase in CD8+ T cell infiltration after PD-1 blockade, and therefore it recapitulates highly mutated human cancers that respond to this therapy.

To generate a mouse model of anti-PD-1 resistance, we created *JAK1* (**Figure 15**)*, JAK2* (**Figure 16**) and *B2M* (**Figure 17**) knockout sublines of MC38 using CRISPR/Cas9 gene editing. All established sublines were validated by TIDE analysis and western blot (see “Methods” section).

Once multiple KO clones were selected and validated for each gene, we evaluated the *in vitro* cellular growth of these clones, as well as the basal surface expression of PD-L1 and MHC class I, in order to select only the sublines that behaved similarly to the parental cell line. All three established KO sublines (*JAK1* sgRNA1 c5, *JAK2* sgRNA2 c3 and *B2M* sgRNA2 c6) had similar proliferation rates *in vitro* and *in vivo* growth curves compared to that of the parental cell lines (**Figure 18**), and were used for subsequent in vivo studies.

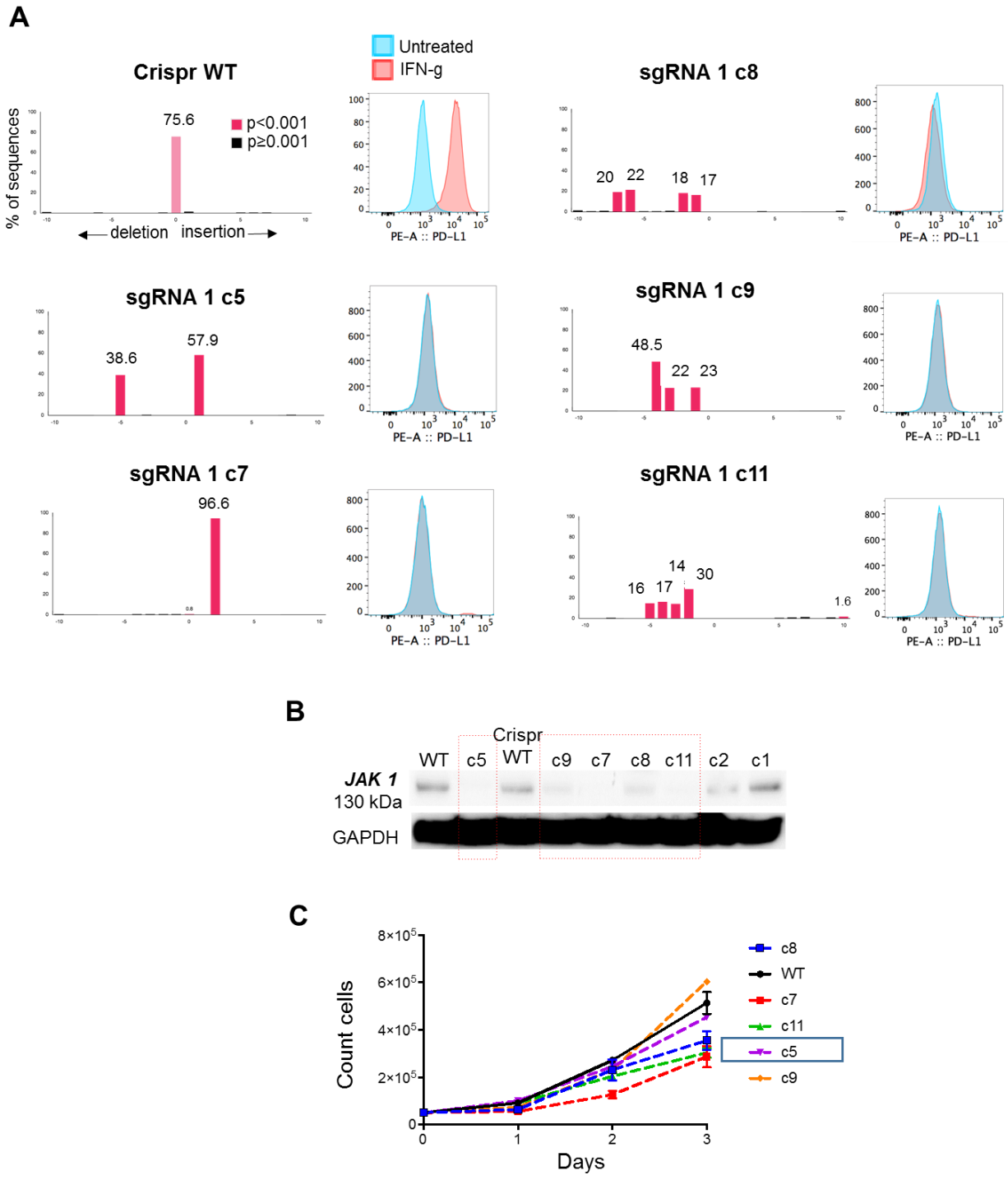

Figure 15. Validation of the generation of *JAK1* KO sublines from MC38 cell line. (A) TIDE analysis histogram showing the percentage of each insertion and deletion ranging from -10 to +10 and PD-L1 expression by flow cytometry after IFNγ stimulation **(B)** Western blot validation and **(C)** *In vitro* growth curves in selected *JAK1* established KO sublines from MC38 cell line.

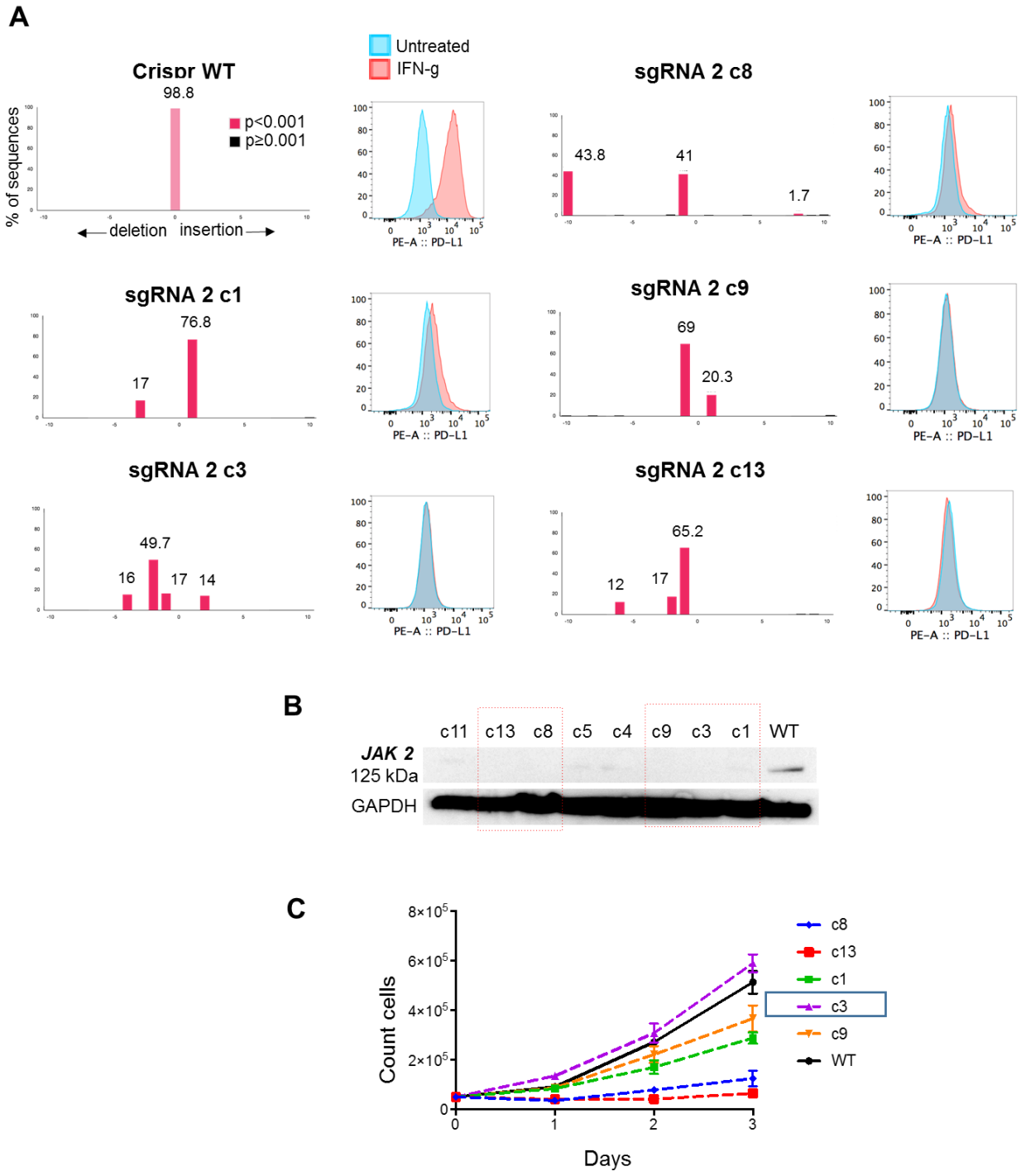

Figure 16. Validation of the generation of *JAK2* KO sublines from MC38 cell line. (A) TIDE analysis histogram showing the percentage of each insertion and deletion ranging from -10 to +10 and PD-L1 expression by flow cytometry after IFNγ stimulation **(B)** Western blot validation and **(C)** *In vitro* growth curves in selected *JAK2* established KO sublines from MC38 cell line

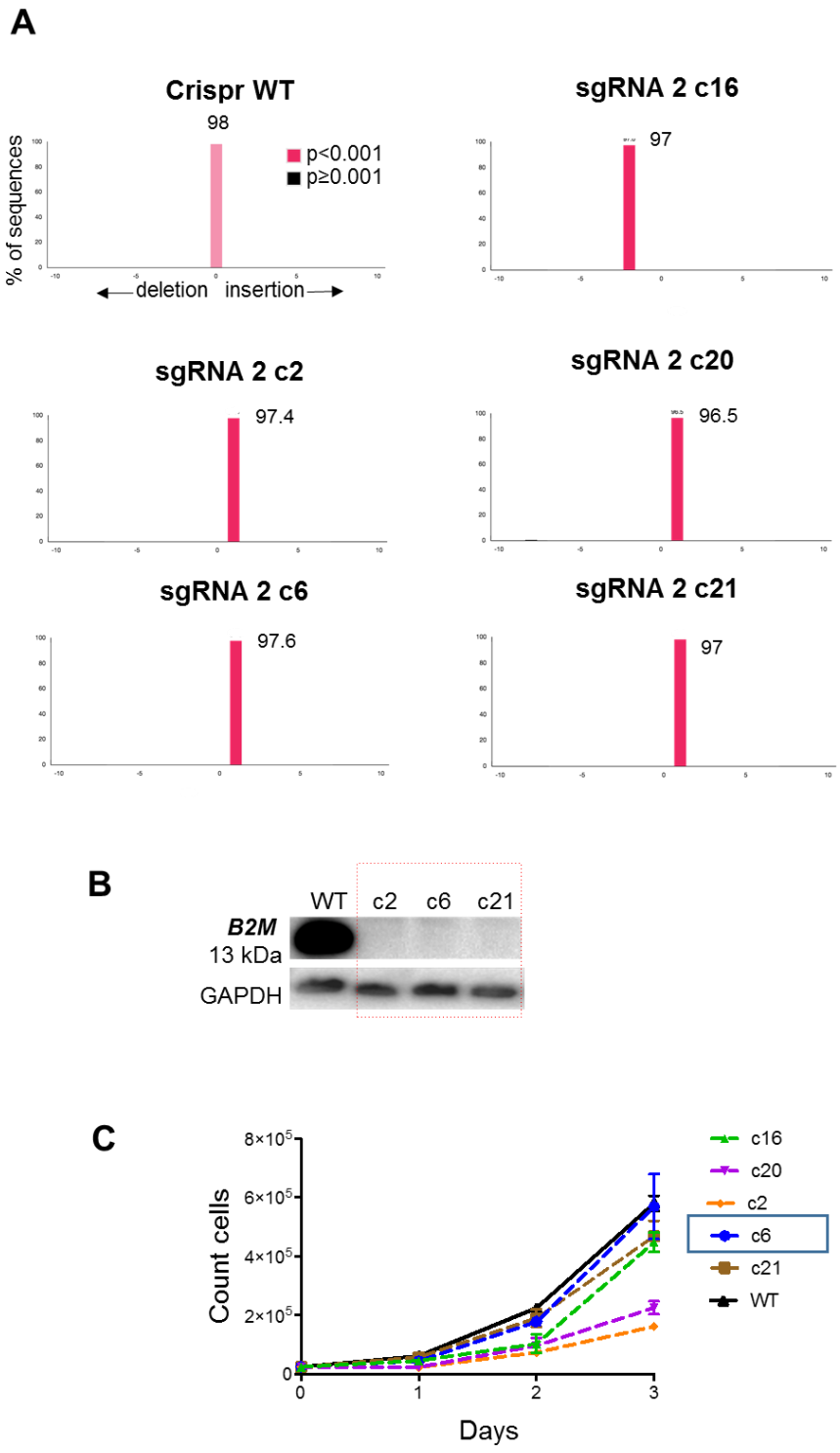

Figure 17. Validation of the generation of *B2M* KO sublines from MC38 cell line. (A) TIDE analysis histogram showing the percentage of each insertion and deletion ranging from -10 to +10 and PD-L1 expression by flow cytometry after IFNγ stimulation **(B)** Western blot validation and **(C)** *In vitro* growth curves in selected *B2M* established KO sublines from MC38 cell line.

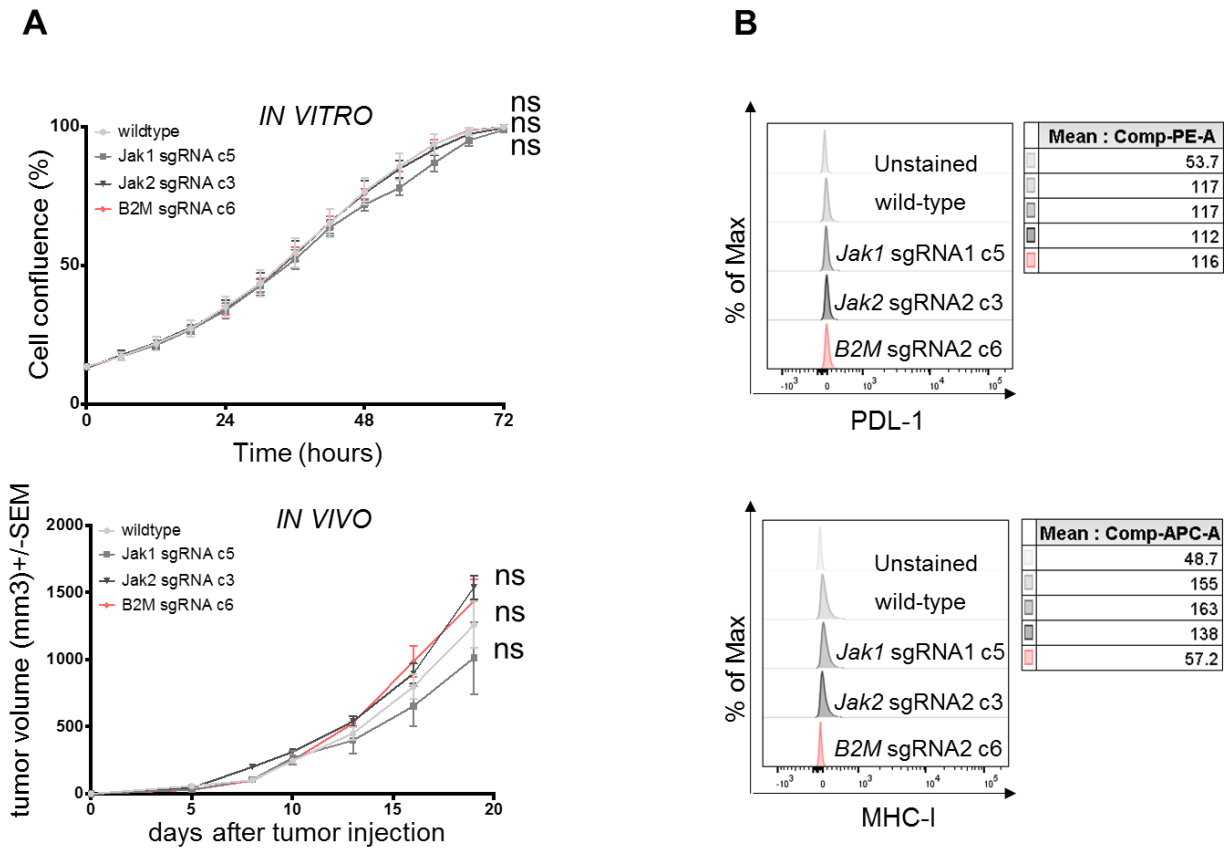

Figure 18. Selection of Knockout Clones in MC38 model. (A) *In vitro* and *in vivo* growth curves in *JAK1*, *JAK2* and *B2M* knockout comparing to wild-type. Growth curves represent the percent in the confluence of cells (y-axis) over time (x-axis) as measured by IncuCyte continuous live-cell imaging. Error bars reflecting the standard error of the mean across six replicates of each subline. ns, not significant for the percent in growth at the 72-hour endpoint as compared with the wild-type group, with Dunnett's multiple-comparison test. *In vivo* growth curves of these cell lines with 5 mice in each group (mean ± SEM) treated with Isotype control. ns, not significant was determined by unpaired t test on day 19, *JAK1/2* and *B2M* KO versus wild-type. **(B)** Basal expression by flow cytometry in MC38 wild-type cell line and *JAK1/2* and *B2M* knockout selected tumors. Histograms represent changes in MFI by flow cytometry compared to baseline.

5.2.2 Functional effects of *JAK1/2* and *B2M* KO mutations in MC38 murine carcinoma

We found that the functional effects of IFNs exposure in terms of growth inhibition, PD-L1 and MHC class I surface expression were broadly comparable with those of the human cell lines with the corresponding knockout genes. MC38 *JAK1* knockout was insensitive to all three IFNs and MC38 *JAK2* knockout was insensitive to only IFNγ (**Figure 19**).

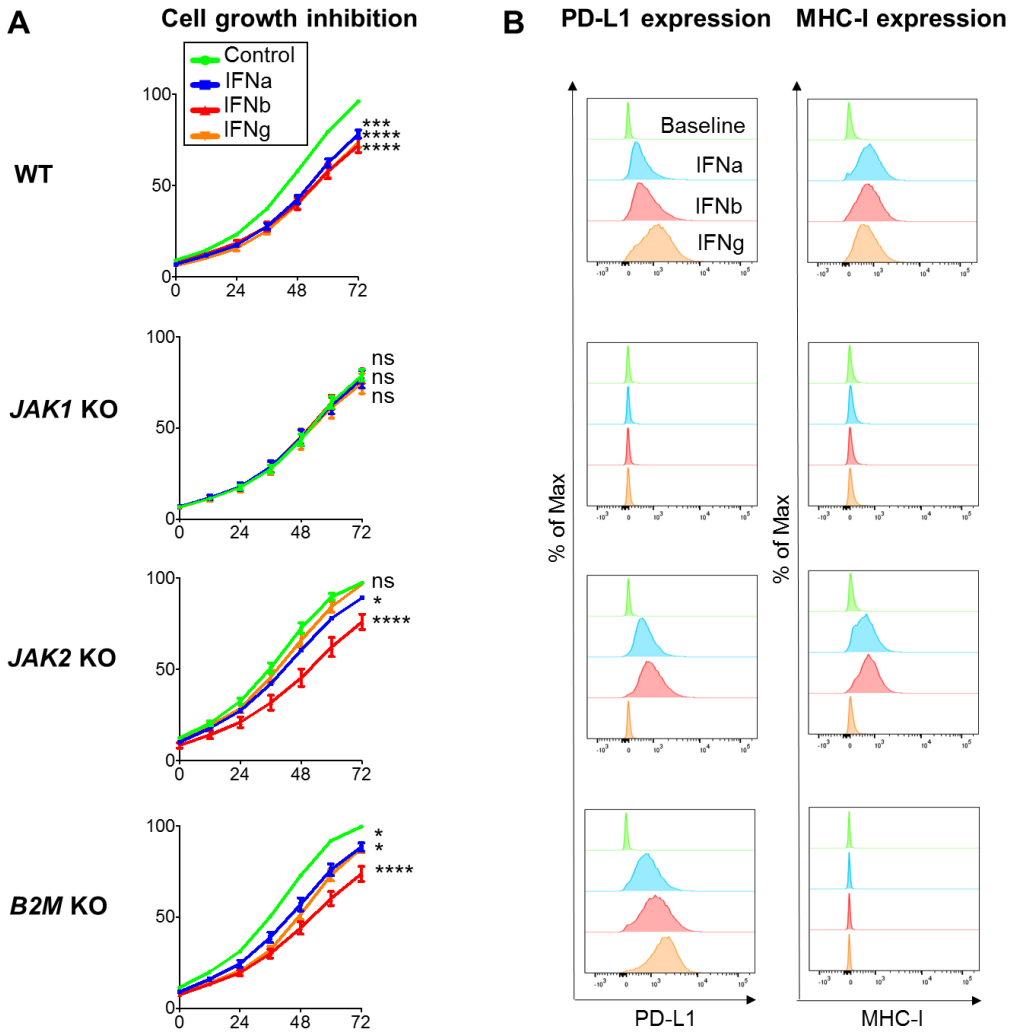

Figure 19. Functional effects of MC38 *JAK1/2* and *B2M* KO tumors. **(A)** Growth inhibition in response to direct *in vitro* treatment with IFNs in MC38 WT and KO cell lines. **(B)** The measure of PD-L1 and MHC class I surface expression by flow cytometry after IFN stimulation. Histograms represent changes in MFI by flow cytometry compared with baseline.

5.2.3 Modeling resistance to PD-1 blockade in MC38 murine carcinoma

To model *in vivo* resistance to PD-1 blockade, we injected MC38 wild-type or genetically modified MC38 sublines subcutaneously in the lower flank of the mice. When tumors became palpable (at day 5), mice received the first out of four injections of anti-PD-1 therapy or isotype control. MC38 wild-type tumors in C57BL/6 mice responded to anti-PD1 therapy, with a statistically significant difference in growth inhibition when compared with tumors treated with isotype control (**Figure 20**, $P < 0.01$, unpaired *t* test, $n = 5$, mean ± SEM). In three replicate studies we demonstrated that MC38 *JAK1*, *JAK2* and *B2M* knockout mutations result in the complete abrogation of the benefit of anti-PD-1 therapy (**Figure 20**, *P* = ns, unpaired *t* test, mean ± SEM), as has been shown in patient biopsy-based studies (18–23,25,33) and prior mouse models of *B2M* knockout (25).

We confirmed our results based on other established clones generated in each condition to reduce the possibility of selection bias or off-target effects, which in our experience are rare but need to be ruled out. These three established KO tumor sublines (*JAK1* sgRNA1 c9, *JAK2* sgRNA2 c9 and *B2M* sgRNA2 c21) result in the complete abrogation of the benefit of anti-PD-1 therapy (**Figure 21**, *P* = ns, unpaired *t* test, mean ± SEM) compared to MC38 wild-type tumors or MC38 wild-type CRISPR control tumors generated following the same procedures but that did not end up having the specific gene knockout. Of note, the lack of anti-PD-1 antitumor activity was validated in a slow-growing *JAK2* knockout tumor (sgRNA2 clone 9) suggesting that the loss of a-PD-1 response is independent of MC38 tumor growth rates in mice (**Figure 21**).

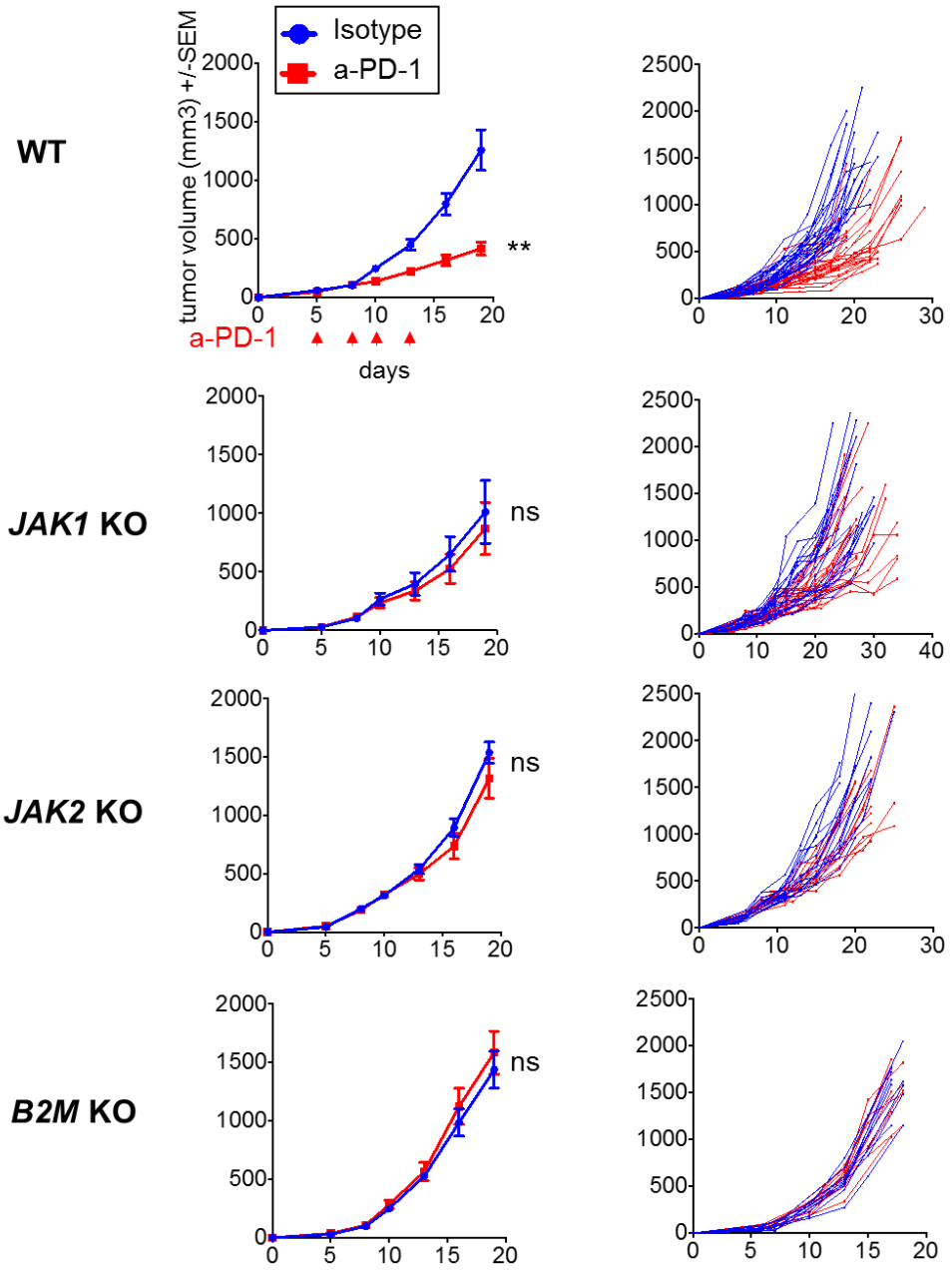

Figure 20. MC38 *JAK1/2* and *B2M* KO tumors result in resistance to anti–PD-1 therapy. *In vivo* tumor growth curves (left) of *JAK1*- or *JAK2*- or *B2M*-KO cell lines with 5 mice in each group (mean ± SEM) after anti–PD-1 (a-PD-1) or isotype control. The arrow indicates the days of treatment with a–PD-1 or isotype control was started. *P* value was determined by unpaired t test on day 19, a–PD-1 versus isotype control. ns, not significant; **, $P < 0.01$. One representative experiment of three independently conducted experiments is shown. *In vivo* tumor growth curves of individual mice (right): MC38 WT (n =28 per group), *JAK1*-KO clone 5 (n = 22 per group), *JAK2*-KO clone 3 (n = 15 per group), and *B2M*-KO clone 6 (n = 10 per group). Treated tumors received four doses of a–PD-1 in total. ns, not significant.

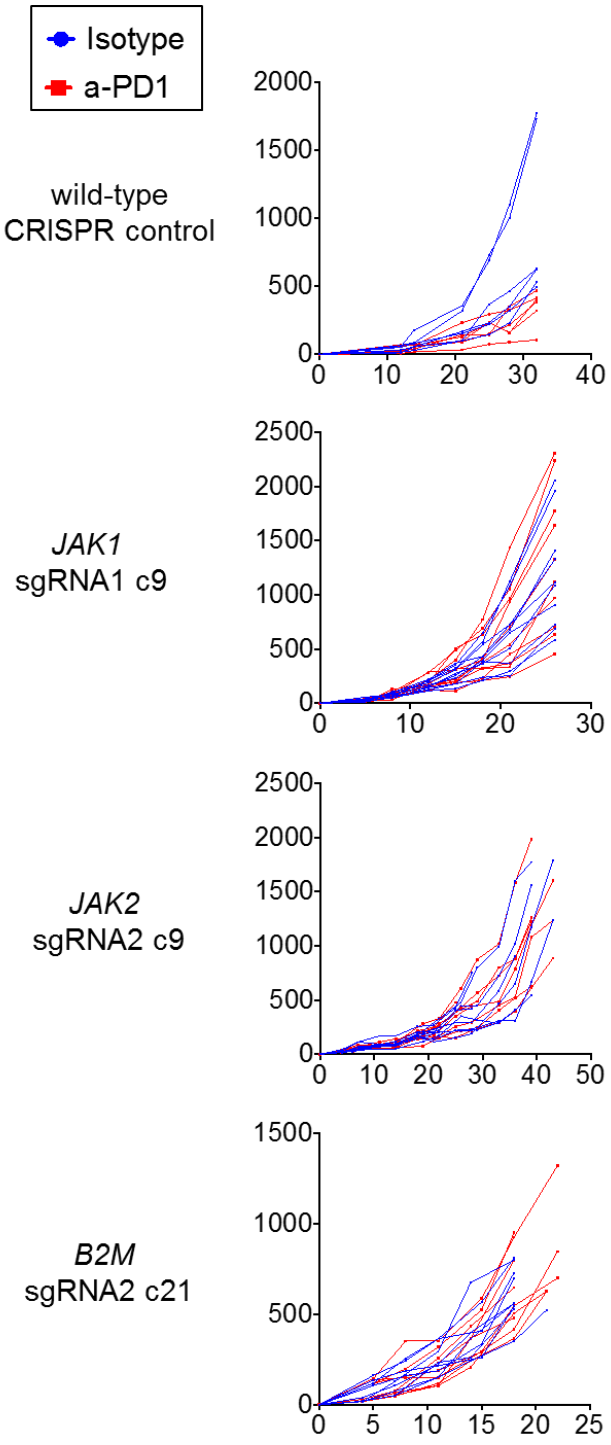

Figure 21. Modeling resistance to PD1-blockade: *In vivo* tumor growth curves of individual mice after anti-PD-1 (red) or isotype control (blue) in MC38 wild-type CRISPR control (n=6 per group), MC38 *JAK1* KO clone 9 (n=10 per group), MC38 *JAK2* KO clone 9 (n=8 per group) and MC38 *B2M* KO clone 21 (n=8 per group). Treated tumors received four doses of anti-PD-1 in total.

5.2.4 Characterization of the tumor immune contexture by CyTOF

To characterize and define the tumor-infiltrating immune cell populations in both MC38 wild-type and resistant tumors treated with either isotype or anti-PD-1 therapy, we performed cytometry by time-of-flight (CyTOF) analysis. A total of 19 independent cell clusters were identified using a panel with 28 markers (**Supplementary Figure 1 and Figure 22A**).

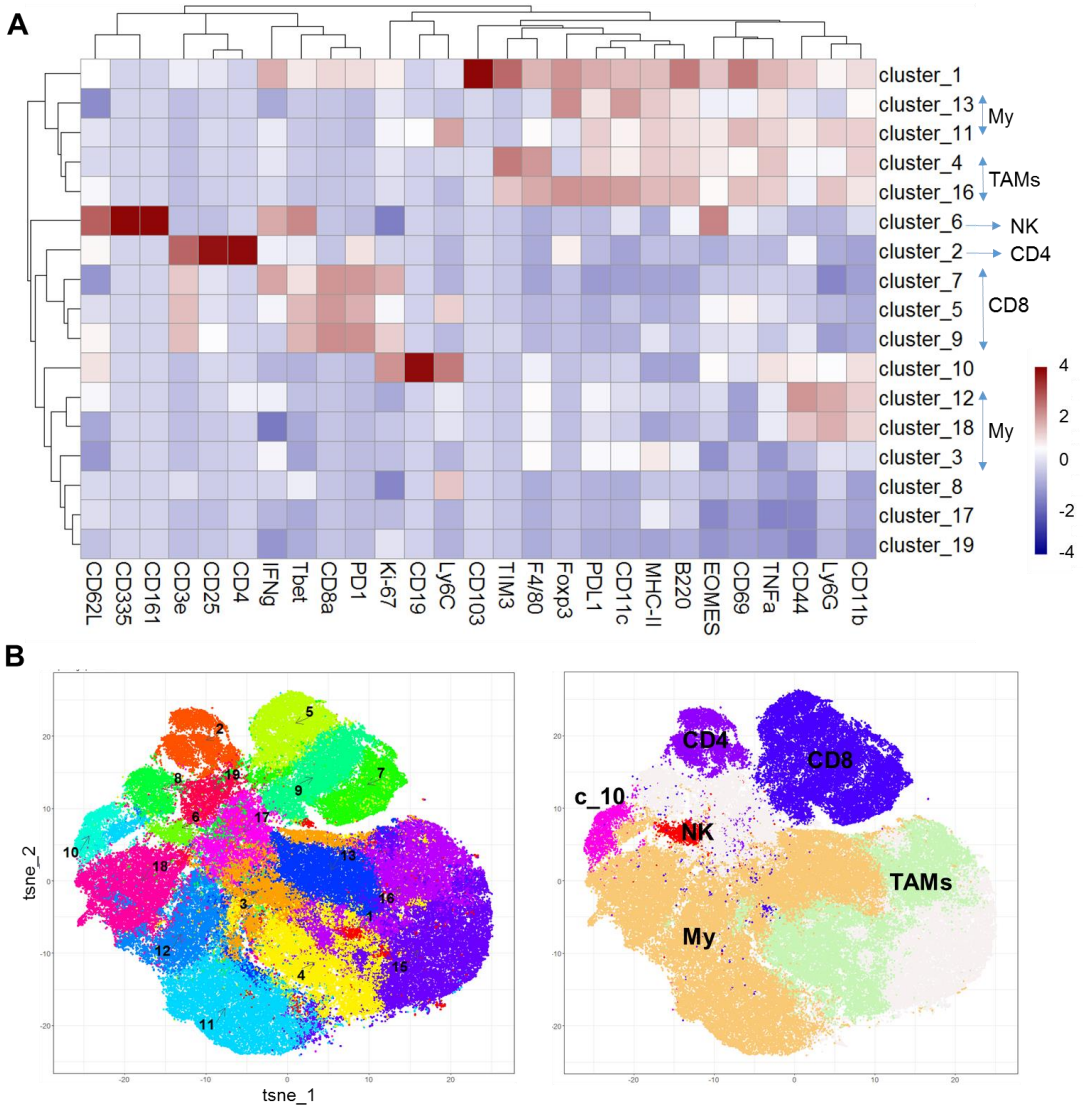

Figure 22. Identification of MC38 tumor CD8+ T immune cell population by CyTOF. (A) Heat map with the normalized median percentages for each of the immune markers. Clusters > 0.5% frequency were analyzed. **(B)** t-SNE plot of total CD45+ cells from all samples overlaid with color coded clusters.

The T-cell population was defined by four clusters, including a CD4 T-cell cluster positive for CD3e, CD4, and CD25, and three CD8 T-cell clusters positive for CD3e, CD8e, TBET, and PD-1. An NK-cell cluster positive for CD335 and CD161 was also identified (**Figure 22 and 23**). Using this approach, we analyzed MC38 tumors from mice after three doses of isotype or anti–PD-1 (day 13). Anti–PD-1–treated wild-type control MC38 tumors presented increased T-cell infiltration (P = 0.04) and a trend toward statistical significance (P = 0.07) of increased CD8+ T-cell infiltration compared with isotype control antibody-treated tumors, which is in line with data from prior studies (61). We did not observe significant changes in the CD4+ and NK-cell infiltration. However, anti–PD-1 did not induce any significant changes in T, CD4+ T, CD8+ T, and NK immune cell populations in MC38 *JAK1*, *JAK2*, and *B2M* KO tumors (**Figure 24**).

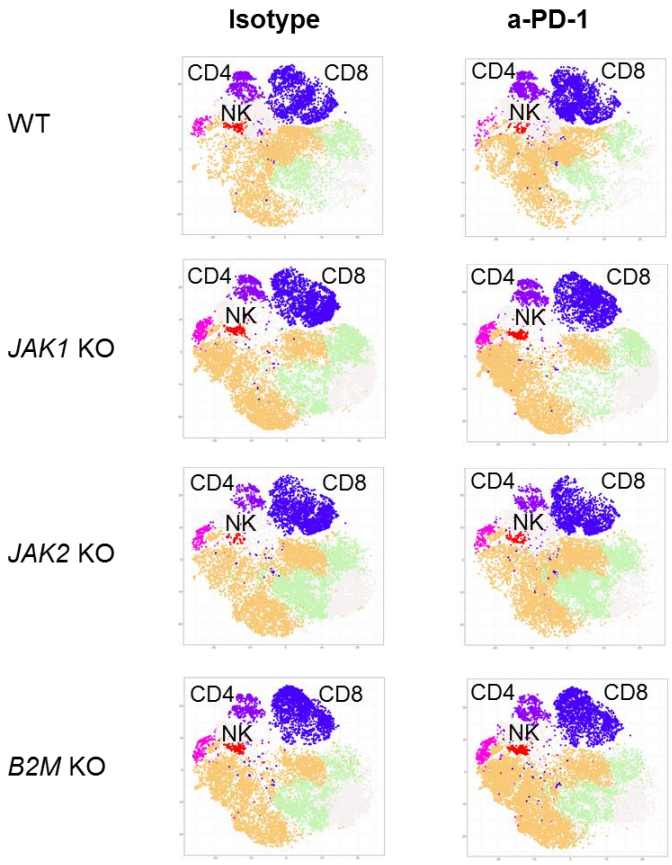

Figure 23. Groups of treatment overlaid with color-coded clusters and subsequent classification in immune cell populations.

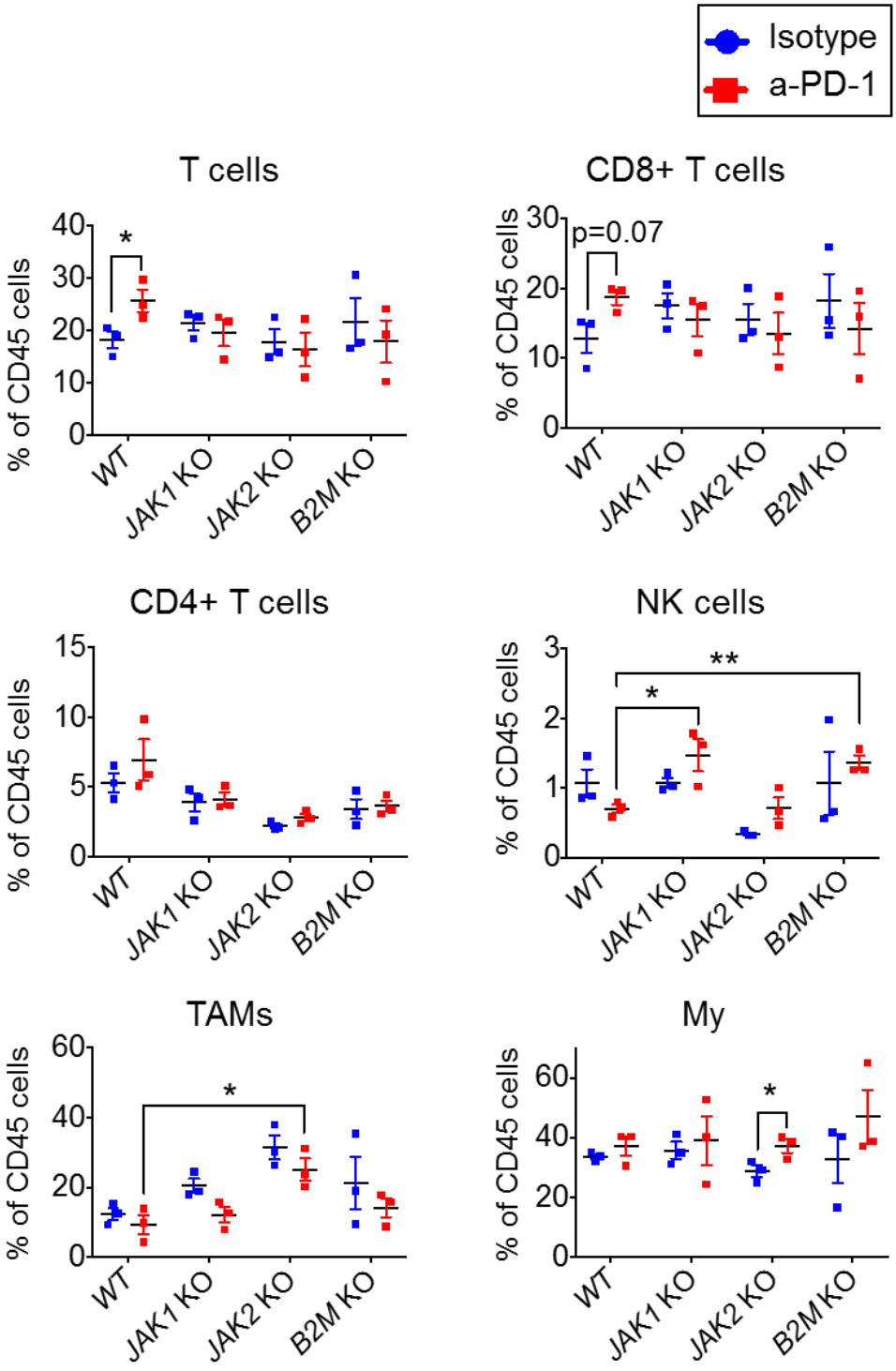

Figure 24. Percentage of T, CD8+ T, CD4+ T, NK, tumor-associated macrophages (TAM), and myeloid cells (My) from CD45+ cells in MC38 wild-type (WT), *JAK1*-, *JAK2*-, and *B2M*-knockout (KO) tumors treated with anti-PD-1 (a-PD-1) or isotype mAb.. Mean ± SEM, unpaired t test, n = 3. *, $P < 0.05$; **, $P < 0.01$.

Separate FlowSOM clustering was performed on manually gated CD8+ T cell population subsets to better dissect their heterogeneity. Cluster 6 expressed markers of terminally CD8+ T exhausted cells (CD3e+, CD8a+, PD1+, TIM3+, EOMES+, and TBET+), while cluster 7 was distinguished by markers associated with progenitor CD8+ T exhausted cells (CD3e+, CD8a+, PD1+, TBET+, and CD69+). A small cluster (cluster 8) expressed markers of CD8+ T (CD3+CD8+) (**Figure 25**).

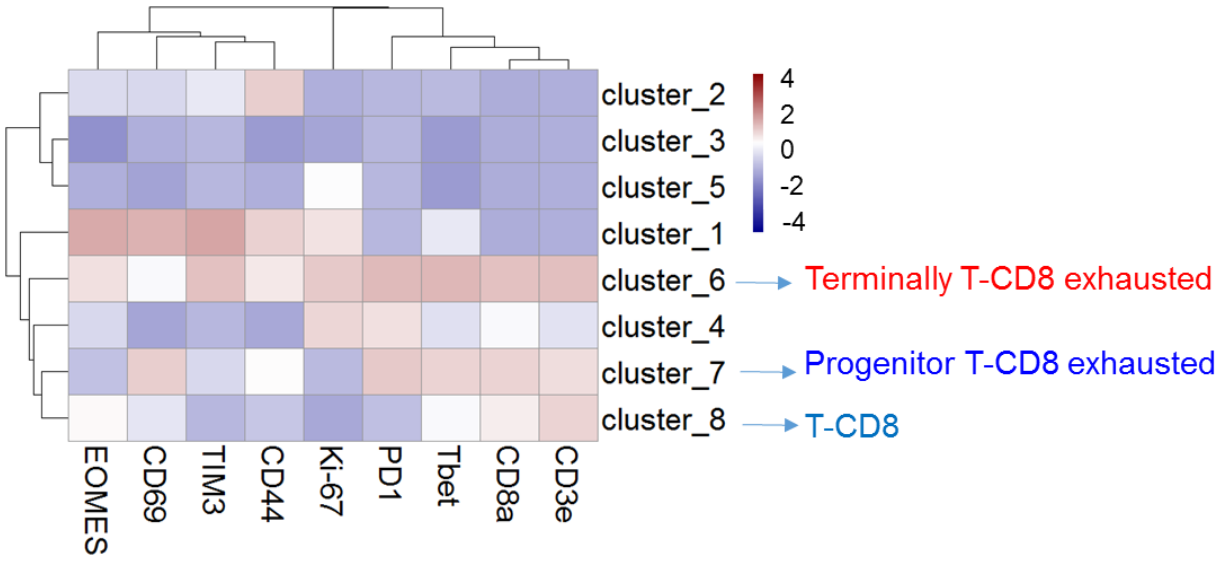

Figure 25. Heat map with the normalized median percentage for each cluster obtained with FlowSOM on CD8+ T-cell markers. Clusters with >0.5% frequency were analyzed

Interestingly, *JAK1/2* and *B2M* knockout tumors showed a significantly basal increased percentage in terminally CD8+ T exhausted cells when compared to the MC38 wild-type tumors (**Figure 26 and 27**, $P < 0.05$, unpaired *t* test, n=3, mean± SEM), which have been reported to be unable to respond to anti–PD-1 therapy (36–38), in line with the observed lack of response to anti–PD-1 therapy *in vivo.*

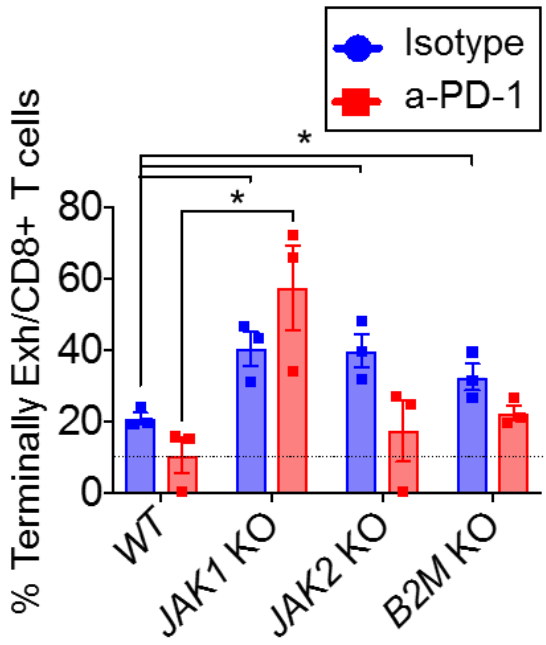

Figure 26. Percentage of terminally CD8+ T exhausted cells from CD8+ cells in MC38 wild-type, *JAK1*-, *JAK2*-, and *B2M*-knockout tumors treated with anti–PD-1 or isotype mAb. Mean ± SEM, unpaired t test, n = 3. *, $P < 0.05$.

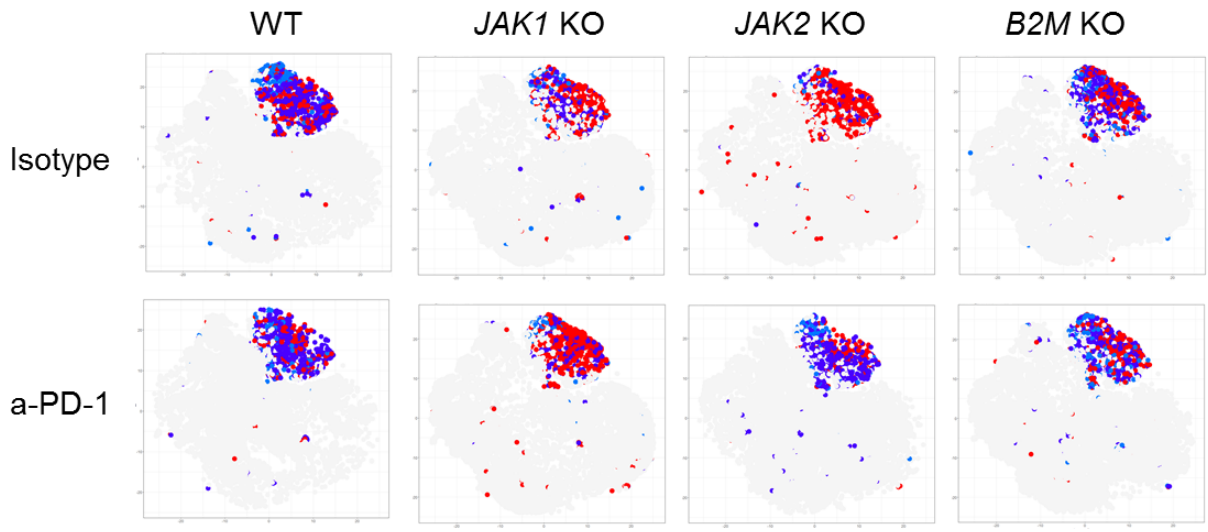

Figure 27. t-SNE plot of MC38 CD8+ T infiltrating population cells overlaid with color-coded clusters and the differentiation of exhausted T cells, representing terminally CD8+ T exhausted cells in red and progenitor CD8+ T exhausted or CD8+ T cells in blue.

5.3 Overcome resistance with combination immunotherapy

5.3.1 Intratumoral TLR-9 agonist administration overcomes resistance to anti-PD-1 therapy in *JAK1/2* knockout tumors

Our results thus far demonstrate that the major effect of *JAK1/2* knockouts is the inability of cancer cells to respond and express an IFN-induced transcriptional profile that leads to downstream immune activation. Additionally, *JAK1/2* knockout tumors were less immune infiltrated with functional CD8 T cells compared to wild-type tumors after anti-PD-1 treatment. Therefore, we investigated whether upstream activation with agents that trigger a type I IFN response in the tumor microenvironment could overcome resistance mediated by *JAK1/2* loss.

Type I IFN responses could be triggered by recognition of foreign DNA sequences through pattern recognition receptors such as TLR9 signaling. TLR9 stimulation of pDCs, which are high producers of IFNα, could initiate a strong antitumor immune response (41) in tumors lacking JAK signaling since they can still be recognized and killed by antigen-specific T cells as shown in **Figure 10** and **12** . To this end, we bilaterally injected wild-type and *JAK1/2* knockout cells into mice and when tumors became detectable, mice were treated with intratumoral TLR9 agonist SD-101 injections into the right flank tumors. We observed antitumor effects in both the injected and contralateral non-injected left flank tumors, with or without systemic anti–PD-1 therapy. In three replicate experiments, the combined therapy of SD-101 and anti-PD-1 provided superior antitumor activity against *JAK1/2* knockout tumors, overcoming resistance in both injected and contralateral non-injected sites, as well as increased survival (**Figure 28 and Supplementary Figure 2** and **3**)**.** This effect was consistent when replicated using tumors from additional MC38 *JAK1/2* knockout sublines (**Figure 29**).

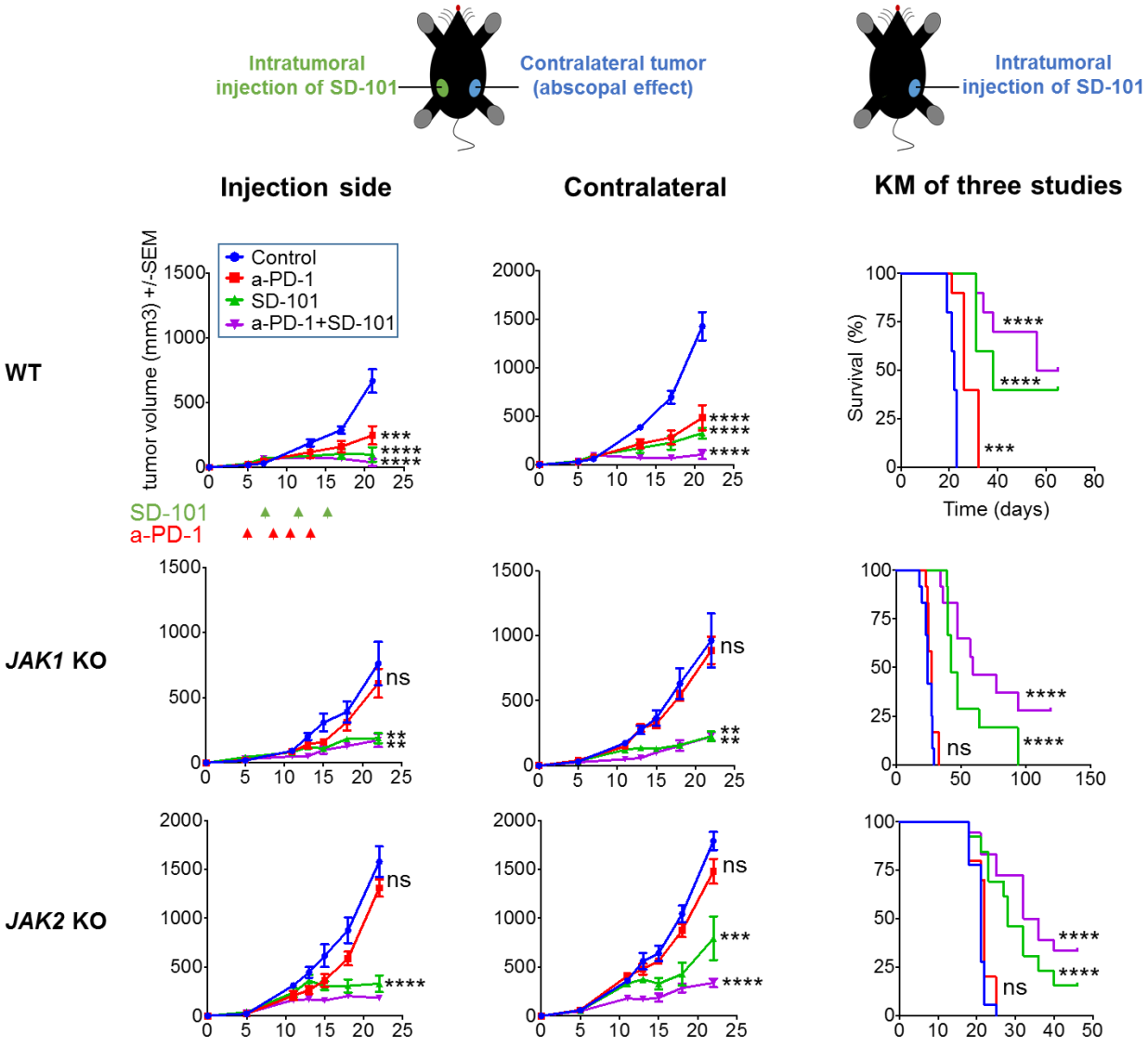

Figure 28. Effect of intratumoral SD-101 on tumor growth at treated and nontreated contralateral sites (left). Date represented as mean ± SEM from an n = 5. Dunnett multiple comparisons test for control versus a–PD-1 or SD-101 or a–PD-1 plus SD-101. Long-term survival for mice inoculated with WT and JAK1/2- KO tumor cells in one flank (right). MC38 wild-type (n = 10 per group), *JAK1* knockout (n = 12 per group), and *JAK2* knockout (control, n = 18; anti–PD-1, n = 10; SD-101, n = 13; and SD-101 plus anti–PD-1, n = 18). Differences in survival were examined using log-rank (Mantel–Cox) test. ns, not significant; *, $P < 0.05$; **, $P < 0.01$; ***, $P < 0.001$; ****, $P < 0.0001$.

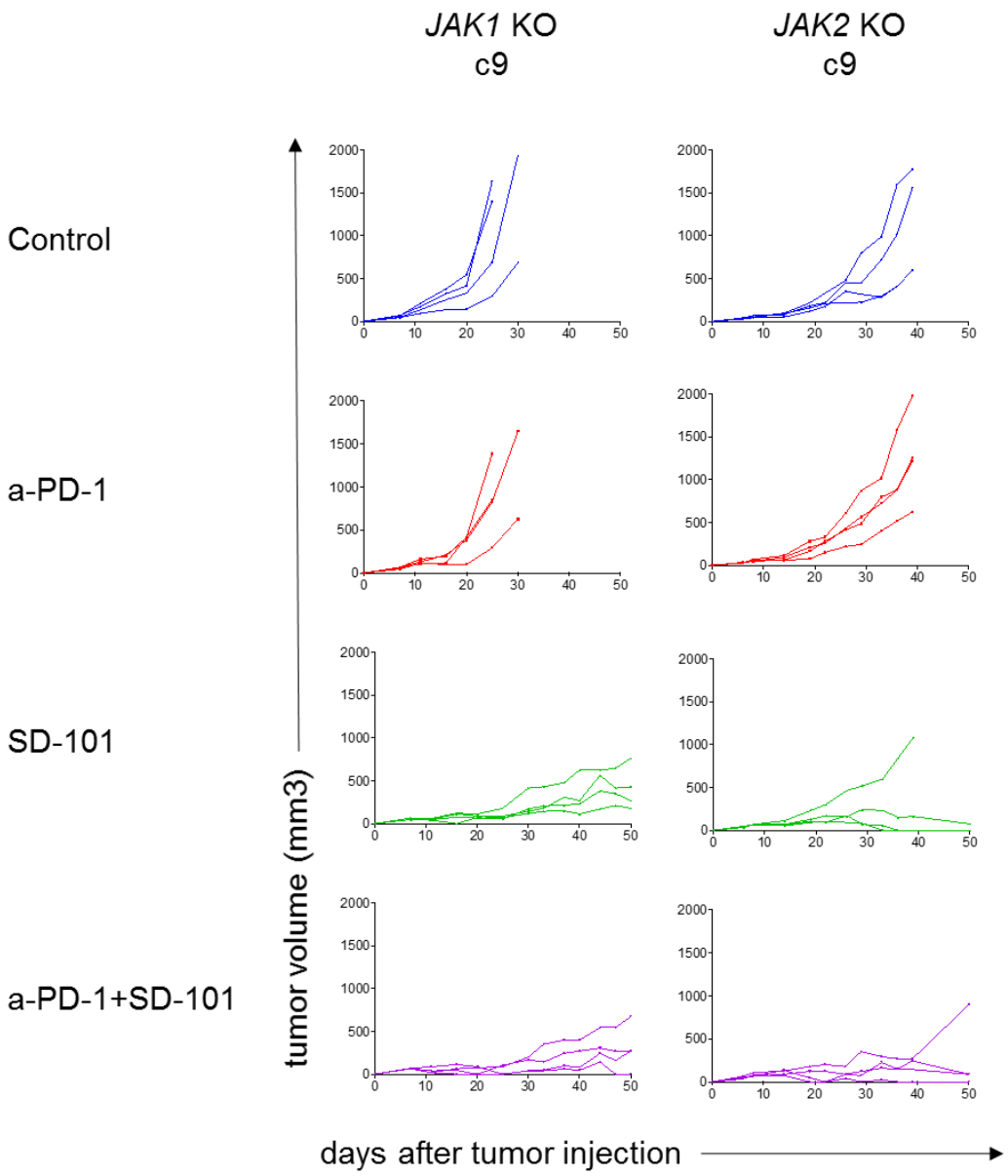

Figure 29: An intratumoral TLR-9 agonist (SD-101) to reverse resistance to anti-PD-1 therapy. In vivo tumor growth curves of individual C57/BL6 mice after Control-PBS, anti-PD-1, SD-101 or anti-PD-1 plus SD-101 in *JAK1* sgRNA1 c9 and *JAK2* sgRNA2 c9 knockout tumors according to the treatment timeline of Figure 28.

IFNγ requires both *JAK1* and *JAK2* for signaling, while type I IFNs use *JAK1* and *TYK2* (64). To directly test the role of type I IFN signaling in our model, we generated and validated IFNα receptor (*IFNAR1*) knockout tumors (**Figure 30**) and performed *in vivo* experiments. Interestingly, both SD-101 and anti-PD-1 alone or in combination can significantly enhance antitumor activity in MC38 *IFNAR1* knockout tumors (**Figure 31**)**.** These results suggested that the anti-PD-1 antitumor effect was not lost with the absence of *IFNAR1* on tumor cells and hence, provides evidence that the systemic antitumor effect of SD-101 is independent on type I IFN sensing and response by cancer cells.

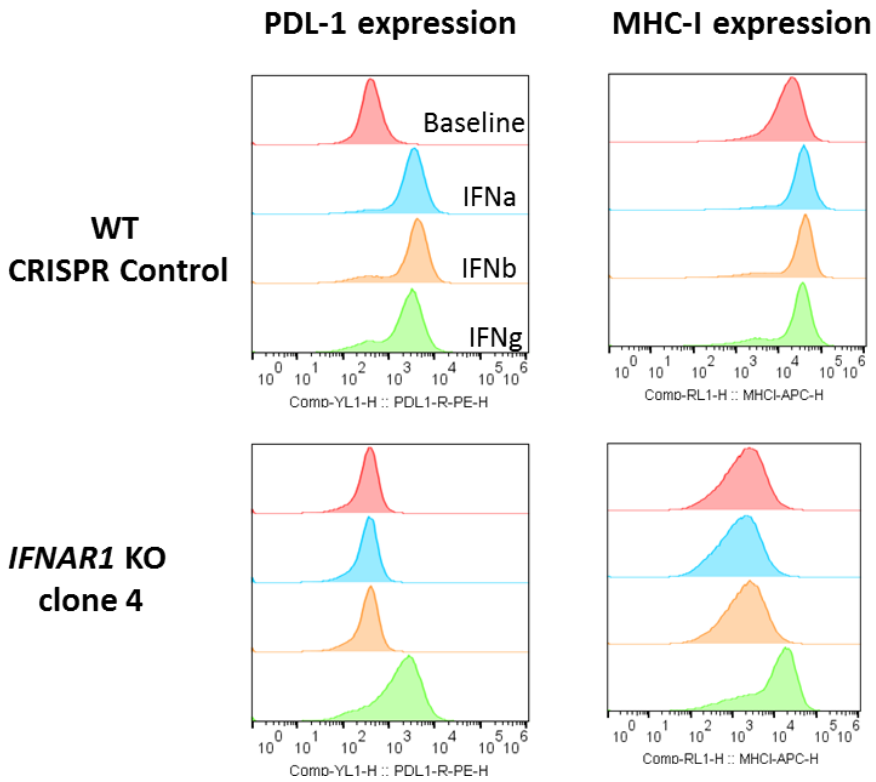

Figure 30. Impact of IFN on PD-L1 and MHC class I expression in *IFNAR1* knockout tumor. The measure of PD-L1 and MHC class I expression by flow cytometry after IFNs stimulation in MC38 wild-type CRISPR control and *IFNAR1* sgRNA c4 knockout. *IFNAR1* knockout ability to up-regulate both expressions upon IFNα and β were dramatically reduced compared to the parental cell line. Histograms represent changes in MFI by flow cytometry compared to baseline.

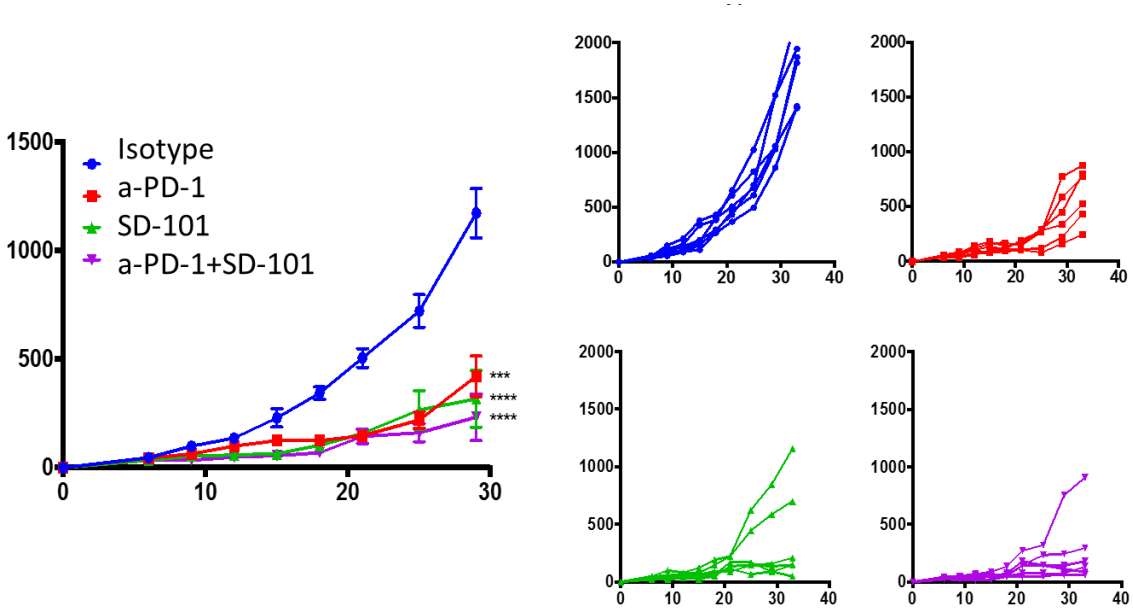

Figure 31. Intratumoral TLR-9 agonist (SD-101) have antitumor activity in MC38 *IFNAR1* KO tumors. Effect of anti-PD-1 and intratumoral SD-101 on tumor growth in one side. $3x10^5$ MC38 *IFNAR1* KO tumor cells were injected in the left flank of C57/BL6 mice on day 0. Anti-PD-1 (four doses) treatment started at day 5. Mice were treated with anti-PD-1 or Isotype administered on days 5, 8, 10, 13 and 16. After first anti-PD-1 injection, mice started receiving intratumoral SD-101 (50 ug) or CTRL-PBS administered on days 7, 11, 15 and 19. A separate group of mice received SD-101 alone. Date represented as mean +/- SEM from an n of 6. Dunnett's multiple comparison tests for Isotype versus anti-PD-1 or SD-101 or anti-PD-1 plus SD-101. In vivo tumor growth curves of individual C57/BL6 mice (right) after Control-Isotype, anti-PD-1, SD-101 or anti-PD-1 plus SD-101. ***, $P < 0.001$; ****, $P < 0.0001$.

To analyze the role of T and NK cells, we performed antibody-mediated CD4+ T-cell, CD8+ T-cell and NK1.1+ cell depletion studies in mice with *JAK1/2* knockout tumors treated unilaterally with intratumoral SD-101 or combination therapy with systemic anti-PD-1 therapy. Antibody-mediated depletion was confirmed by flow cytometric analysis of splenocytes (**Figure 32**)**.** In *JAK1* knockout tumors, depletion of NK and CD4+ T cells, but not CD8+ T cells, partially abrogated the SD-101 antitumor activity (**Figure 33 and Supplementary Figure 4**). In contrast, the CD8+ T-cell depletion completely ablated the effect of the combination therapy (**Figure. 33 and Supplementary Figure 5**). In *JAK2* knockout tumors, depletion of CD4+ and NK cells

resulted in a partial abrogation of antitumor activity, whereas CD8+ T-cell depletion resulted in complete abrogation of the antitumor efficacy of SD-101 alone and in combination with anti–PD-1 (**Figure 33 and Supplementary Figure 4 and 5**).

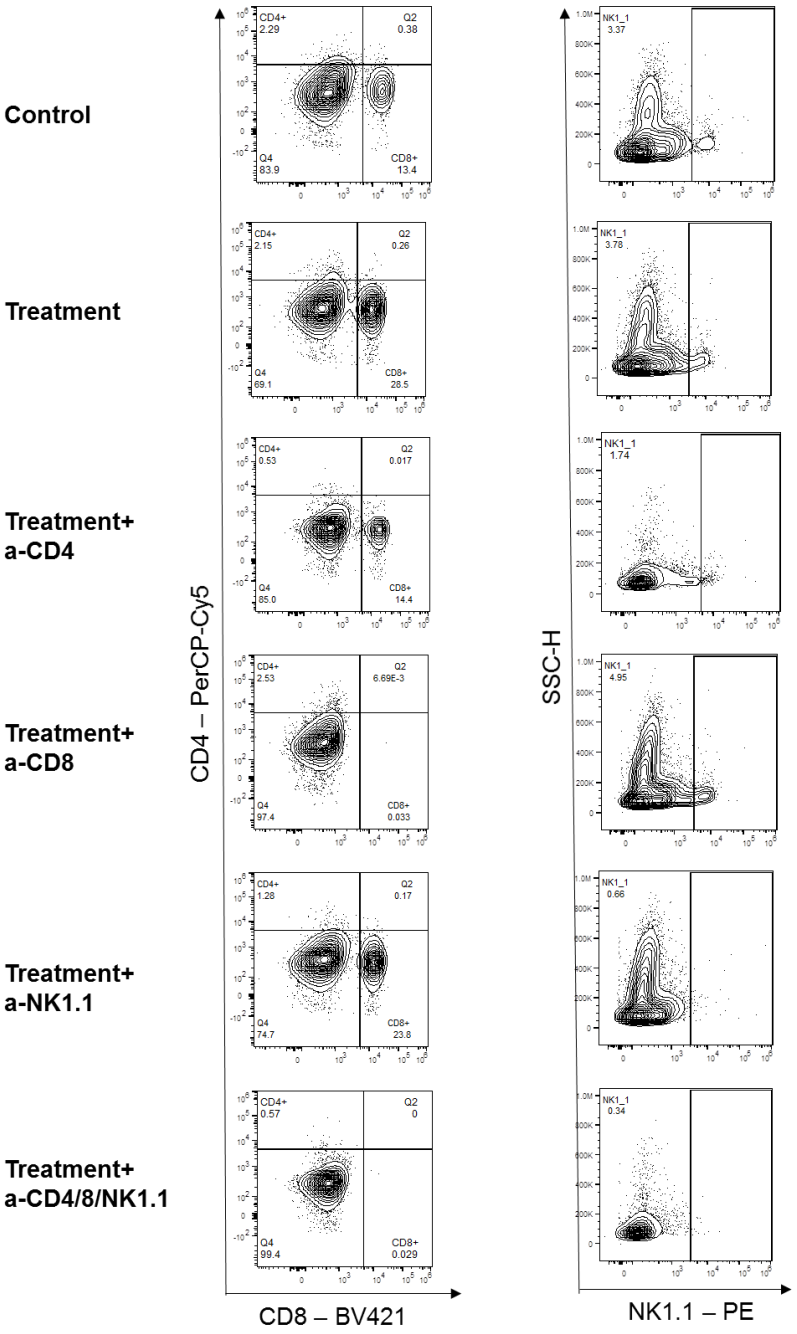

Figure 32. FACS analysis validation of depletion studies. Confirmation of CD4+ T, CD8+ T and NK depletion using FACS analysis of splenocytes treated with combined treatment (representative graph) at day 18 after tumor inoculation.

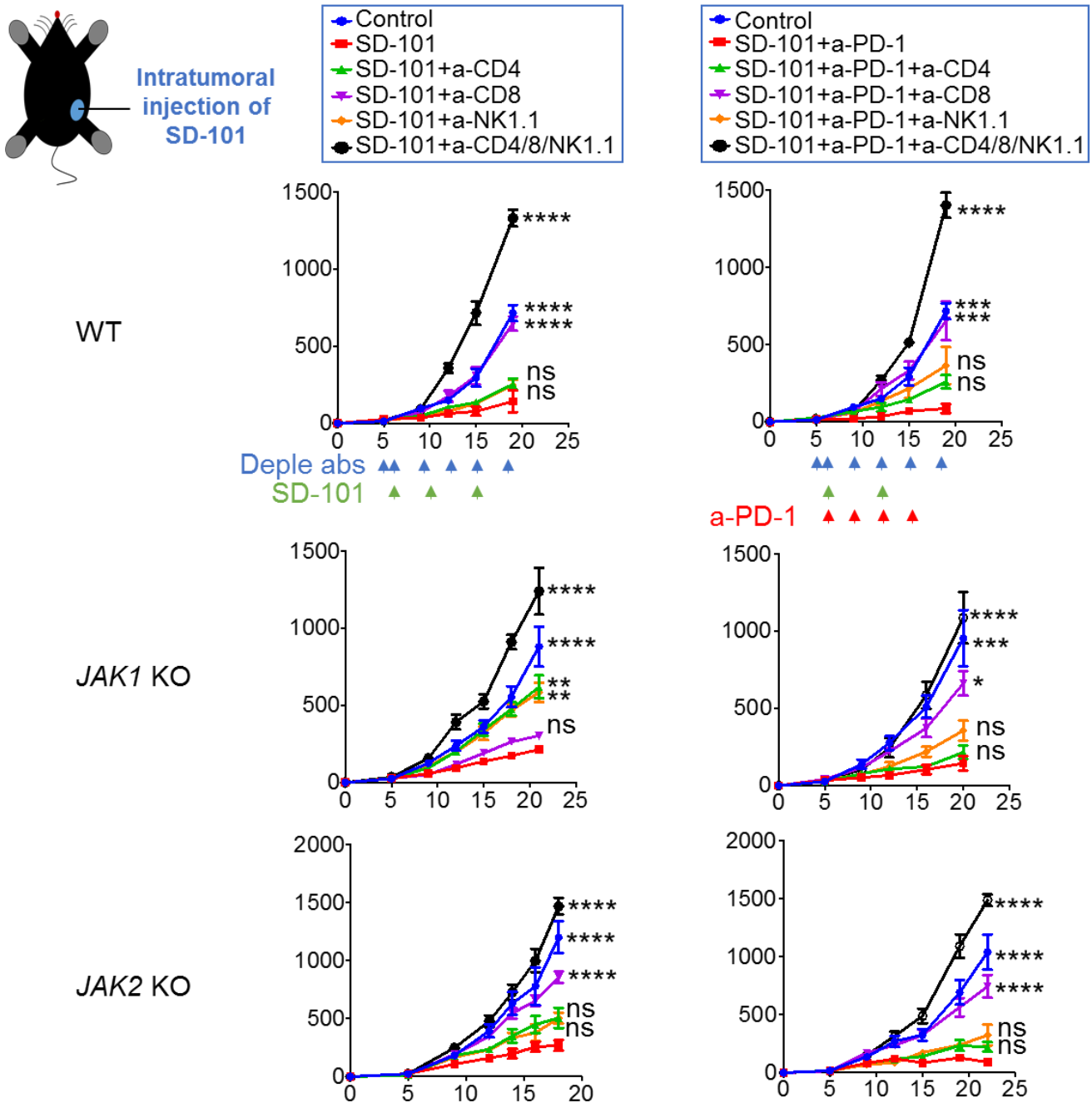

Figure 33. Tumor growth curves for wild-type control and *JAK1/2*-KO–resistant tumors with anti-CD4, anti-CD8, and anti-NK1.1 depletion studies after intratumoral SD-101 treatment (one-side). Date represented as mean ± SEM. In MC38 wild-type, n = 5 per group. In *JAK1* KO depletion: control, n = 10; SD-101, n = 12; SD-101 plus anti-CD4, n = 10; SD-101 plus anti-CD8, n = 12; SD-101 plus anti-NK1.1, n = 12; and SD-101 plus anti-CD4/8/NK1.1, n = 6. In *JAK2* KO depletion: n = 8 per group. ns, not significant; *, $P < 0.05$; **, $P < 0.01$; ***, $P < 0.001$; ****, $P < 0.0001$.

To have the power to distinguish tumor-specific immune cell changes from combinatorial treatments, we integrated data from replicate mass cytometry experiments (**Table 6**) using an automated meta-analysis of CyTOF data, MetaCyto (39). We merged cytometry data across a wide range of cell surface and intracellular markers (**Table 5**) and identified immune cell populations using predefined cluster analysis (**Table 7**).

Anti–PD-1 therapy did not change the frequency of CD4+ and CD8+ T effector subsets in both *JAK1/2* knockout tumors (**Figure 34, left column**). These results are in line with **Figure 24** and suggest a lack of maintained T-cell activation in *JAK1/2* knockout tumors. Treatment with single-agent SD-101 increased NK-cell mobilization in *JAK1* knockout and also CD8+ and CD4+ T cells in *JAK2* knockout tumors. Interestingly, the addition of anti–PD-1 treatment improved immune responses and increased the levels of CD3+ T, CD4+ T, CD8+ T, and B cells compared with SD-101 alone of both injected and non-injected tumor sites (**Figure 34**), in line with our depletion experiments in **Figure 33**.

As we documented the increase in T-cell infiltration when adding anti–PD-1 to intratumoral TLR9 administration, we next wanted to elucidate whether the combinatorial treatment increased expression of the T-cell chemoattracting chemokines CXCL9 and CXCL10 within the tumor microenvironment. Therefore, we performed qRT-PCR from MC38 wild-type control and knockout tumors after two doses of intratumoral SD-101 and three doses of anti–PD-1 compared with anti–PD-1 or isotype control. No differential expression of CXCL9 or CXCL10 was detected in *JAK1/2* knockout tumors treated with anti–PD-1 comparable to isotype control. Interestingly, the combination of SD-101 with anti–PD-1 treatment produced higher levels of CXCL9 and CXCL10 than did tumors treated with anti–PD-1 or isotype control, in wild-type and *JAK1/2*-knockout tumors (**Figure 35**).

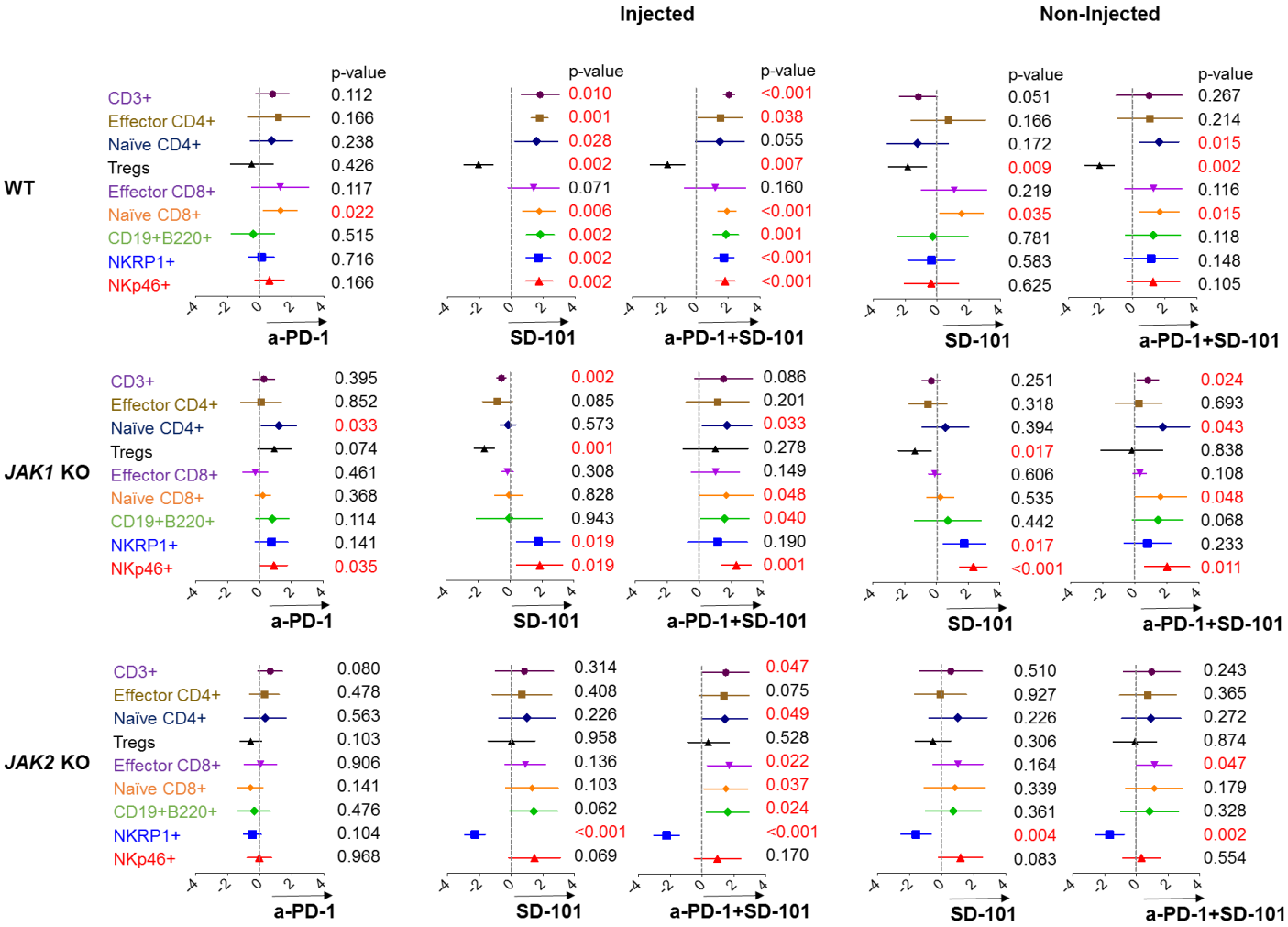

Figure 34. Meta-analysis of CyTOF data using MetaCyto in MC38 wild-type and *JAK1/2* KO tumors. Plots showing the effect size of treatments: control-isotype versus anti–PD-1 or control-isotype versus SD-101 or combination SD-101 plus anti–PD-1 therapy in wild-type and *JAK1/2* KO tumors (effect of injected and non-injected sites). Dots and whiskers represent the means and 95% confidence intervals. The *P* value is calculated using a random effect model, adjusted using Benjamini–Hochberg correction.

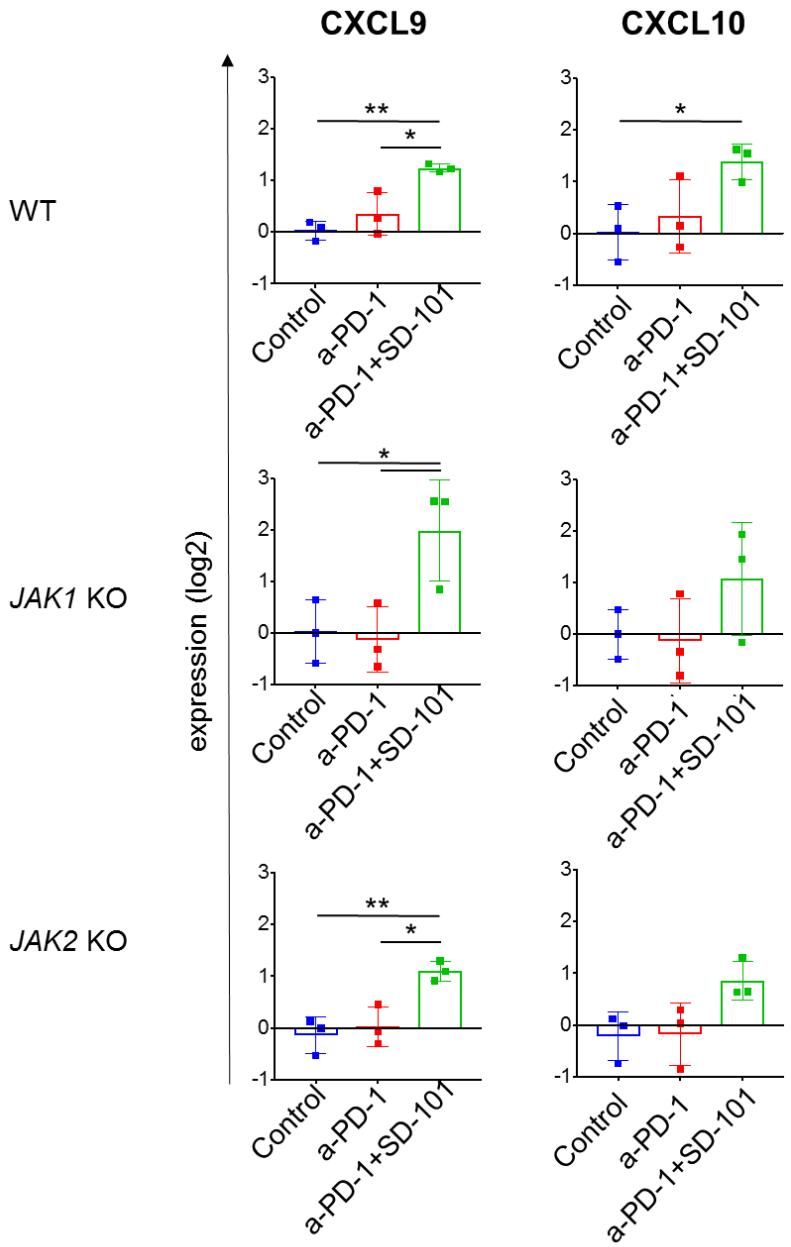

Figure 35. RT-PCR for CXCL9 and CXCL10 expression shows that SD-101 plus anti–PD-1 increase the expression levels of these genes. Showing means ± SD. Results are normalized to control-isotype level in each group and then log2 transformed (n = 3). *, $P < 0.05$; **, $P < 0.01$.

Taken together, our results demonstrate that SD-101 is able to overcome resistance in both *JAK1* and *JAK2* knockout models by increasing infiltration of T cells and NK cells as a result of markedly increased levels of both CXCL9 and CXCL10 in the tumor microenvironment.

5.3.2 The CD122 preferential IL2 pathway agonist (NKTR-214, bempegaldesleukin) overcomes resistance in *B2M* knockout tumors

We reasoned that the absence of *B2M* and subsequent lack of surface expression of MHC class I may sensitize cancer cells to NK cells, as MHC class I is the major inhibitory ligand for NK cell function (42–44). Therefore, we tested a CD122 preferential IL2 pathway agonist, bempegaldesleukin, also known as NKTR-214 (60), administered either alone or in combination with anti-PD-1. In two replicate experiments, the systemic administration of bempegaldesleukin overcame therapeutic resistance to anti-PD-1 in *B2M* knockout tumors, with significantly longer survival compared to the control groups (**Figure 36** and **Supplementary Figure 6**). To assess the influence of T and NK cells in the bempegaldesleukin response, depletion studies were performed and confirmed by splenocyte flow cytometric analysis. Depletion of CD8+ T cells did not affect the antitumor effect, as expected from the low MHC class I expression on the tumors. However, the depletion of either CD4+ T or NK cells abrogated the antitumor effect of bempegaldesleukin in the MC38 *B2M* knockout tumors (**Figure 37** and **Supplementary Figure 7**) .

Applying MetaCyto across a set of mass cytometry data, knockout of *B2M* in tumors resulted in the loss of MHC class I and the reduction of CD8+ T-cell infiltration (**Figure 38**). However, treatment with bempegaldesleukin was able to overcome resistance through increased infiltration of CD4+ T as well as NK cells, resulting in the rejection of *B2M* knockout tumors (**Figure 38**). Taken together, our combined meta-analysis and depletion studies suggest that the immune compartment is distinct in the B2M knockout and wild-type tumors due to the lack of MHC class I expression. However, an effective antitumor immune response, consisting of CD4+ T cells and NK cells, can still be mounted in these tumors by treatment with bempegaldesleukin.

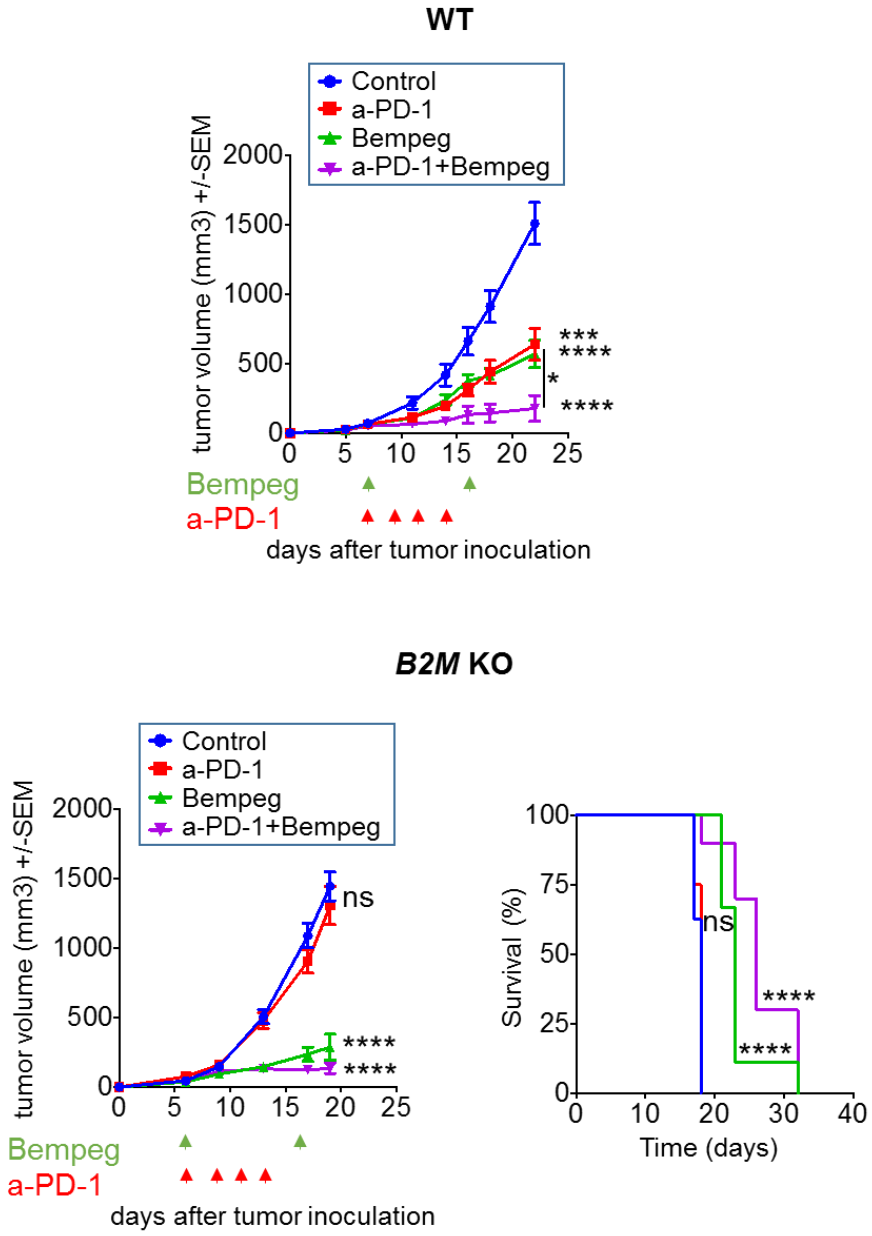

Figure 36. Bempegaldesleukin to reverse resistance in *B2M*-KO tumors. Effect of bempegaldesleukin on tumor growth of MC38 wild-type (WT) and *B2M*-KO tumors. In MC38 wild-type, control, n = 6; anti–PD-1 (a-PD-1), n = 5; bempegaldesleukin (bempeg), n = 8; and anti–PD-1 plus bempegaldesleukin n = 9. In *B2M* KO: control, n = 10; anti–PD-1, n = 8; bempegaldesleukin, n = 10; and anti–PD-1 plus bempegaldesleukin, n = 9. Dunnett multiple comparisons test for control versus anti–PD-1 or bempegaldesleukin or anti–PD-1 plus bempegaldesleukin. Long-term survival for mice inoculated with wild-type and *B2M*-KO tumors (right). n = 9 mice per group. Differences in survival were examined using log-rank (Mantel–Cox) test. ns, not significant; *, $P < 0.05$; ***, $P < 0.001$; ****, $P < 0.0001$.

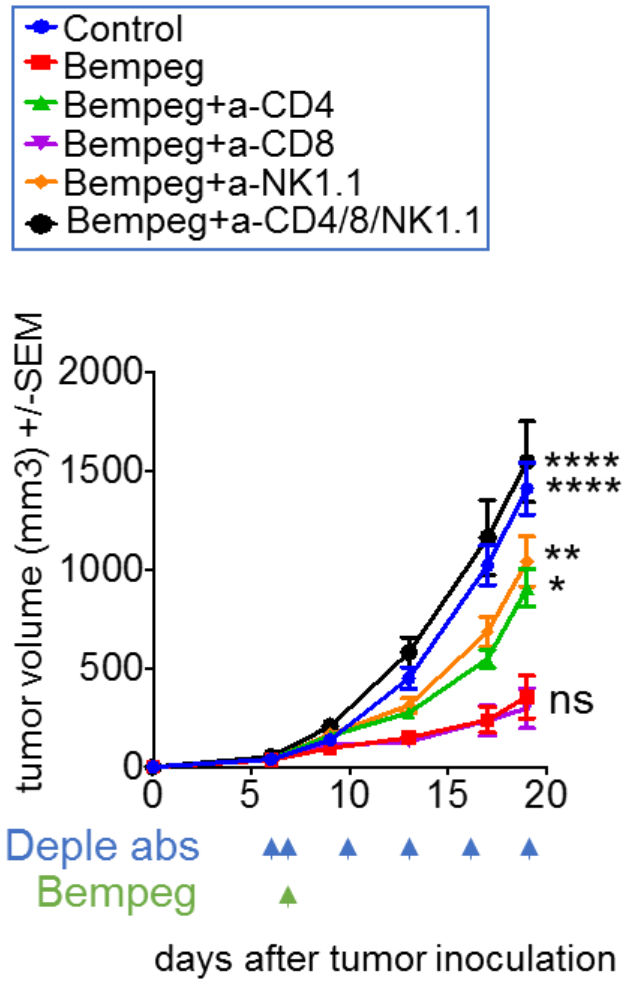

Figure 37. Tumor growth curves for *B2M*-KO resistant tumors with anti-CD4, anti-CD8, and anti-NK1.1 depletion studies after 0.8 mg/kg intravenous bempegaldesleukin. Data represented as mean ± SEM from an n of 8 per group, except bempegaldesleukin plus anti-CD4/8/NK1.1, n = 6. Dunnett multiple comparisons tests for bempegaldesleukin versus control or bempegaldesleukin plus anti-CD4 or bempegaldesleukin plus anti-CD8 or bempegaldesleukin plus anti-NK1.1 or bempegaldesleukin plus anti-CD4/8/NK1.1. ns, not significant; *, $P < 0.05$; **, $P < 0.01$; ****, $P < 0.001$.

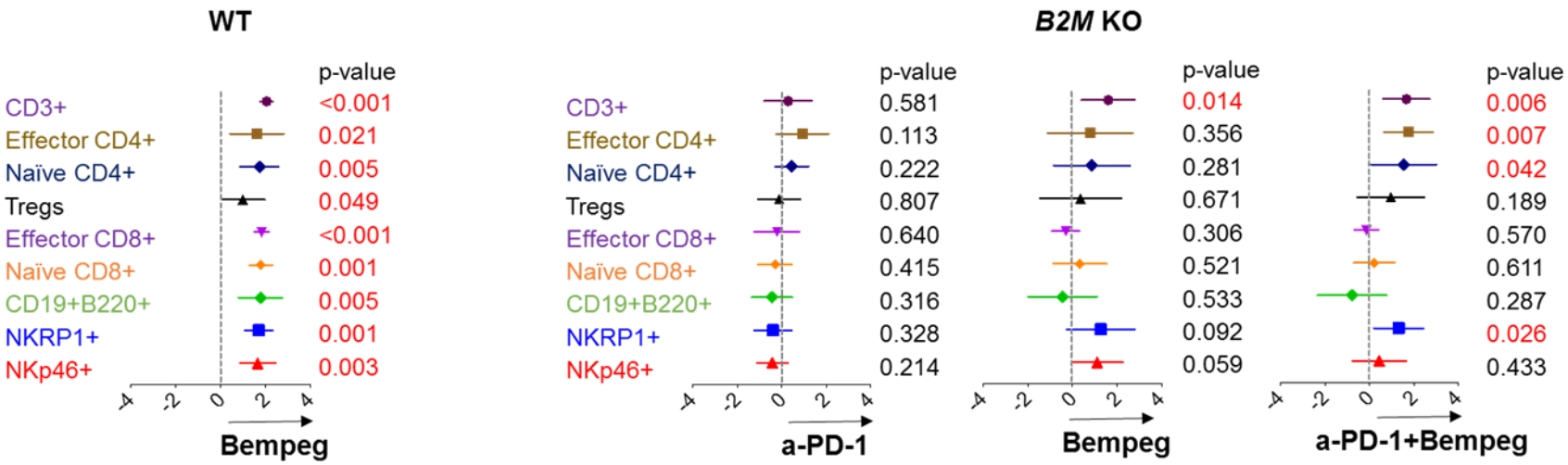

Figure 38. Meta-analysis of CyTOF data using MetaCyto. Plots showing the effect size of treatments: control-isotype versus bempegaldesleukin in wild-type tumors and control-isotype versus anti–PD-1, bempegaldesleukin or combination of bempegaldesleukin plus anti–PD-1 in *B2M* knockout tumors. Dots and whiskers represent the means and 95% confidence intervals. The P value is calculated using a random effect model, adjusted using Benjamini–Hochberg correction.

5.3.3 Overcoming *JAK1/2* and *B2M* knockout–resistant tumors in an aggressive B16 murine melanoma model

To validate the concepts underlying the combinatorial strategies to overcome resistance in *JAK1/2* and *B2M* knockout tumors, we used a second mouse tumor model, the B16 melanoma model, which exhibits primary resistance to PD-1 blockade (30). Functional effects of IFN exposure were consistent with their defective signaling: B16 *JAK1* knockout did not upregulate PD-L1 and MHC class I surface expression to all three IFNs, and B16 *JAK2* knockout to only IFNγ (**Figure 39**).

To evaluate the impact of the combinatorial treatment, TLR9 agonist plus anti–PD-1 in this model, we bilaterally implanted B16 wild-type control and *JAK1/2* knockout cells into mice and treated with intratumoral SD-101 with or without systemic anti–PD-1 therapy, as we had done with the MC38 experiments. Combination of SD-101 with anti–PD-1 resulted in a significant growth delay in *JAK1* and *JAK2* knockout tumors, overcoming resistance in both injected and contralateral non-injected sites (**Figure 40 and Supplementary Figure 8 and 9**).

We also examined the effect of bempegaldesleukin alone or in combination with anti–PD-1 in B16 *B2M* knockout tumors. Consistent with the results in the MC38 model, combination of bempegaldesleukin with anti–PD-1 overcame therapeutic resistance to anti–PD-1 in *B2M* knockout tumors (**Figure 41** and **Supplementary Figure 10**), with a significant improved survival in *B2M* knockout tumors compared with wild-type control. We confirmed that both MC38 and B16/F10 tumors showed significant tumor growth inhibition in the anti-PD-1 plus bempegaldesleukin group from around 7 days after the first injection of combined therapy.

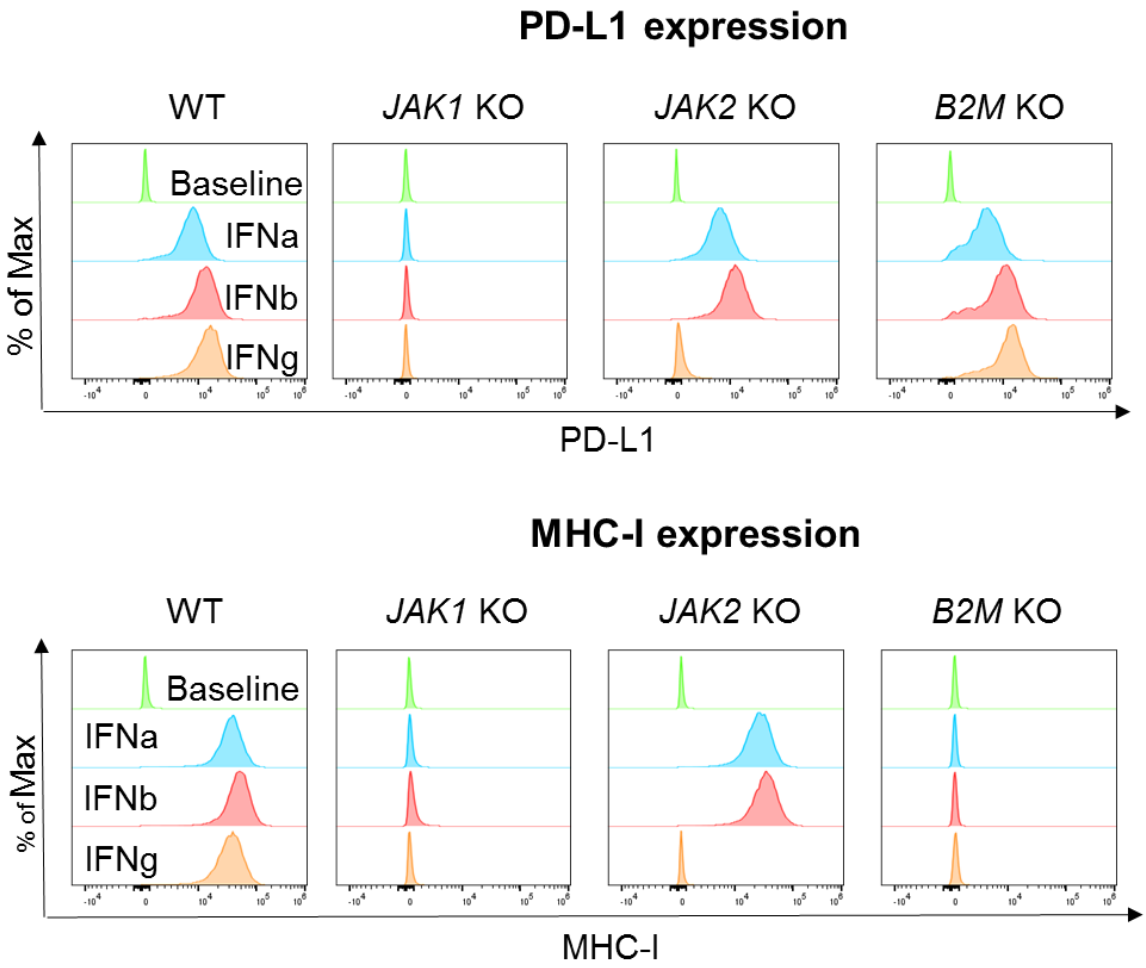

Figure 39. PD-L1 and MHC class I surface expression by flow cytometry after IFN stimulation. Histograms represent changes in MFI by flow cytometry compared with baseline.

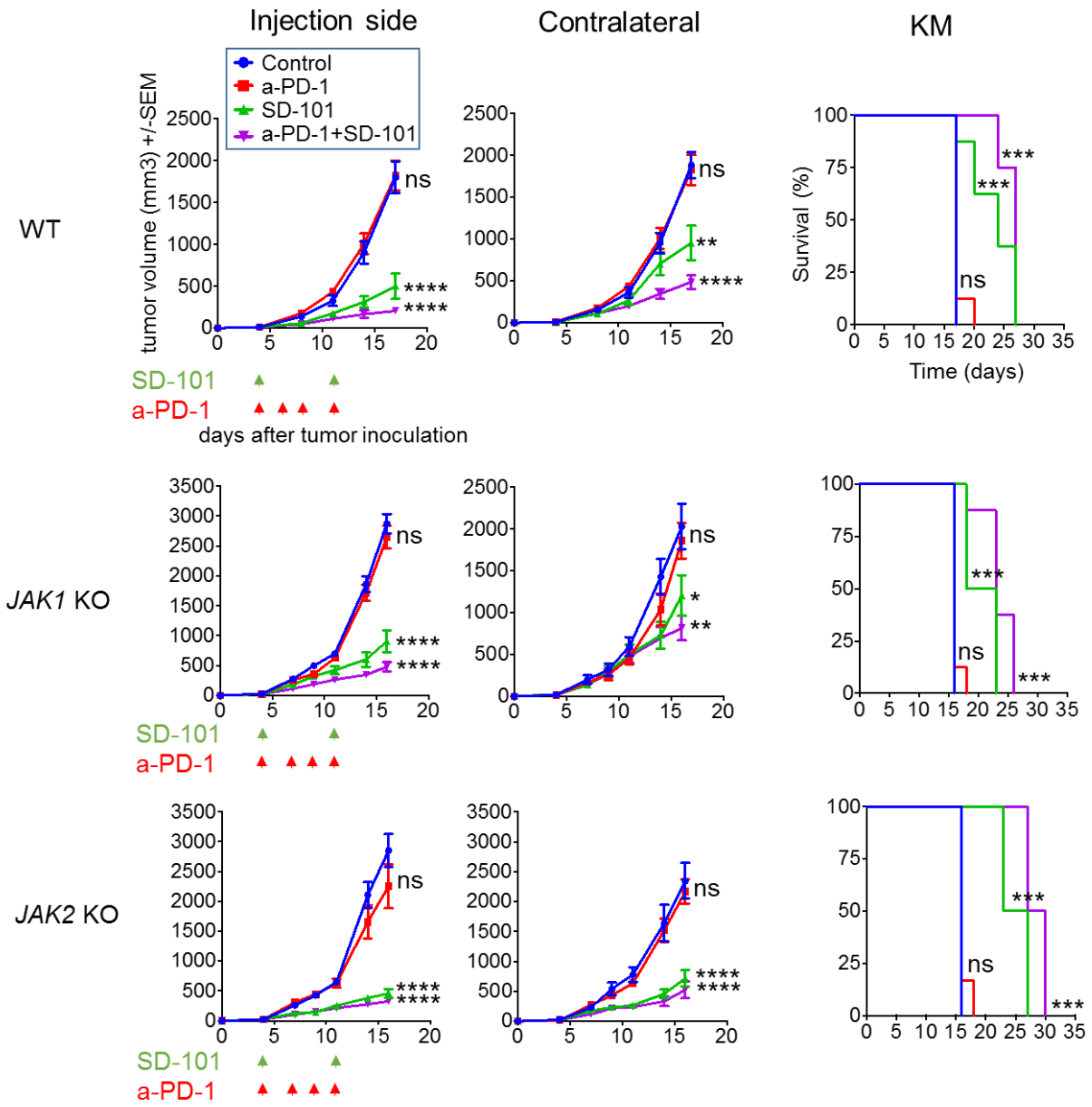

Figure 40. Effect of intratumoral SD-101 on tumor growth at treated and nontreated contralateral sites and long-term survival. Data represented as mean ± SEM. In B16 wild-type (WT) and *JAK1* knockout (KO) tumors, n = 8 per group. In B16 *JAK2* knockout tumors, control, n = 6; anti–PD-1 (a-PD-1), n = 6; SD-101, n = 8; and SD-101 plus anti–PD-1, n = 8. Dunnett multiple comparisons test for control versus anti–PD-1 or SD-101 or anti–PD-1 plus SD-101. Differences in survival were examined using logrank (Mantel–Cox) test. ns, not significant; *, $P < 0.05$; **, $P < 0.01$; ***, $P < 0.001$; ****, $P < 0.0001$.

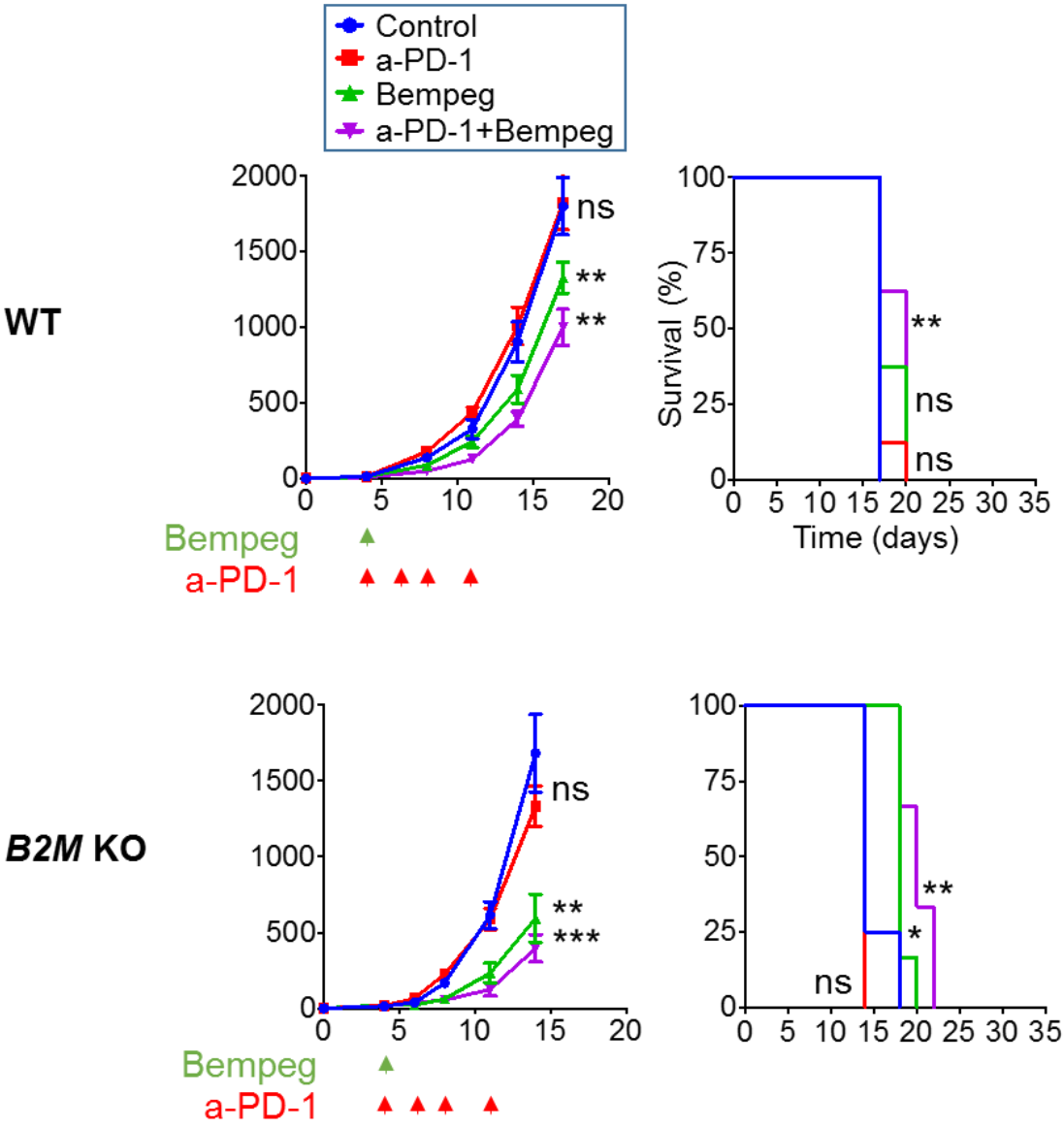

Figure 41. Effect of bempegaldesleukin on tumor growth of B16 wild-type and *B2M* knockout tumors and long-term survival. In B16 wild-type, n = 8 per group. In B16 *B2M* knockout: control, n = 4; anti–PD-1, n = 4; bempegaldesleukin (bempeg), n = 6; and anti–PD-1 plus bempegaldesleukin, n = 6. Dunnett multiple comparisons test for control versus anti–PD-1 or bempegaldesleukin or anti–PD-1 plus bempegaldesleukin. Differences in survival were examined using logrank (Mantel–Cox) test. ns, not significant; *, $P < 0.05$; **, $P < 0.01$; ***, $P < 0.001$.

6. DISCUSSION

Here we characterized the significance of *JAK1/2* and *B2M* loss-of-function mutations in tumor cells as resistance mechanism to anti-PD-1 therapy. Our functional data showed that *JAK1/2* knockout mutations resulted in insensitivity to IFNγ-induced antitumor effects maintained the ability to be recognized and killed by T cells, while *B2M* knockout led to the lack of antigen presentation, cancer cell recognition and cytotoxicity by T cells. This information allowed us to design combinatorial strategies to successfully overcome these anti-PD-1 resistance mechanisms in mouse models.

We initially generated acquired resistant murine sublines from a MC38 syngeneic mouse model, a model that recapitulates cancers of high mutational burden and are particularly sensitive to the PD-1 blockade such as in MSI-high colorectal tumors (67). Resistant tumors grew progressively in fully immunocompetent syngeneic mice at the same rate as the parental controls. Despite clonal selection limitations by the CRISPR-Cas9 system, we showed that these established knockout tumors result in resistance to anti–PD-1 therapy. Our CyTOF data revealed that the expansion of terminally exhausted CD8+ T cells, which correlated with poor anti-PD-1 response (68,69), was enriched in *JAK1, JAK2* and *B2M* knockout tumors. This result suggested to us that these CD8+ T cells are seemingly impaired in their ability to efficiently kill tumor cells *in vivo* with defects of IFNγ signaling and antigen presentation.

Defects leading to lack of sensitivity to the IFN signaling pathway have been described as a mechanism of tumor escape and immunoresistance (70–75). Baseline *JAK1* or *JAK2* mutations are infrequent in human cancers, representing less than 1% of all cases (19), with an increase in incidence in *JAK1* mutations in endometrial carcinomas with microsatellite instability (MSI, 20,74,75). Interestingly, other study including TCGA cohorts suggested that tumors with chromosomal *CDKN2A* losses increased the susceptibility to resistance of IFNγ and

immunotherapy by concomitant *JAK2* losses (78) indicating additional genetic associations involved in the pathway. Therefore, the knowledge of the consequence of these key mutations in the IFN pathway, including *IFNAR1* (as a type I IFN signaling reference) help to understand the role of the pathway in the response and resistance to anti-PD-1 therapy.

Upon pressure from the immune system, some cancer cells may escape by developing an inactivating mutation in one JAK allele and losing the second wild-type allele, resulting in a homozygous loss-of-function mutation in the IFNγ response pathway. Such events have been documented in patients with melanoma treated with immune checkpoint blockade therapy with acquired resistance induced by mutations in *JAK1* or *JAK2* (18,21), and in patients with metastatic cervical cancer receiving adoptive cell transfer therapy with a TCR specific for the E6 viral antigen mediated by the development of mutations in the IFNγ receptor 1 (74). Our data suggest that once the tumor cells with *JAK1/2* knockout grow in vivo past the point of tumor implantation, then they become resistant to anti–PD-1 therapy due to the inability to respond to IFNγ and amplify the antitumor immune response.

The realization that IFN signaling by cancer cells is critical for anti–PD-1 response led us to hypothesize that changing the tumor microenvironment to have a strong IFN response by triggering pattern recognition receptors may overcome resistance due to lack of IFNγ signaling, and may improve the antitumor activity of immune checkpoint blockade therapy. Synthetic CpG-ODN agonists of TLR9 are being tested in the clinic in combination with the human anti–PD-1 antibody therapy. The combination of intratumoral SD-101 with pembrolizumab resulted in antitumor responses in patients with advanced melanoma who were refractory or resistant to prior anti–PD-1 therapy (79). In the same way, early clinical trials using two other TLR9 agonists, CMP-001 (80) and IMO-2125 (81), or the double-stranded RNA (poly I:C) BO-112

(82), in combination with immune checkpoint inhibitors, resulted in objective antitumor responses in patients who had previously progressed on treatment with anti–PD-1. Together, these clinical data validate our mouse model findings and suggest a strategic approach for overcoming resistance to PD-1 blockade therapy. We observed that the *JAK1/2*-knockout tumors were still being recognized by antigen-specific T cells and could lead to specific cytotoxicity independent of IFNγ signaling, which provides evidence that if a TLR9 agonist could reactivate type I IFN signaling in tumor microenvironment cells despite the cancer cells not being able to signal through the IFN receptor, then T cells will be able to exert antitumor activity.

Antitumor immune response involved in *JAK1*-knockout tumors was NK and CD4 T cell–dependent when treated with single-agent SD-101, observed preferentially expansion of innate immunity without the need of activation of both type I and II IFN signaling on tumor cells. These findings were consistent with the SD-101 retained antitumor efficacy against *IFNAR1*-knockout tumors deficient in type I IFN signaling. Surprisingly, the addition of anti–PD-1 improved antitumor response restoring the central function of CD8 T-cell effector, indicating that these tumors may sensitize to the synergistic effect of combined therapy. In contrast, *JAK2*-knockout tumors required mainly CD8+ T cells for tumor suppression, suggesting that the tumors deficient in type II IFN signaling became more favorable for CD8+ T-cell responses. Here, we postulate that the intratumoral injection of SD-101 in combination with a-PD-1 induce favorable changes in the tumor microenvironment, such as increased type I IFN response in tumor cells or pDCs, and increased chemokines CXCL9/10, which are lost in *JAK1/2*-knockout tumors.

In line with our study, other researchers have modeled preclinical approaches to overcome IFN-deficient resistant tumors. These strategies include the TLR3 agonist BO-112, a potent nanoplexed version of poly I:C was able to revert the resistance of *JAK1* deficient tumors to

adoptive T cell therapy by restoring MHC class I expression, and an oncolytic virus, vesicular stomatitis virus (VSV) for IFNγ dysregulated melanomas. Retinoic acid-inducible gene I (RIG-1), which is an essential pathogen recognition receptors sensing types of virus-derived double-stranded RNA, was triggered by an IFN-independent salvage pathway overcoming MHC-I APM silencing and resensitizes IFN-resistant JAK-STAT signaling–defective melanoma cells. All together highlighted the potential use of targets based on pattern recognition receptors (PPRs) to reverse resistance to a-PD-1 in IFN-deficient tumors.

Loss-of-function in *B2M* mutations have been reported in microsatellite stable and MSI-high colorectal (83), melanoma (22,84) and lung cancers (85), and promote resistance to immunotherapy mediated by loss of antigen presentation (18,22,23,25,33). Some studies have found the loss of *B2M* in biopsies from patients who respond to a-PD-1 (36,37,86), with corresponding supportive results when knocking out *B2M* in mouse models of immunotherapy (25,34), but the exact mechanism mediating this response remains unknown. We indirectly suggested that activation of MHC class I–independent CD4+ T cells or innate immune cells such as NK cells may contribute to *B2M*-deficient tumor response.

Bempegaldesleukin is a CD122 preferential IL2 pathway agonist that preferentially activates and expands effector CD4+ T, CD8+ T and NK cells (46,60). Combination therapy with bempegaldesleukin and nivolumab has shown encouraging objective responses in patients with treatment-naive melanoma regardless of baseline PD-L1 status and baseline levels of tumor-infiltrating lymphocytes (87–89). Consistent with our hypothesis, we obtained durable tumor responses with this combination in *B2M* knockout tumors. In line with the lack of MHC class I antigen presentation, depletion studies suggested that NK and CD4+ T cells, which are

not restricted by-MHC class I, play a key role in the antitumor immunity in *B2M*-knockout tumors.

Furthermore, Ardolino and colleagues (90) had also described that IL2 therapy could induce antitumor responses in a model of MHC class I–deficient mouse tumor, and other preclinical study (91) revealed that recombinant human IL2 combined with immune checkpoint inhibitors was more effective than either monotherapy by stimulating both CD8+ T cells and NK cells. These studies provide strong mechanistic support for a strategy of IL2-based therapy with anti–PD-1 for treating patients with MHC class I deficient tumors who have progressed on prior anti–PD-1 therapy, and may also enhance the antitumor activity in previously untreated tumors.

We provided the scientific basis of combinatorial therapies for patients whose tumors have not responded to anti-PD-1 therapy or other tumors capable of developing resistance in the same way. The combination therapies of PD-1 blockade, bempegaldesleukin (89) and toll-like receptor 9 (79–81) that were identified in the study are now being assessed in human clinical trials for patients with tumors have not responded to anti-PD-1 therapy.

7. CONCLUSIONS

1. Our study links the disruption of genes in the IFNγ receptor and antigen presentation pathways with mechanisms of resistance to PD-1 blockade therapy and gives clues to how cancer tries to escape and how we could reverse the resistance process.

2. Combination therapies aimed at increasing an interferon inflammatory intratumoral signaling response may broaden the antitumor activity of PD-1 blockade

3. Even in the extreme setting of genetic resistance to PD-1 blockade by *JAK1/2* loss of function mutation, resistance can be overcome by the intratumoral injection of a TLR9 agonist, whereas resistance through *B2M* loss can be overcome by an IL2 pathway agonist potently activating an antitumor CD4+ T cell and NK cell response. Our findings strongly support the testing of these rational combinatorial strategies in patients with such mechanisms of anti-PD-1 resistance.

8. FUTURE RESEARCH LINES

From a preclinical perspective

In our studies, we used the CRISPR/Cas9 gene-editing approach to generate murine and human cancer cell lines that replicate mechanisms of resistance to immune checkpoint blockade found in patient biopsies. This refined framework has allowed a defined understanding of the signaling networks being used by cancer cells to escape from an immune attack. Impressively, we had then taken this knowledge and used it to hypothesize how to overcome the cancer cell resistance to immunotherapy.

Thus, we reasoned that the activation of IFN signaling through pattern recognition receptors and the stimulation of CD4+ T cells and NK cells overcome genetic mechanisms of resistance to PD-1 blockade therapy mediated through deficient IFN receptor and antigen presentation pathways. Having already established murine models of immunotherapy resistance we are then positioned to continue to proactively explore other alternative therapeutic strategies that target emerging resistance mechanisms to prevent or inhibit resistance will have a direct translational impact on ongoing trials and improve the therapeutic outcome.

Novel combined approaches to treat tumors have become insensitive to interferon exploit the combination of immune checkpoint inhibitors with STING (stimulator of interferon gene) agonists that is capable of promoting STAT activation independent of *JAK2* (18) or oncolytic virotherapy may be more effective without the anti-viral activity of interferon-response genes and reactive PD-L1 expression (92). Other likely targets include additional immune checkpoint ligands that are not IFN-response genes and can provide this immune privilege such as adenosine A2A receptor (93,94); ICOS (inducible T cell co-stimulator); T cell immunoglobulin and ITIM domain (TIGIT, which counterbalances the costimulatory function of CD226); TIM3

(marker of exhaustion, also known as HAVCR2 or CD366) (95); and V-domain Ig suppressor of T cell activation (VISTA) known to inhibit T-cell function as well as promote the differentiation of naive T-cells into Tregs (96,97).

While alterations in *B2M* and APM have long been known as a route to resistance, the precise mechanisms of *B2M* inactivation among distinct tumor types or how the immune cells orchestrate the response between cancer cells and tumor microenvironment have not been characterized. We demonstrated that anti-PD-1 resistance in *B2M* loss could be overcome with the activation of NK cells and CD4+ T cells, and a very recent study also identified a unique role for CD4+ T cells in *Mlh1*/*B2M* knockout tumors (98). Thus, the knowledge of these effector mechanisms in these models would be of high interest, in particular because we could explain why some patients with *B2M* loss tumors are be able to respond to treatment.

Several strategies to enhance NK cells to recognize and destroy the tumor cells in MHC class I-deficient tumors have been investigated. Our findings corroborated the role of cytokine-based immunotherapy, as a potential strategy. Alternatively, consideration could also be a modified Interleukin 15 (IL15, NKTR-255) that expands more potently activate NK cells (99) might be used in combination with immune checkpoint inhibitors for future research in *B2M* loss tumors. The fact that CD8+ T cells could not orchestrate the response in these tumors is intriguing. Significant questions remain regarding the failure of NK-cell surveillance or the interplay between macrophage differentiation and CD4+ T cell might therefore be an attractive avenue warranting further study.

From a clinical perspective

The identification of specific mutations responsible for PD-1/PD-L1 resistance will inform the selection of patients who will likely respond or not respond to anti-PD1/PD-L1 therapy for advanced melanoma and other cancers. The results of these studies have direct implications for the design and interpretation of ongoing and planned studies combining targeted therapy and immunotherapy to prevent or treat resistance to cancer immunotherapy.

Based on our work we identify which strategies are best in combination and how best to improve immune responses based on underlying mechanisms to treat patients with cancer that are resistant to the first-generation immune checkpoint blockade therapies. In particular, our preclinical studies are guiding how best to use the clinical testing of combinations of anti-PD-1 immune activating antibodies with intratumoral Toll-Like Receptor 9 (TLR9) agonists (79–81) and provided compelling evidence that a combination of IL-2 pathway agonist, NKTR-214 with anti-PD-1, has effective antitumoral activity for *B2M* loss tumors. Furthermore, the results of these studies also support the clinical testing of anti-PD-1 immune activating antibodies with other strategies such as STING agonists, oncolytic viruses or cytokines in patients who are progressing on prior single-agent anti-PD-1 therapy (**Table 8**), although these require a better understanding of mechanisms of combinatorial synergy.

Table 8. Clinical trials investigating combination strategies in patients with tumors refractory to PD-1 blockade

Target	Drug	ICI	Tumor(s)*	Phase	Results	N	ORR	Identifier	Study
CTLA-4	Ipilimumab (low-dose)	pembrolizumab	Advanced melanoma	II	Y	67	**31%**, 4 pts with CR.	NCT02743819	Olson et al. (2020)
TIM3	MBG453	spartalizumab	Advanced solid tumors	I/Ib	Y	23	**4.3%**, 0% in melanoma cohort	NCT02608268	Mach et al. (2019)
GITR	MK-4166	pembrolizumab	Advanced solid tumors	I	Y	7	**0%**	NCT02132754	Papadopoulos et al. (2019)
LAG3	Relatlimab	nivolumab	Advanced melanoma (57% prior a-CTLA-4)	I/II	Y	61	**11.5%**, 1 pt with CR.	NCT01968109	Ascierto et al. (2017)
TLR3	BO-112 (i.t.)	nivolumab o pembrolizumab	Advanced solid tumors	I	Y	28	**10.7%**, 35.7% with SD.	NCT02828098	Marquez-Rodas et al (2020) (82)
TLR 7/8	BDB001		Advanced solid tumors	I	Y	32	**6%**	NCT04819373	Patel et al (2020)
TLR9	SD-101 (i.t.)	pembrolizumab	Advanced melanoma	Ib/II	Y	2 mg (n=31) 8 mg (n=30)	**19.4%** (2mg) **13.3%** (8 mg), 1 pt with CR.	NCT02521870	Ribas et al. (2018) (79), Milhem et al (2019)
	CMP-001 (i.t.) (Vidutolimod)	pembrolizumab	Advanced melanoma	Ib	Y	98	**23.5%**, 7 pts with CR.	NCT02680184	Milhem et al. (2020)
	IMO-2125 (i.t.) (Tilsotolimod)	ipilimumab	Advanced melanoma	I/II	Y	49	**22.4%**, 2 pts with CR.	NCT03445533	ILLUMINATE-204 Haymaker et al. (2021) (100)

STING	ADU-S100 (MIW815)	spartalizumab	Advanced solid tumors or lymphomas	I	Y	25	**8%**	NCT03172936	Meric-Bernstam et al. (2019)
Herpes Simplex	HF10 Canerpaturev (i.t).	ipilimumab	Advanced melanoma	II	Y	27	**7%**	NCT03153085	Isei, et al (2018)
	RP1 (i.t.)	nivolumab	Advanced melanoma	I/II	Y	25	**16%**	NCT03767348	Middleton, et al. (2020)
	T-VEC (i.t.)	pembrolizumab	Advanced melanoma	II	N			NCT02965716	
Adenovirus	ONCOS-102 (i.t.)	pembrolizumab	Advanced melanoma	I	Y	20	**35%**	NCT03003676	
Poliovirus	PVSRIPO (i.t.)	Anti-PD-1	Advanced melanoma	II	N			NCT04577807	LUMINOS-102
Cytokines	Tavokinogene Telseplasmid (i.t.)**	pembrolizumab	Advanced melanoma	II	Y	54	**30%**, 3 pts with CR.	NCT03132675	KEYNOTE 695 Daud et al. (2020)
	MEDI1191 (mRNA IL-12) (i.t.)	durvalumab	Advanced solid tumors	I	Y	6	2 pts with PR. (HNSCC and melanoma)	NCT03946800	Hamid et al. (2021)
	IL-2 (i.t.)	pembrolizumab + RT	Advanced solid tumors	I/II	N			NCT03474497	
TIL	E7 TCR T cells		Human Papillomavirus-Associated Cancers	I/II	Y	8	**50%**	NCT02858310	Nagarsheth, et al. (2021) (101)

TIL	LN-144, lifileucel		Advanced melanoma (80% prior a-CTLA-4)	II	Y	66	**36.4%**, 4.5% with CR.	NCT02360579	C-144-01 Chesney, et al. (2021)
FMT	Fecal microbiota transplant		Advanced melanoma	I	Y	10	**30%**, 1 pt with CR.	NCT03341143	Baruch et al. (2021) (102)
mRna FixVAc	mRNA-based BNT111 FixVac	cemiplimab	Advanced melanoma	II	N			NCT04526899	
HDAC	Domatinostat (4SC-202)	pembrolizumab	Advanced melanoma	I/II	N			NCT03278665	
TIGIT or VEGRF1-3	Vibostolimab or Lenvatinib	pembrolizumab + quavonlimab	Advanced melanoma	I/II	N			NCT04305041	
VEGFR1-3	Axitinib	nivolumab	Advanced melanoma	II	N			NCT04493203	

* Must have received prior PD-1
** tavo, pIL 12 plus Electroporation (ImmunoPulse)
ORR, overall response rate; CR, complete response; SD, stable disease, TIL, Tumor infiltrating lymphocytes therapy; i.t. intratumoral; pt, patient.

9. BIBLIOGRAPHY

1. Bray F, Jemal A, Grey N, Ferlay J, Forman D. Global cancer transitions according to the Human Development Index (2008–2030): a population-based study. The Lancet Oncology. 2012 Aug;13(8):790–801.

2. Bray F, Ferlay J, Soerjomataram I, Siegel RL, Torre LA, Jemal A. Global cancer statistics 2018: GLOBOCAN estimates of incidence and mortality worldwide for 36 cancers in 185 countries. CA: A Cancer Journal for Clinicians. 2018 Nov;68(6):394–424.

3. Leach DR, Krummel MF, Allison JP. Enhancement of Antitumor Immunity by CTLA-4 Blockade. Science. 1996 Mar 22;271(5256):1734–6.

4. Chambers CA, Kuhns MS, Egen JG, Allison JP. CTLA-4-mediated inhibition in regulation of T cell responses: mechanisms and manipulation in tumor immunotherapy. Annu Rev Immunol. 2001;19:565–94.

5. Hui E, Cheung J, Zhu J, Su X, Taylor MJ, Wallweber HA, et al. T cell costimulatory receptor CD28 is a primary target for PD-1–mediated inhibition. Science. 2017 Mar 31;355(6332):1428–33.

6. Kamphorst AO, Wieland A, Nasti T, Yang S, Zhang R, Barber DL, et al. Rescue of exhausted CD8 T cells by PD-1–targeted therapies is CD28-dependent. Science. 2017 Mar 31;355(6332):1423–7.

7. Sharma P, Hu-Lieskovan S, Wargo JA, Ribas A. Primary, Adaptive, and Acquired Resistance to Cancer Immunotherapy. Cell. 2017 Feb;168(4):707–23.

8. Gide TN, Wilmott JS, Scolyer RA, Long GV. Primary and Acquired Resistance to Immune Checkpoint Inhibitors in Metastatic Melanoma. Clin Cancer Res. 2018 Mar 15;24(6):1260–70.

9. Kalbasi A, Ribas A. Tumour-intrinsic resistance to immune checkpoint blockade. Nat Rev Immunol. 2020 Jan;20(1):25–39.

10. Yang Y, Xiang Z, Ertl HC, Wilson JM. Upregulation of class I major histocompatibility complex antigens by interferon gamma is necessary for T-cell-mediated elimination of recombinant adenovirus-infected hepatocytes in vivo. Proceedings of the National Academy of Sciences. 1995 Aug 1;92(16):7257–61.

11. Grasso CS, Tsoi J, Onyshchenko M, Abril-Rodriguez G, Ross-Macdonald P, Wind-Rotolo M, et al. Conserved Interferon-γ Signaling Drives Clinical Response to Immune Checkpoint Blockade Therapy in Melanoma. Cancer Cell. 2020 Oct;38(4):500-515.e3.

12. Pardoll DM. The blockade of immune checkpoints in cancer immunotherapy. Nat Rev Cancer. 2012 Apr;12(4):252–64.

13. Ribas A. Adaptive Immune Resistance: How Cancer Protects from Immune Attack. Cancer Discovery. 2015 Sep;5(9):915–9.

14. Garcia-Diaz A, Shin DS, Moreno BH, Saco J, Escuin-Ordinas H, Rodriguez GA, et al. Interferon Receptor Signaling Pathways Regulating PD-L1 and PD-L2 Expression. Cell Reports. 2017 May;19(6):1189–201.

15. Leone P, Shin E-C, Perosa F, Vacca A, Dammacco F, Racanelli V. MHC Class I Antigen Processing and Presenting Machinery: Organization, Function, and Defects in Tumor Cells. JNCI Journal of the National Cancer Institute. 2013 Aug 21;105(16):1172–87.

16. D'Urso CM, Wang ZG, Cao Y, Tatake R, Zeff RA, Ferrone S. Lack of HLA class I antigen expression by cultured melanoma cells FO-1 due to a defect in B2m gene expression. J Clin Invest. 1991 Jan 1;87(1):284–92.

17. Restifo NP, Marincola FM, Kawakami Y, Taubenberger J, Yannelli JR, Rosenberg SA. Loss of Functional Beta2-Microglobulin in Metastatic Melanomas From Five Patients Receiving Immunotherapy. JNCI Journal of the National Cancer Institute. 1996 Jan 17;88(2):100–8.

18. Zaretsky JM, Garcia-Diaz A, Shin DS, Escuin-Ordinas H, Hugo W, Hu-Lieskovan S, et al. Mutations Associated with Acquired Resistance to PD-1 Blockade in Melanoma. N Engl J Med. 2016 Sep;375(9):819–29.

19. Shin DS, Zaretsky JM, Escuin-Ordinas H, Garcia-Diaz A, Hu-Lieskovan S, Kalbasi A, et al. Primary Resistance to PD-1 Blockade Mediated by *JAK1/2* Mutations. Cancer Discov. 2017 Feb;7(2):188–201.

20. Albacker LA, Wu J, Smith P, Warmuth M, Stephens PJ, Zhu P, et al. Loss of function JAK1 mutations occur at high frequency in cancers with microsatellite instability and are suggestive of immune evasion. Reis RM, editor. PLoS ONE. 2017 Nov 9;12(11):e0176181.

21. Sucker A, Zhao F, Pieper N, Heeke C, Maltaner R, Stadtler N, et al. Acquired IFNγ resistance impairs anti-tumor immunity and gives rise to T-cell-resistant melanoma lesions. Nat Commun. 2017 Aug;8(1):15440.

22. Sade-Feldman M, Jiao YJ, Chen JH, Rooney MS, Barzily-Rokni M, Eliane J-P, et al. Resistance to checkpoint blockade therapy through inactivation of antigen presentation. Nat Commun. 2017 Dec;8(1):1136.

23. Huang AC, Orlowski RJ, Xu X, Mick R, George SM, Yan PK, et al. A single dose of neoadjuvant PD-1 blockade predicts clinical outcomes in resectable melanoma. Nat Med. 2019 Mar;25(3):454–61.

24. Lee JH, Shklovskaya E, Lim SY, Carlino MS, Menzies AM, Stewart A, et al. Transcriptional downregulation of MHC class I and melanoma de- differentiation in resistance to PD-1 inhibition. Nat Commun. 2020 Dec;11(1):1897.

25. Gettinger S, Choi J, Hastings K, Truini A, Datar I, Sowell R, et al. Impaired HLA Class I Antigen Processing and Presentation as a Mechanism of Acquired Resistance to Immune Checkpoint Inhibitors in Lung Cancer. Cancer Discov. 2017 Dec;7(12):1420–35.

26. Manguso RT, Pope HW, Zimmer MD, Brown FD, Yates KB, Miller BC, et al. In vivo CRISPR screening identifies Ptpn2 as a cancer immunotherapy target. Nature. 2017 Jul;547(7664):413–8.

27. Patel SJ, Sanjana NE, Kishton RJ, Eidizadeh A, Vodnala SK, Cam M, et al. Identification of essential genes for cancer immunotherapy. Nature. 2017 Aug;548(7669):537–42.

28. Pan D, Kobayashi A, Jiang P, Ferrari de Andrade L, Tay RE, Luoma AM, et al. A major chromatin regulator determines resistance of tumor cells to T cell–mediated killing. Science. 2018 Feb 16;359(6377):770–5.

29. Kearney CJ, Vervoort SJ, Hogg SJ, Ramsbottom KM, Freeman AJ, Lalaoui N, et al. Tumor immune evasion arises through loss of TNF sensitivity. Sci Immunol. 2018 May 18;3(23):eaar3451.

30. Vredevoogd DW, Kuilman T, Ligtenberg MA, Boshuizen J, Stecker KE, de Bruijn B, et al. Augmenting Immunotherapy Impact by Lowering Tumor TNF Cytotoxicity Threshold. Cell. 2019 Jul;178(3):585-599.e15.

31. Hellmann MD, Nathanson T, Rizvi H, Creelan BC, Sanchez-Vega F, Ahuja A, et al. Genomic Features of Response to Combination Immunotherapy in Patients with Advanced Non-Small-Cell Lung Cancer. Cancer Cell. 2018 May;33(5):843-852.e4.

32. Riaz N, Havel JJ, Makarov V, Desrichard A, Urba WJ, Sims JS, et al. Tumor and Microenvironment Evolution during Immunotherapy with Nivolumab. Cell. 2017 Nov;171(4):934-949.e16.

33. Miao D, Margolis CA, Gao W, Voss MH, Li W, Martini DJ, et al. Genomic correlates of response to immune checkpoint therapies in clear cell renal cell carcinoma. Science. 2018 Feb 16;359(6377):801–6.

34. Benci JL, Johnson LR, Choa R, Xu Y, Qiu J, Zhou Z, et al. Opposing Functions of Interferon Coordinate Adaptive and Innate Immune Responses to Cancer Immune Checkpoint Blockade. Cell. 2019 Aug;178(4):933-948.e14.

35. Liu D, Schilling B, Liu D, Sucker A, Livingstone E, Jerby-Amon L, et al. Integrative molecular and clinical modeling of clinical outcomes to PD1 blockade in patients with metastatic melanoma. Nat Med. 2019 Dec;25(12):1916–27.

36. Rizvi H, Sanchez-Vega F, La K, Chatila W, Jonsson P, Halpenny D, et al. Molecular Determinants of Response to Anti–Programmed Cell Death (PD)-1 and Anti–Programmed Death-Ligand 1 (PD-L1) Blockade in Patients With Non–Small-Cell Lung Cancer Profiled With Targeted Next-Generation Sequencing. JCO. 2018 Mar;36(7):633–41.

37. Rodig SJ, Gusenleitner D, Jackson DG, Gjini E, Giobbie-Hurder A, Jin C, et al. MHC proteins confer differential sensitivity to CTLA-4 and PD-1 blockade in untreated metastatic melanoma. Sci Transl Med. 2018 Jul 18;10(450):eaar3342.

38. Blank CU, Rozeman EA, Fanchi LF, Sikorska K, van de Wiel B, Kvistborg P, et al. Neoadjuvant versus adjuvant ipilimumab plus nivolumab in macroscopic stage III melanoma. Nat Med. 2018 Nov;24(11):1655–61.

39. Paulson KG, Voillet V, McAfee MS, Hunter DS, Wagener FD, Perdicchio M, et al. Acquired cancer resistance to combination immunotherapy from transcriptional loss of class I HLA. Nat Commun. 2018 Dec;9(1):3868.

40. Patel SA, Minn AJ. Combination Cancer Therapy with Immune Checkpoint Blockade: Mechanisms and Strategies. Immunity. 2018 Mar;48(3):417–33.

41. Siegal FP. The Nature of the Principal Type 1 Interferon-Producing Cells in Human Blood. Science. 1999 Jun 11;284(5421):1835–7.

42. Rezvani K, Rouce R, Liu E, Shpall E. Engineering Natural Killer Cells for Cancer Immunotherapy. Molecular Therapy. 2017 Aug;25(8):1769–81.

43. Kärre K, Ljunggren HG, Piontek G, Kiessling R. Selective rejection of H–2-deficient lymphoma variants suggests alternative immune defence strategy. Nature. 1986 Feb;319(6055):675–8.

44. Bix M, Liao N-S, Zijlstra M, Loring J, Jaenisch R, Raulet D. Rejection of class I MHC-deficient haemopoietic cells by irradiated MHC-matched mice. Nature. 1991 Jan;349(6307):329–31.

45. Mitra S, Leonard WJ. Biology of IL-2 and its therapeutic modulation: Mechanisms and strategies. J Leukoc Biol. 2018 Apr;103(4):643–55.

46. Charych D, Khalili S, Dixit V, Kirk P, Chang T, Langowski J, et al. Modeling the receptor pharmacology, pharmacokinetics, and pharmacodynamics of NKTR-214, a kinetically-controlled interleukin-2 (IL2) receptor agonist for cancer immunotherapy. Tsirka SE, editor. PLoS ONE. 2017 Jul 5;12(7):e0179431.

47. Parisi G, Saco JD, Salazar FB, Tsoi J, Krystofinski P, Puig-Saus C, et al. Persistence of adoptively transferred T cells with a kinetically engineered IL-2 receptor agonist. Nat Commun. 2020 Dec;11(1):660.

48. Homet Moreno B, Zaretsky JM, Garcia-Diaz A, Tsoi J, Parisi G, Robert L, et al. Response to Programmed Cell Death-1 Blockade in a Murine Melanoma Syngeneic Model Requires Costimulation, CD4, and CD8 T Cells. Cancer Immunology Research. 2016 Oct 1;4(10):845–57.

49. Mosely SIS, Prime JE, Sainson RCA, Koopmann J-O, Wang DYQ, Greenawalt DM, et al. Rational Selection of Syngeneic Preclinical Tumor Models for Immunotherapeutic Drug Discovery. Cancer Immunol Res. 2017 Jan;5(1):29–41.

50. Ran FA, Hsu PD, Wright J, Agarwala V, Scott DA, Zhang F. Genome engineering using the CRISPR-Cas9 system. Nat Protoc. 2013 Nov;8(11):2281–308.

51. Brinkman EK, Chen T, Amendola M, van Steensel B. Easy quantitative assessment of genome editing by sequence trace decomposition. Nucleic Acids Research. 2014 Dec 16;42(22):e168–e168.

52. Kim D, Langmead B, Salzberg SL. HISAT: a fast spliced aligner with low memory requirements. Nat Methods. 2015 Apr;12(4):357–60.

53. Anders S, Pyl PT, Huber W. HTSeq--a Python framework to work with high-throughput sequencing data. Bioinformatics. 2015 Jan 15;31(2):166–9.

54. Subramanian A, Tamayo P, Mootha VK, Mukherjee S, Ebert BL, Gillette MA, et al. Gene set enrichment analysis: A knowledge-based approach for interpreting genome-wide expression profiles. Proceedings of the National Academy of Sciences. 2005 Oct 25;102(43):15545–50.

55. Kanehisa M. KEGG: Kyoto Encyclopedia of Genes and Genomes. Nucleic Acids Research. 2000 Jan 1;28(1):27–30.

56. Fabregat A, Jupe S, Matthews L, Sidiropoulos K, Gillespie M, Garapati P, et al. The Reactome Pathway Knowledgebase. Nucleic Acids Research. 2018 Jan 4;46(D1):D649–55.

57. Wickham H. ggplot2 [Internet]. Cham: Springer International Publishing; 2016 [cited 2019 Aug 20]. (Use R!). Available from: http://link.springer.com/10.1007/978-3-319-24277-4

58. Escuin-Ordinas H, Atefi M, Fu Y, Cass A, Ng C, Huang RR, et al. COX-2 inhibition prevents the appearance of cutaneous squamous cell carcinomas accelerated by BRAF inhibitors. Molecular Oncology. 2014 Mar;8(2):250–60.

59. Marshall JD, Fearon KL, Higgins D, Hessel EM, Kanzler H, Abbate C, et al. Superior Activity of the Type C Class of ISS *In Vitro* and *In Vivo* Across Multiple Species. DNA and Cell Biology. 2005 Feb;24(2):63–72.

60. Charych DH, Hoch U, Langowski JL, Lee SR, Addepalli MK, Kirk PB, et al. NKTR-214, an Engineered Cytokine with Biased IL2 Receptor Binding, Increased Tumor Exposure, and Marked Efficacy in Mouse Tumor Models. Clinical Cancer Research. 2016 Feb 1;22(3):680–90.

61. Wei SC, Levine JH, Cogdill AP, Zhao Y, Anang N-AAS, Andrews MC, et al. Distinct Cellular Mechanisms Underlie Anti-CTLA-4 and Anti-PD-1 Checkpoint Blockade. Cell. 2017 Sep;170(6):1120-1133.e17.

62. Chen H, Lau MC, Wong MT, Newell EW, Poidinger M, Chen J. Cytofkit: A Bioconductor Package for an Integrated Mass Cytometry Data Analysis Pipeline. Schneidman D, editor. PLoS Comput Biol. 2016 Sep 23;12(9):e1005112.

63. Hu Z, Jujjavarapu C, Hughey JJ, Andorf S, Lee H-C, Gherardini PF, et al. MetaCyto: A Tool for Automated Meta-analysis of Mass and Flow Cytometry Data. Cell Reports. 2018 Jul;24(5):1377–88.

64. Parker BS, Rautela J, Hertzog PJ. Antitumour actions of interferons: implications for cancer therapy. Nat Rev Cancer. 2016 Mar;16(3):131–44.

65. Chodon T, Comin-Anduix B, Chmielowski B, Koya RC, Wu Z, Auerbach M, et al. Adoptive Transfer of MART-1 T-Cell Receptor Transgenic Lymphocytes and Dendritic Cell Vaccination in Patients with Metastatic Melanoma. Clinical Cancer Research. 2014 May 1;20(9):2457–65.

66. Johnson LA, Morgan RA, Dudley ME, Cassard L, Yang JC, Hughes MS, et al. Gene therapy with human and mouse T-cell receptors mediates cancer regression and targets normal tissues expressing cognate antigen. Blood. 2009 Jul 16;114(3):535–46.

67. Efremova M, Rieder D, Klepsch V, Charoentong P, Finotello F, Hackl H, et al. Targeting immune checkpoints potentiates immunoediting and changes the dynamics of tumor evolution. Nat Commun. 2018 Dec;9(1):32.

68. Thommen DS, Schumacher TN. T Cell Dysfunction in Cancer. Cancer Cell. 2018 Apr;33(4):547–62.

69. Miller BC, Sen DR, Al Abosy R, Bi K, Virkud YV, LaFleur MW, et al. Subsets of exhausted CD8+ T cells differentially mediate tumor control and respond to checkpoint blockade. Nat Immunol. 2019 Mar;20(3):326–36.

70. Dunn GP, Bruce AT, Ikeda H, Old LJ, Schreiber RD. Cancer immunoediting: from immunosurveillance to tumor escape. Nat Immunol. 2002 Nov;3(11):991–8.

71. Kaplan DH, Shankaran V, Dighe AS, Stockert E, Aguet M, Old LJ, et al. Demonstration of an interferon -dependent tumor surveillance system in immunocompetent mice. Proceedings of the National Academy of Sciences. 1998 Jun 23;95(13):7556–61.

72. Dunn GP, Sheehan KCF, Old LJ, Schreiber RD. IFN Unresponsiveness in LNCaP Cells Due to the Lack of *JAK1* Gene Expression. Cancer Res. 2005 Apr 15;65(8):3447–53.

73. Fish EN, Platanias LC. Interferon Receptor Signaling in Malignancy: A Network of Cellular Pathways Defining Biological Outcomes. Molecular Cancer Research. 2014 Dec 1;12(12):1691–703.

74. Doran SL, Stevanović S, Adhikary S, Gartner JJ, Jia L, Kwong MLM, et al. T-Cell Receptor Gene Therapy for Human Papillomavirus–Associated Epithelial Cancers: A First-in-Human, Phase I/II Study. JCO. 2019 Oct 20;37(30):2759–68.

75. Nguyen T-T, Ramsay L, Ahanfeshar-Adams M, Lajoie M, Schadendorf D, Alain T, et al. Mutations in the IFNγ-JAK-STAT pathway causing resistance to immune checkpoint inhibitors in melanoma increase sensitivity to oncolytic virus treatment. Clin Cancer Res. 2021 Feb 16;clincanres.3365.2020.

76. Ren Y, Zhang Y, Liu RZ, Fenstermacher DA, Wright KL, Teer JK, et al. JAK1 truncating mutations in gynecologic cancer define new role of cancer-associated protein tyrosine kinase aberrations. Sci Rep. 2013 Nov;3(1):3042.

77. Stelloo E, Versluis MA, Nijman HW, de Bruyn M, Plat A, Osse EM, et al. Microsatellite instability derived *JAK1* frameshift mutations are associated with tumor immune evasion in endometrioid endometrial cancer. Oncotarget. 2016 Jun 28;7(26):39885–93.

78. Horn S, Leonardelli S, Sucker A, Schadendorf D, Griewank KG, Paschen A. Tumor CDKN2A-Associated JAK2 Loss and Susceptibility to Immunotherapy Resistance. JNCI: Journal of the National Cancer Institute. 2018 Jun 1;110(6):677–81.

79. Ribas A, Medina T, Kummar S, Amin A, Kalbasi A, Drabick JJ, et al. SD-101 in Combination with Pembrolizumab in Advanced Melanoma: Results of a Phase Ib, Multicenter Study. Cancer Discov. 2018 Oct;8(10):1250–7.

80. Milhem M, Zakharia Y, Davar D, Buchbinder E, Medina T, Daud A, et al. O85 Durable responses in anti-PD-1 refractory melanoma following intratumoral injection of a toll-like receptor 9 (TLR9) agonist, CMP-001, in combination with pembrolizumab. J Immunother Cancer. 2020 Apr;8(Suppl 1):A2.2-A3.

81. Diab A, Rahimian S, Haymaker CL, Bernatchez C, Andtbacka RHI, James M, et al. A phase 2 study to evaluate the safety and efficacy of Intratumoral (IT) injection of the TLR9 agonist IMO-2125 (IMO) in combination with ipilimumab (ipi) in PD-1 inhibitor refractory melanoma. JCO. 2018 May 20;36(15_suppl):9515–9515.

82. Márquez-Rodas I, Longo F, Rodriguez-Ruiz ME, Calles A, Ponce S, Jove M, et al. Intratumoral nanoplexed poly I:C BO-112 in combination with systemic anti–PD-1 for patients with anti–PD-1–refractory tumors. Sci Transl Med. 2020 Oct 14;12(565):eabb0391.

83. Grasso CS, Giannakis M, Wells DK, Hamada T, Mu XJ, Quist M, et al. Genetic Mechanisms of Immune Evasion in Colorectal Cancer. Cancer Discov. 2018 Jun;8(6):730–49.

84. del Campo AB, Kyte JA, Carretero J, Zinchencko S, Méndez R, González-Aseguinolaza G, et al. Immune escape of cancer cells with beta2-microglobulin loss over the course of metastatic melanoma: Immune escape of cancer cells. Int J Cancer. 2014 Jan 1;134(1):102–13.

85. McGranahan N, Rosenthal R, Hiley CT, Rowan AJ, Watkins TBK, Wilson GA, et al. Allele-Specific HLA Loss and Immune Escape in Lung Cancer Evolution. Cell. 2017 Nov;171(6):1259-1271.e11.

86. Middha S, Yaeger R, Shia J, Stadler ZK, King S, Guercio S, et al. Majority of *B2M* -Mutant and -Deficient Colorectal Carcinomas Achieve Clinical Benefit From Immune Checkpoint Inhibitor Therapy and Are Microsatellite Instability-High. JCO Precision Oncology. 2019 Dec;(3):1–14.

87. Hurwitz ME, Cho DC, Balar AV, Curti BD, Siefker-Radtke AO, Sznol M, et al. Baseline tumor-immune signatures associated with response to bempegaldesleukin (NKTR-214) and nivolumab. JCO. 2019 May 20;37(15_suppl):2623–2623.

88. Sharma M, Khong H, Fa'ak F, Bentebibel S-E, Janssen LME, Chesson BC, et al. Bempegaldesleukin selectively depletes intratumoral Tregs and potentiates T cell-mediated cancer therapy. Nat Commun. 2020 Dec;11(1):661.

89. Diab A, Tannir NM, Bentebibel S-E, Hwu P, Papadimitrakopoulou V, Haymaker C, et al. Bempegaldesleukin (NKTR-214) plus Nivolumab in Patients with Advanced Solid Tumors: Phase I Dose-Escalation Study of Safety, Efficacy, and Immune Activation (PIVOT-02). Cancer Discov. 2020 Aug;10(8):1158–73.

90. Ardolino M, Azimi CS, Iannello A, Trevino TN, Horan L, Zhang L, et al. Cytokine therapy reverses NK cell anergy in MHC-deficient tumors. J Clin Invest. 2014 Nov 3;124(11):4781–94.

91. Hutmacher C, Gonzalo Núñez N, Liuzzi AR, Becher B, Neri D. Targeted Delivery of IL2 to the Tumor Stroma Potentiates the Action of Immune Checkpoint Inhibitors by Preferential Activation of NK and CD8 $^{+}$ T Cells. Cancer Immunol Res. 2019 Apr;7(4):572–83.

92. Ribas A, Dummer R, Puzanov I, VanderWalde A, Andtbacka RHI, Michielin O, et al. Oncolytic Virotherapy Promotes Intratumoral T Cell Infiltration and Improves Anti-PD-1 Immunotherapy. Cell. 2017 Sep;170(6):1109-1119.e10.

93. Vijayan D, Young A, Teng MWL, Smyth MJ. Targeting immunosuppressive adenosine in cancer. Nat Rev Cancer. 2017 Dec;17(12):709–24.

94. Chen L, Diao L, Yang Y, Yi X, Rodriguez BL, Li Y, et al. CD38-Mediated Immunosuppression as a Mechanism of Tumor Cell Escape from PD-1/PD-L1 Blockade. Cancer Discov. 2018 Sep;8(9):1156–75.

95. Sun F, Guo ZS, Gregory AD, Shapiro SD, Xiao G, Qu Z. Dual but not single PD-1 or TIM-3 blockade enhances oncolytic virotherapy in refractory lung cancer. J Immunother Cancer. 2020 May;8(1).

96. Le Mercier I, Chen W, Lines JL, Day M, Li J, Sergent P, et al. VISTA Regulates the Development of Protective Antitumor Immunity. Cancer Res. 2014 Apr 1;74(7):1933–44.

97. Kakavand H, Jackett LA, Menzies AM, Gide TN, Carlino MS, Saw RPM, et al. Negative immune checkpoint regulation by VISTA: a mechanism of acquired resistance to anti-PD-1 therapy in metastatic melanoma patients. Mod Pathol. 2017 Dec;30(12):1666–76.

98. Germano G, Lu S, Rospo G, Lamba S, Rousseau B, Fanelli S, et al. CD4 T cell dependent rejection of beta 2 microglobulin null mismatch repair deficient tumors. Cancer Discov. 2021 Mar 2;candisc.0987.2020.

99. Miyazaki T, Kivimäe S, Hennessy M, Pena R, Quach P, Moffet A, et al. NKTR-255, a Polymer-Conjugated IL-15 Enhances Antibody-Dependent Cellular Cytotoxicity Mediated By NK Cells in a B Cell Lymphoma Model. Blood. 2019 Nov 13;134(Supplement_1):5302–5302.

100. Haymaker C, Johnson DH, Murthy R, Bentebibel S-E, Uemura MI, Hudgens CW, et al. Tilsotolimod with ipilimumab drives tumor responses in anti-PD-1 refractory melanoma. Cancer Discov. 2021 Mar 11;candisc.1546.2020.

101. Nagarsheth NB, Norberg SM, Sinkoe AL, Adhikary S, Meyer TJ, Lack JB, et al. TCR-engineered T cells targeting E7 for patients with metastatic HPV-associated epithelial cancers. Nat Med. 2021 Mar;27(3):419–25.

102. Baruch EN, Youngster I, Ben-Betzalel G, Ortenberg R, Lahat A, Katz L, et al. Fecal microbiota transplant promotes response in immunotherapy-refractory melanoma patients. Science. 2021 Feb 5;371(6529):602–9.

10. ANNEXES

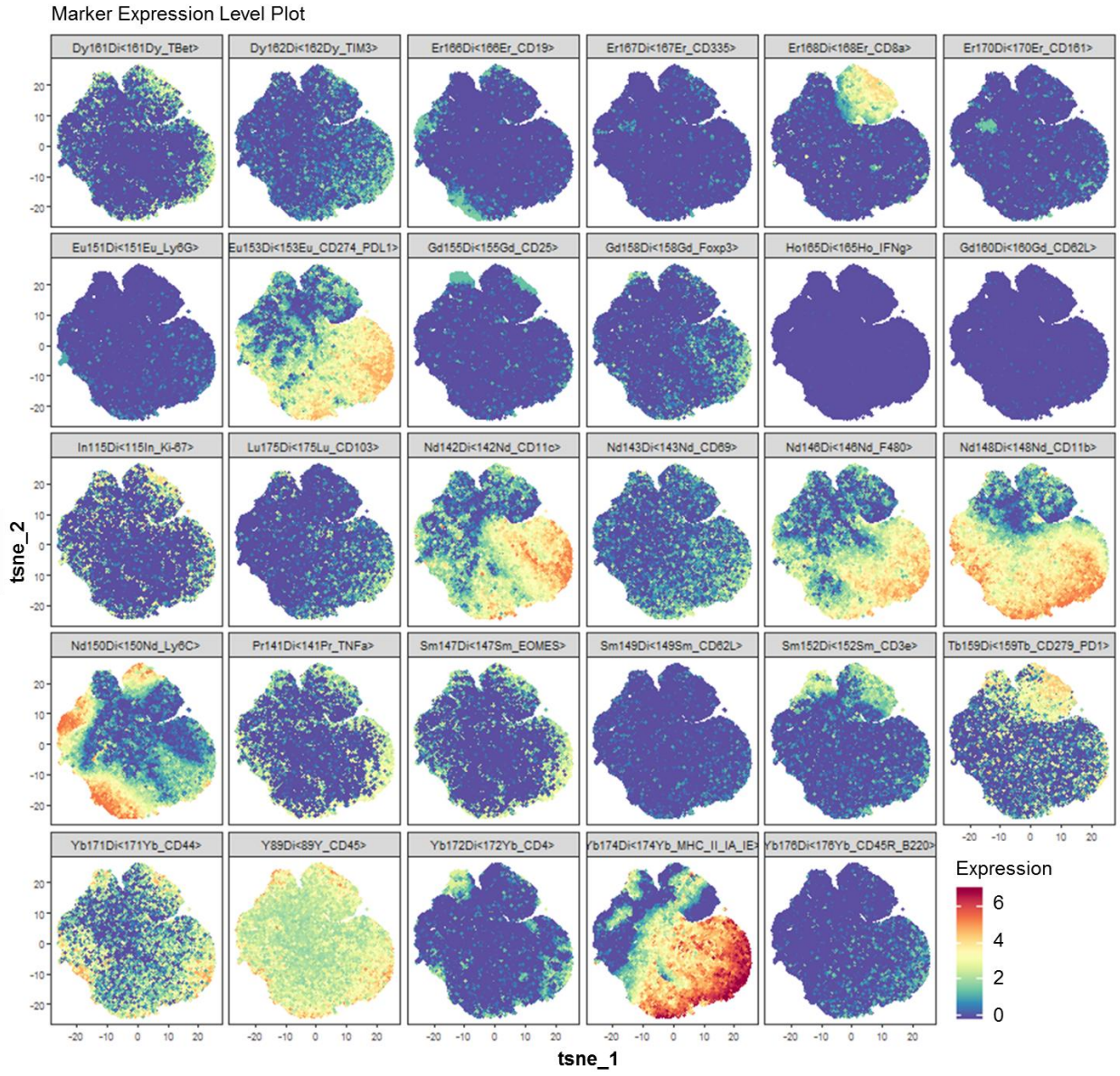

Supplementary Figure 1. Modeling resistance to PD1-blockade: t-SNE plots of total CD45+ cells from all samples overlaid with the expression of selected markers.

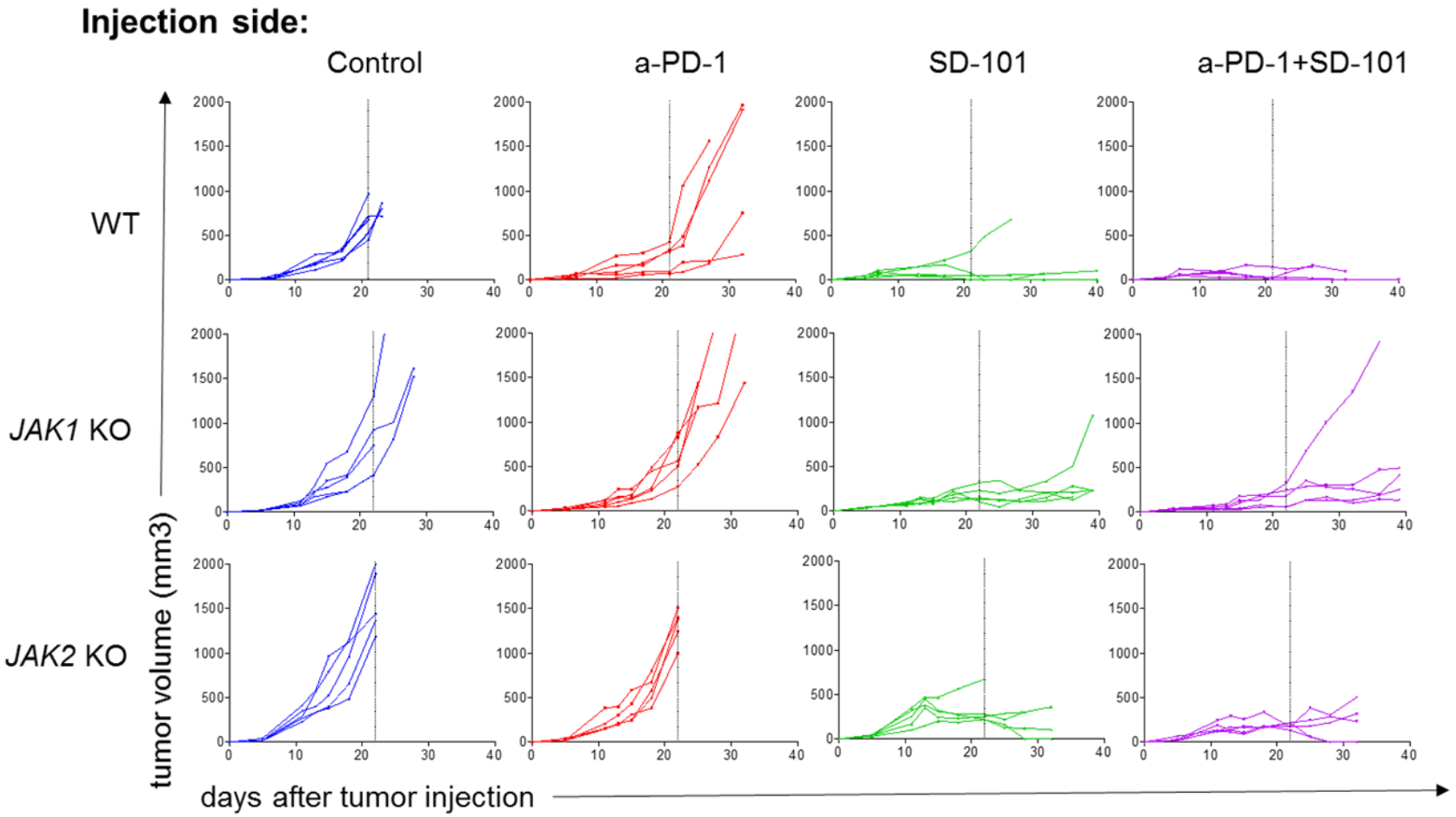

Supplementary Figure 2. An intratumoral TLR-9 agonist (SD-101) to reverse resistance to anti-PD-1 therapy. *In vivo* tumor growth curves of individual C57/BL6 mice after control-PBS, anti-PD-1, SD-101 or anti-PD-1 plus SD-101 in injection sites.

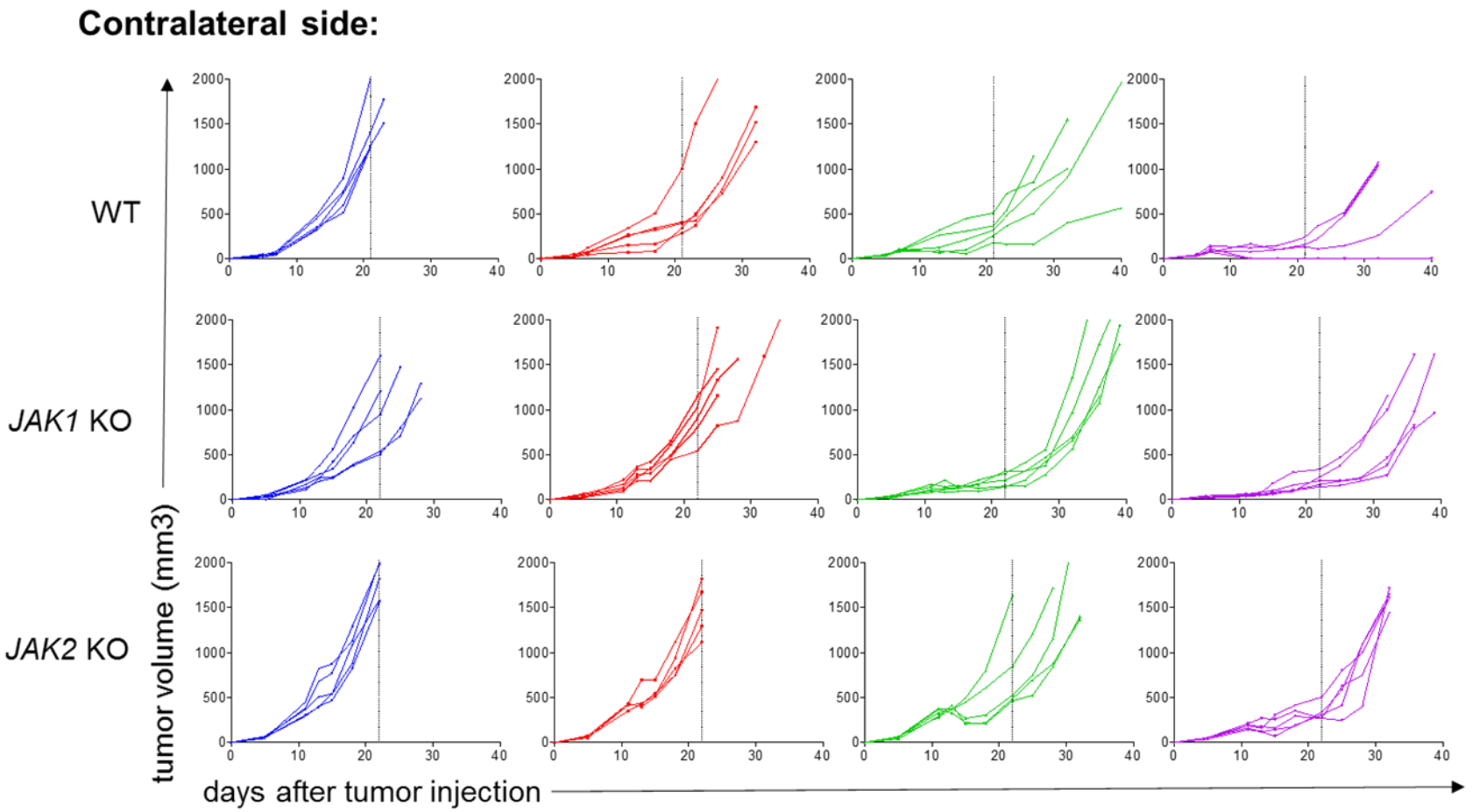

Supplementary Figure 3: An intratumoral TLR-9 agonist (SD-101) to reverse resistance to anti-PD-1 therapy. *In vivo* tumor growth curves of individual C57/BL6 mice after control-PBS, anti-PD-1, SD-101 or anti-PD-1 plus SD-101 in non-injection or contralateral sites.

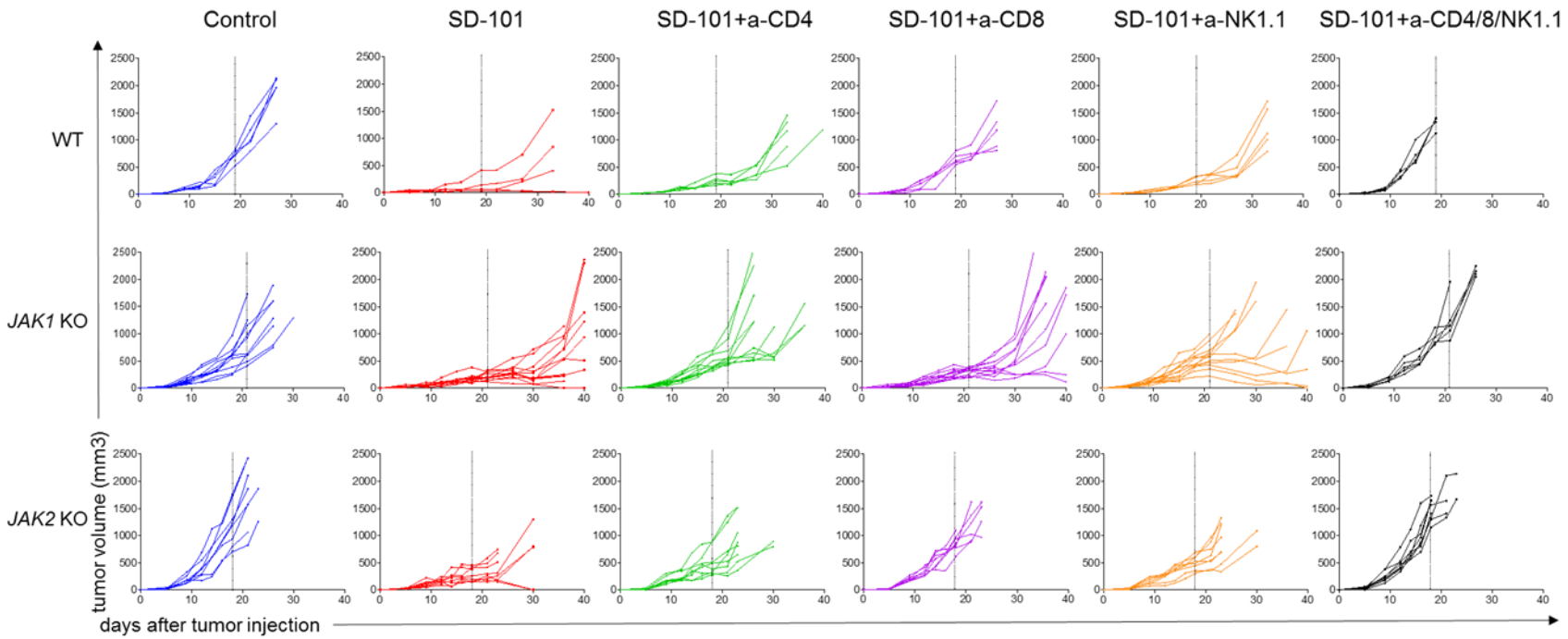

Supplementary Figure 4. *In vivo* depletion studies with intratumoral TLR-9 agonist. *In vivo* tumor growth curves of individual C57/BL6 mice for wild-type control and *JAK1/2* knockout resistant tumors with anti-CD4, anti-CD8 and anti-NK1.1 depletion studies after intratumoral (i.t) SD-101 therapy,

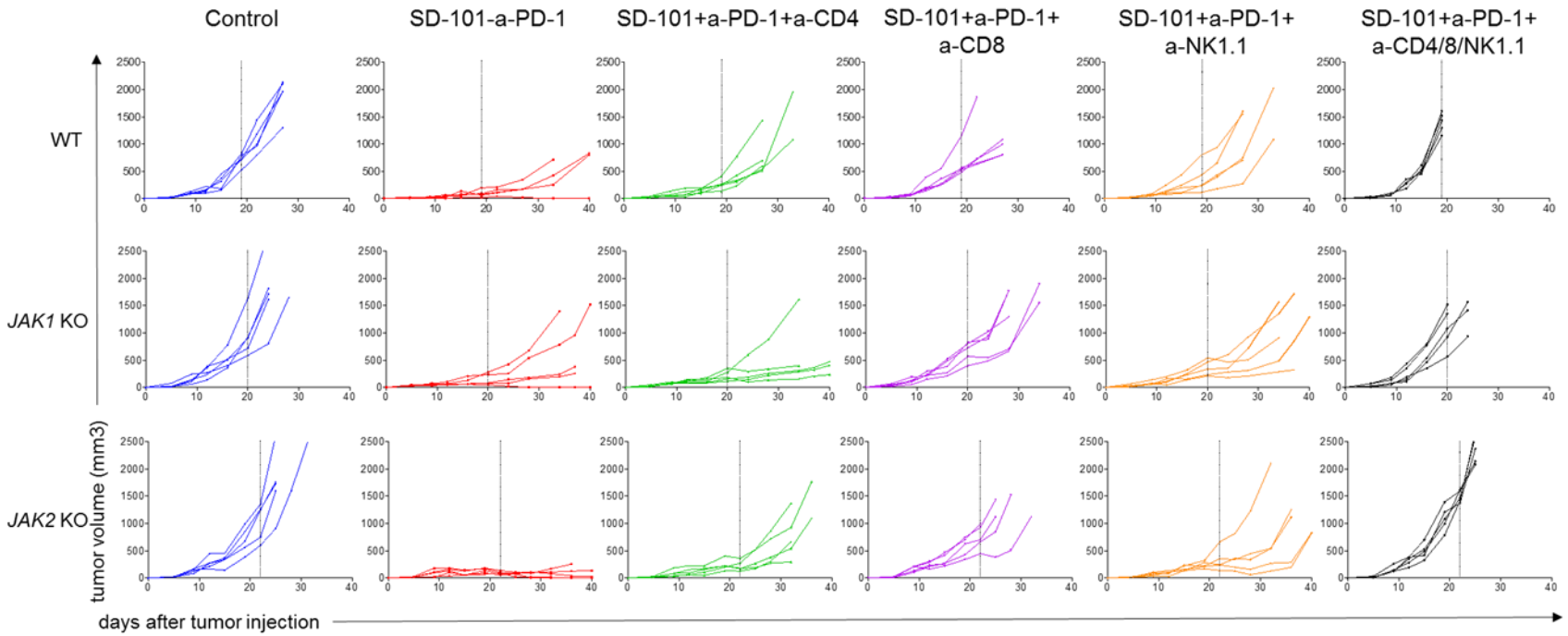

Supplementary Figure 5*. In vivo* depletion studies with intratumoral TLR-9 agonist in combination with anti-PD-1 therapy. *In vivo* tumor growth curves of individual C57/BL6 mice for wild-type control and *JAK1/2* knockout resistant tumors with anti-CD4, anti-CD8 and anti-NK1.1 depletion studies after intratumoral (i.t) SD-101 combined with anti-PD-1 therapy, according Figure 33.

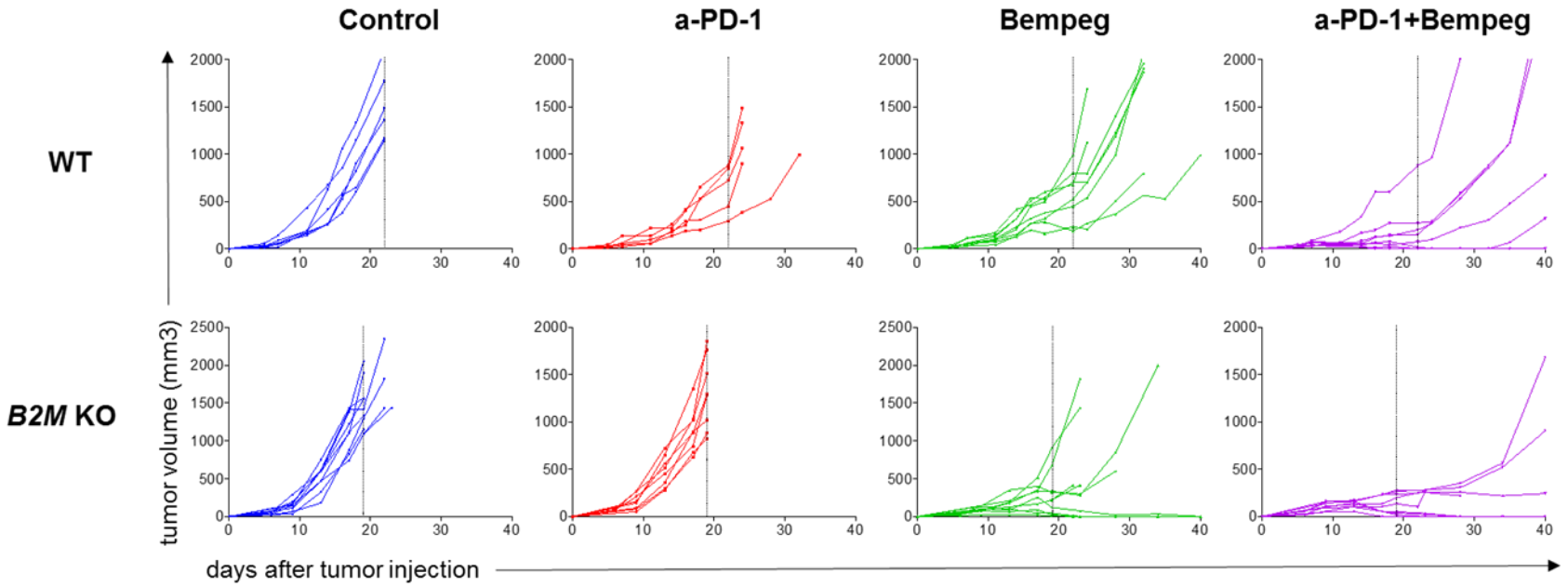

Supplementary Figure 6. A CD122 preferential IL2 pathway agonist (bempegaldesleukin, NKTR-214) to reverse resistance in *B2M* deficient tumors. *In vivo* tumor growth curves of individual C57/BL6 mice after Control-Isotype, anti-PD-1, bempegaldesleukin or anti-PD-1 plus bempegaldesleukin, according Figure 36 .Bempeg, bempegaldesleukin

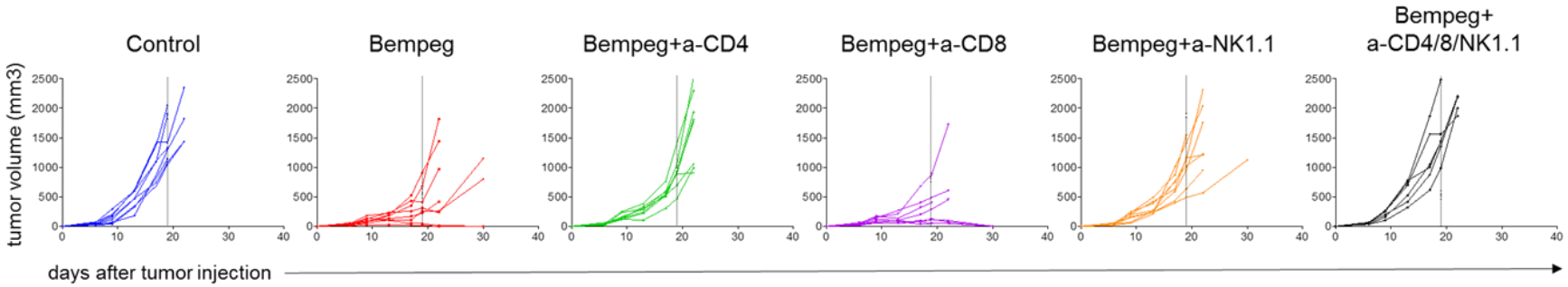

Supplementary Figure 7: A CD122 preferential IL2 pathway agonist (bempegaldesleukin, NKTR-214) to reverse resistance in *B2M* deficient tumors. *In vivo* tumor growth curves of individual C57/BL6 mice for *B2M* knockout resistant tumors with anti-CD4, anti-CD8 and anti-NK1.1 depletion studies after 0.8 mg/kg IV bempegaldesleukin, according Figure . Bempeg, bempegaldesleukin.

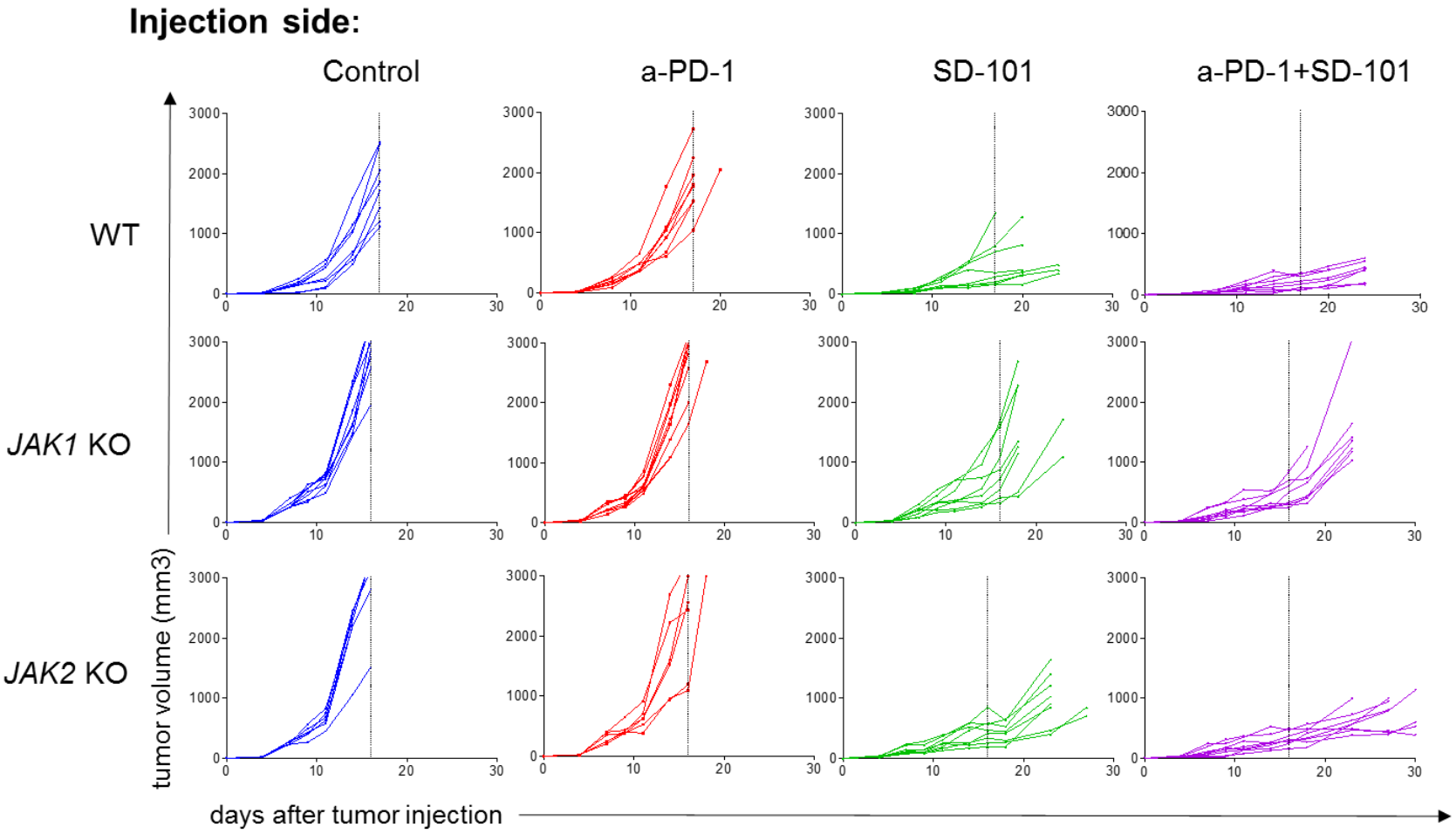

Supplementary Figure 8: Overcoming *JAK1/2* and *B2M* resistant tumors in an aggressive B16 murine melanoma model. *In vivo* tumor growth curves of individual C57/BL6 mice after Control-Isotype, anti-PD-1, SD-101 or anti-PD-1 plus SD-101, in B16 wild-type and *JAK1/2* knockout tumors, according Figure 40. Effect on tumor growth at treated (injection site)

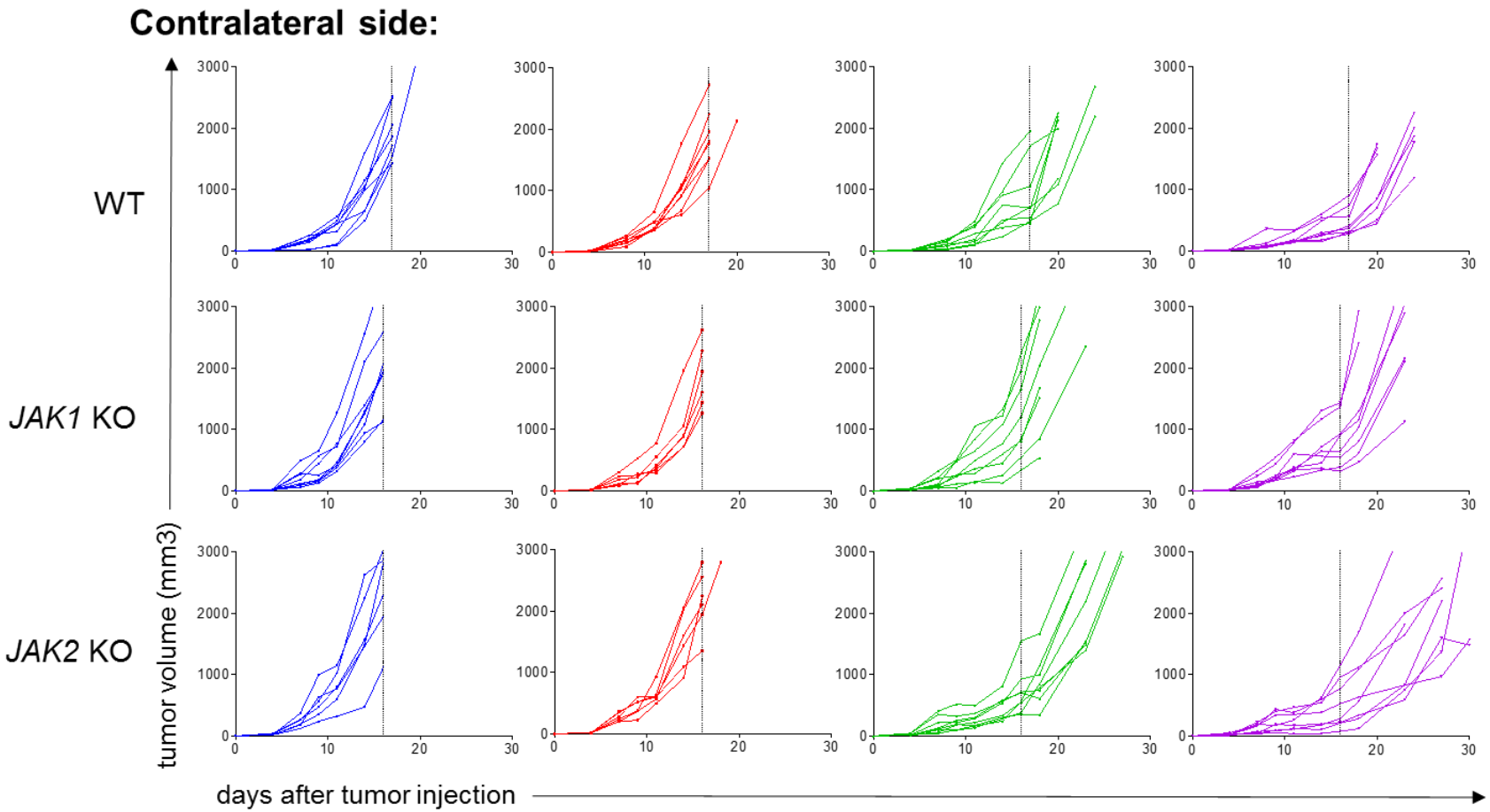

Supplementary Figure 9: Overcoming *JAK1/2* resistant tumors in an aggressive B16 murine melanoma model. *In vivo* tumor growth curves of individual C57/BL6 mice after Control-Isotype, anti-PD-1, SD-101 or anti-PD-1 plus SD-101, in B16 wild-type and *JAK1/2* knockout tumors, according Figure 40. Effect on tumor growth at treated (non-injection or contralateral site)

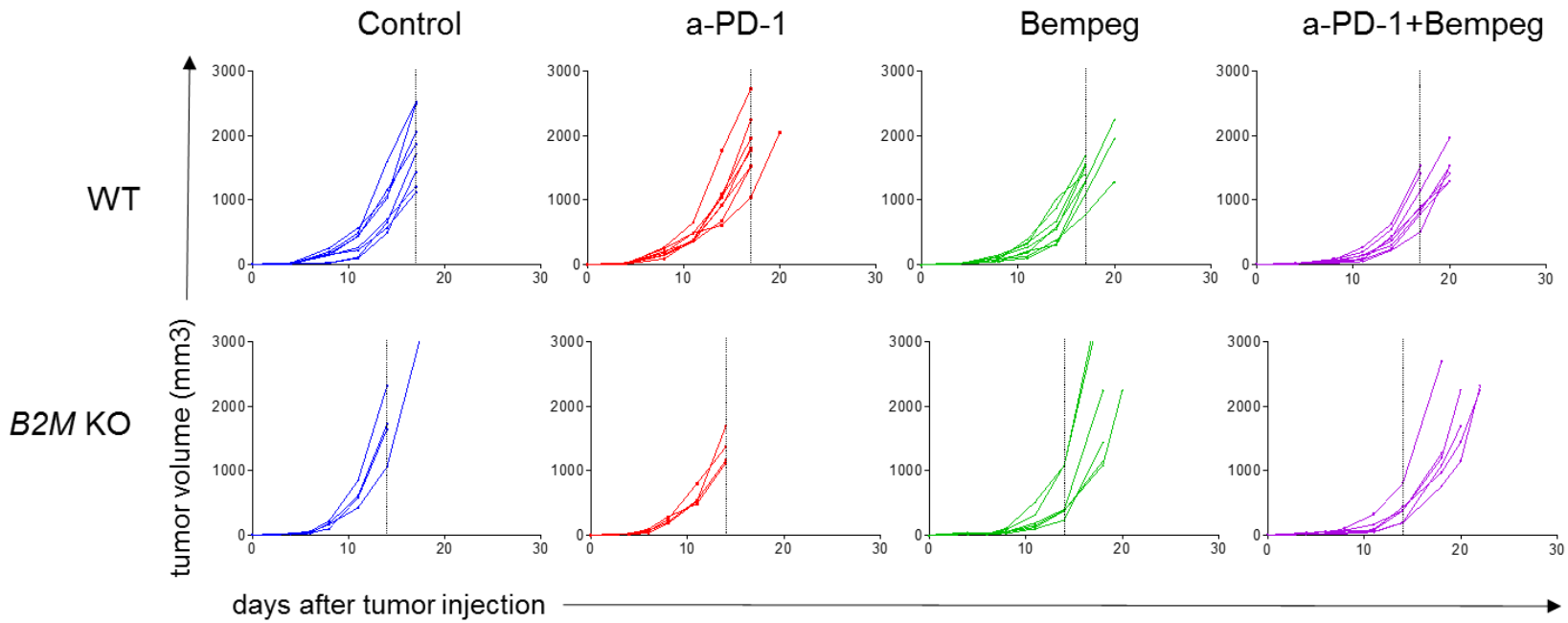

Supplementary Figure 10: Overcoming *B2M* resistant tumors in an aggressive B16 murine melanoma model. *In vivo* tumor growth curves of individual C57/BL6 mice for B16 wild-type control and *B2M* knockout resistant tumors treated with control isotype, anti-PD-1 according Figure 41, bempeg and anti-PD-1 plus bempeg. Bempeg, bempegaldesleukin